

AD-782 178

POLARIZED EMITTANCE. VOLUME 1:
POLARIZED BIDIRECTIONAL REFLECTANCE
WITH LAMBERTIAN OR NON-LAMBERTIAN
DIFFUSE COMPONENTS

J. R. Maxwell, et al

Environmental Research Institute of Michigan

Prepared for:

Ballistic Research Laboratories

May 1974

DISTRIBUTED BY:

NTIS

National Technical Information Service
U. S. DEPARTMENT OF COMMERCE
5285 Port Royal Road, Springfield Va. 22151

UNCLASSIFIED

SECURITY CLASSIFICATION OF THIS PAGE(When Data Entered)

Block 20. Abstract

The model makes it possible to calculate bidirectional reflectance data from a very small amount of measured data. Accuracy demonstrated indicates that the model is very effective, although improvement can still be obtained at large receiver zenith angles.

ja

UNCLASSIFIED

SECURITY CLASSIFICATION OF THIS PAGE(When Data Entered)

FOREWORD

The work reported herein, covering the period 10 April 1972 to 31 December 1972, was carried out by the Infrared and Optics Division of the Environmental Research Institute of Michigan (formerly the Willow Run Laboratories of The University of Michigan), Ann Arbor, Michigan. The work, which was performed under Contract DAAD05-72-C-0246 for the Army Ballistic Research Laboratories, was done in three parts, each of which represents one volume.

The three volumes comprising the present series on polarized radiance are:

- I - Polarized Bidirectional Reflectance with Lambertian or Non-Lambertian Diffuse Components
- II - Polarized Spectral Emittance from 4 to 14 μm
- III - Wavelength Dependence of Polarized Bidirectional Reflectance

The ERIM number for Volume I of this report is 192500-1-T(I).

PREFACE

Under contract commitments with the Air Force Avionics Laboratory (Contract F33615-70-C-1123), a bidirectional reflectance model was developed to predict reflectance from rough surfaces as a function of the zenith and azimuth angles of source and receiver, given a set of input parameters derived from limited measurements. It was observed, however, that the model required further extension to account for anomalies in the comparison of measured data with calculated model predictions. Specifically, it was determined that the model would be more accurate if it could account for a non-Lambertian, non-specular component of the reflectance which was assumed to result from scattering within the target material. Extension of the model to take the non-Lambertian angular dependence into account was carried out under this BRL contract, as well as coding the model in Fortran IV and validating it.

This extension of the bidirectional reflectance model plus other extensions performed under the AFAL contract have considerably improved the fit between model predictions and measured data.

The work done under this contract with BRL has been combined with the work done under the Air Force contract to form a unified model. Therefore, for completeness, the AF-sponsored part of the model is included in this report.

CONTENTS

1. Introduction	1
2. Bidirectional Reflectance	3
3. Background Information	6
4. Surface Model	8
4.1. Available Area	8
4.2. Fresnel Coefficients	8
4.3. Shadowing and Obscuration	10
5. Volume Models	12
5.1. Lambertian	12
5.2. Non-Lambertian	12
6. Model Validation	17
6.1. Reflectance for Sample Material A02018-001	18
6.2. Reflectance for Sample Material A02018-002	26
6.3. Polarization Angle for Sample Materials A02018-001 and A02018-002	26
6.4. Percent Polarization for Sample Materials A02018-001	48
6.5. Reflectance for Sample Material A02100	48
7. Model Parameters	66
7.1. Source Polarization Parameters	66
7.2. Surface Model Parameters	67
7.3. Lambertian Volume Model Parameters	68
7.4. Non-Lambertian Volume Model Parameters	68
Appendix I: Documentation of Bidirectional Reflectance Program (RHOPRIME)	73
Appendix II: Instructions for Use of Program with Sample Computer Output	89
Appendix III: Rhoprime Program Listing	95
References	118
Distribution List	119

v

FIGURES

1. Bidirectional Reflectance Geometry and Parameters	4
2. Example of Reflectance ρ' for A02018-001. θ_r Scanned in Plane	7
3. Volume Scattering Geometry and Parameters	13
4. Fixed Bistatic ρ' for A02018-001. Polarizations $\perp\perp, \perp 45, \perp\parallel$	19
5. Measured ρ' for A02018-001. $\phi_r = 0, 180^\circ$; Polarizations $\perp\perp, \perp 45, \perp\parallel$	21
6. Calculated ρ' for A02018-001 Using Lambertian Volume Model and Non-Lambertian Volume Model With and Without Shadowing and Obscuration Factor, $\theta_i = 40^\circ$; $\phi_r = 0^\circ, 180^\circ$; Polarizations $\perp\perp, \perp\parallel$	22
7. Measured ρ' for A02018-001. $\phi_r = 90^\circ, 270^\circ$; Polarizations $\perp\perp, \perp 45, \perp\parallel$	24
8. Calculated ρ' for A02018-001 Using Lambertian Volume Model and Non-Lambertian Volume Model With and Without Shadowing and Obscuration Factor, $\theta_i = 40^\circ$, $\phi_i = 180^\circ$; $\phi_r = 90^\circ, 270^\circ$; Polarizations $\perp\perp, \perp\parallel$	25
9. Measured ρ' for A02018-001. $\phi_r = 30^\circ, 210^\circ$; Polarizations $\perp\perp, \perp 45, \perp\parallel$	27
10. Calculated ρ' for A02018-001 Using Non-Lambertian Volume Model With Shadowing and Obscuration Factor. $\phi_r = 30^\circ, 210^\circ$; Polarizations $\perp\perp, \perp\parallel$	28
11. Measured ρ' for A02018-001. $\phi_r = 60^\circ, 240^\circ$; Polarizations $\perp\perp, \perp 45, \perp\parallel$	29
12. Calculated ρ' for A02018-001 Using Non-Lambertian Volume Model With Shadowing and Obscuration Factor. $\phi_r = 60^\circ, 240^\circ$; Polarizations $\perp\perp, \perp\parallel$	30
13. Measured ρ' for A02018-001. $\phi_r = 0^\circ, 180^\circ$; Polarizations $-45\perp, -45-45, -45\parallel$	31
14. Calculated ρ' for A02018-001 Using Non-Lambertian Volume Model With Shadowing and Obscuration Factor. $\phi_r = 0^\circ, 180^\circ$; Polarizations $-45\perp, -45\parallel$	32
15. Measured ρ' for A02018-001. $\phi_r = 90^\circ, 270^\circ$; Polarization $\parallel\perp, \parallel-45, \parallel\parallel$	33
16. Calculated ρ' for A02018-001 Using Non-Lambertian Volume Model With Shadowing and Obscuration Factor. $\phi_r = 90^\circ, 270^\circ$; Polarizations $\parallel\perp, \parallel\parallel$	34
17. Measured ρ' for A02018-001. $\phi_r = 30^\circ, 210^\circ$; Polarizations $\parallel\perp, \parallel-45, \parallel\parallel$	35
18. Calculated ρ' for A02018-001 Using Non-Lambertian Volume Model With Shadowing and Obscuration Factor. $\phi_r = 30^\circ, 210^\circ$; Polarizations $\parallel\perp, \parallel\parallel$	36

vi

19. Measured ρ' for A02018-001. $\phi_r = 60^\circ, 240^\circ$; Polarizations $\perp\perp, \perp-45, \parallel\parallel$	37
20. Calculated ρ' for A02018-001 Using Non-Lambertian Volume Model With Shadowing and Obscuration Factor. $\phi_r = 60^\circ, 240^\circ$; Polarizations $\perp\perp, \parallel\parallel$	38
21. Fixed Bistatic ρ' for A02018-002. Polarizations $\perp\perp, 145, \perp\parallel$	39
22. Measured ρ' for A02018-002. $\phi_r = 0^\circ, 180^\circ$; Polarizations $\perp\perp, \perp-45, \perp\parallel$	40
23. Calculated ρ' for A02018-002 Using Lambertian Volume Model. $\phi_r = 0^\circ, 180^\circ$; Polarizations $\perp\perp, \perp\parallel$	41
24. Measured ρ' for A02018-002. $\phi_r = 90^\circ, 270^\circ$; Polarizations $\perp\perp, \perp-45, \perp\parallel$	42
25. Calculated ρ' for A02018-002 Using Lambertian Volume Model. $\phi_r = 90^\circ, 270^\circ$; Polarizations $\perp\perp, \perp\parallel$	43
26. Measured ρ' for A02018-002. $\phi_r = 0^\circ, 180^\circ$; Polarizations $\perp\perp, \perp-45, \parallel\parallel$	44
27. Calculated ρ' for A02018-002 Using Lambertian Volume Model. $\phi_r = 0^\circ, 180^\circ$; Polarizations $\perp\perp, \parallel\parallel$	45
28. Measured ρ' for A02018-002. $\phi_r = 90^\circ, 270^\circ$; Polarizations $\perp\perp, \perp-45, \parallel\parallel$	46
29. Calculated ρ' for A02018-002 Using Lambertian Volume Model. $\phi_r = 90^\circ, 270^\circ$; Polarizations $\perp\perp, \parallel\parallel$	47
30. Variation of Polarization Angle of Reflected Radiance as Function of Source-Receiver Position. $\phi_r = 0^\circ, 180^\circ$	50
31. Variation of Polarization Angle of Reflected Radiance as Function of Source-Receiver Position. $\phi_r = 30^\circ, 210^\circ$	51
32. Variation of Polarization Angle of Reflected Radiance as Function of Source-Receiver Position. $\phi_r = 60^\circ, 240^\circ$	52
33. Variation of Polarization Angle of Reflected Radiance as Function of Source-Receiver Position. $\phi_r = 90^\circ, 270^\circ$	53
34. Percent Polarization Variation for A02018-002 as Function of Source-Receiver Position. $\phi_r = 0^\circ, 180^\circ$; Perpendicular Source	54
35. Percent Polarization Variation for A02018-002 as Function of Source-Receiver Position. $\phi_r = 0^\circ, 180^\circ$; Parallel Source	54
36. Percent Polarization Variation for A02018-001 as Function of Source-Receiver Position. $\phi_r = 0^\circ, 180^\circ$; Perpendicular Source	54
37. Percent Polarization Variation for A02018-001 as Function of Source-Receiver Position. $\phi_r = 90^\circ, 270^\circ$; Perpendicular Source	55
38. Percent Polarization Variation for A02018-001 as Function of Source-Receiver Position. $\phi_r = 90^\circ, 270^\circ$; Parallel Source	55

39. Fixed Bistatic ρ' for A02100. Polarizations $\perp\perp$, \perp -45, $\perp\parallel$	56
40. Measured ρ' for A02100. $\theta_i = 0^\circ$, $\phi_i = 0^\circ$, $\phi_r = 0^\circ, 180^\circ$; Polarizations $\perp\perp$, \perp -45, $\perp\parallel$	57
41. Calculated ρ' for A02100 Using Non-Lambertian Volume Model. $\theta_i = 0^\circ$, $\phi_i = 180^\circ$, $\phi_r = 0^\circ, 180^\circ$; Polarization $\perp\parallel$	58
42. Calculated ρ' for A02100 Using Lambertian Volume Model. $\theta_i = 0^\circ$, $\phi_i = 180^\circ$, $\phi_r = 0^\circ, 180^\circ$; Polarization $\perp\parallel$	59
43. Measured ρ' for A02100. $\theta_i = 20^\circ$, $\phi_i = 180^\circ$, $\phi_r = 0^\circ, 180^\circ$; Polarizations $\perp\perp$, \perp -45, $\perp\parallel$	60
44. Calculated ρ' for A02100 Using Non-Lambertian Volume Model. $\theta_i = 20^\circ$, $\phi_i = 180^\circ$, $\phi_r = 0^\circ, 180^\circ$; Polarization $\perp\parallel$	61
45. Calculated ρ' for A02100 Using Lambertian Volume Model. $\theta_i = 20^\circ$, $\phi_i = 180^\circ$, $\phi_r = 0^\circ, 180^\circ$; Polarization $\perp\parallel$	62
46. Measured ρ' for A02100. $\theta_i = 40^\circ$, $\phi_i = 180^\circ$, $\phi_r = 0^\circ, 180^\circ$; Polarizations $\perp\perp$, \perp -45, $\perp\parallel$	63
47. Calculated ρ' for A02100 Using Non-Lambertian Volume Model. $\theta_i = 40^\circ$, $\phi_i = 180^\circ$, $\phi_r = 0^\circ, 180^\circ$; Polarization $\perp\parallel$	64
48. Calculated ρ' for A02100 Using Lambertian Volume Model. $\theta_i = 40^\circ$, $\phi_i = 180^\circ$, $\phi_r = 0^\circ, 180^\circ$; Polarization $\perp\parallel$	65
49. Bidirectional Reflectance Geometry	75

TABLES

I. Model Parameters for Sample Paints	18
II. True Source Polarization Angles	18
III. $\rho'(\theta_n, \phi_n; \theta_n, \phi_n) \cos^2 \theta_n$ Values for A02017-001.	69
IV. $\rho'(\theta_n, \phi_n; \theta_n, \phi_n) \cos^2 \theta_n$ Values for A02018-001.	70
V. $\rho'(\theta_n, \phi_n; \theta_n, \phi_n) \cos^2 \theta_n$ Values for A02018-002.	71
VI. $\rho'(\theta_n, \phi_n; \theta_n, \phi_n) \cos^2 \theta_n$ Values for A02100	72
VII. RHOPRIME Input Listing	92
VIII. Long Form Output.	93
IX. Short Form Output	94

POLARIZED RADIANCE
Volume I

Polarized Bidirectional Reflectance with Lambertian
or Non-Lambertian Diffuse Components

10 April Through 31 December 1972

1

INTRODUCTION

A model for predicting the radiance at a remote sensor must include the spatial, spectral, and polarization characteristics of the bidirectional reflectance and directional emittance with respect to target and background surfaces. In principle, the directional reflectance and directional emittance properties of materials must be known for all source and receiver angles, polarizations, and wavelengths. A Lambertian assumption may be valid for some types of backgrounds, but for most man-made targets is scarcely adequate. Measurement of all spatial, polarization, and spectral characteristics of the bidirectional reflectance and directional emittance for a large number of material samples is impractical. Even if such measurement were performed, the data could not all be stored efficiently enough to make it accessible for digital computations. Clearly, an empirical model is required to approximate the bidirectional reflectance and directional emittance properties from a limited number of measurements.

The bidirectional reflectance model first developed by the Environmental Research Institute of Michigan (ERIM) for the Air Force [1, 2] is described in this report. The model accounts for effects that produce both specular and diffuse components. In particular, a surface model relates bidirectional reflectance for all source-receiver angles and polarizations to fixed bistatic measurements and a Brewster angle measurement. The model has been extended under this contract to enable calculation of either a Lambertian diffuse component or a non-Lambertian diffuse component. The latter component accounts for angular and depolarization properties arising from internal scattering effects. Our extension of the bidirectional reflectance model has considerably improved the fit between model predictions and measured data, as will be shown in Section 6.

As it now stands, the model permits generation of an enormous amount of bidirectional reflectance data from a very small amount of measured data. The accuracy shown in Section 6 on Model Validation indicates that the model is very effective, although it can still be improved, particularly at large receiver zenith angles. With the ability to account for elliptical (particularly circular) polarization now built in, the model is available for use with circularly polarized sources, if these sources prove useful in the future.

In this report, we compare measured data with results computed from both the initial model and from the extended model, and then evaluate the relative performance of the two. We

establish a domain of validity for each, based on material properties. Since the modeling is empirical, only a limited amount of measured data are required as input parameters. In this case, the parameters are the fixed bistatic data.

All modeling described in Volume I of this report was performed with respect to one wavelength, $\lambda = 1.06 \mu\text{m}$.

2
BIDIRECTIONAL REFLECTANCE

One physical property which can be measured directly from a sample of material is bi-directional reflectance. The physical definition is

$$\rho'(\theta_i, \phi_i; \theta_r, \phi_r) = \frac{\delta L_r(\theta_r, \phi_r)}{\delta E_i(\theta_i, \phi_i)} \quad (1a)$$

where $\delta E_i(\theta_i, \phi_i)$ is the incremental irradiance (power per unit area) impinging on the surface of a material from the direction (θ_i, ϕ_i) , and $L_r(\theta_r, \phi_r)$ is the resulting increment of radiance (power per unit projected area per unit solid angle) scattered from that surface in the direction (θ_r, ϕ_r) . Figure 1 illustrates the situation. The bistatic angle, 2β , is that angle between the vectors which point to the source and the receiver respectively.

Equation (1a) can be rewritten in terms of directly-accessible experimental parameters as

$$\rho'(\theta_i, \phi_i; \theta_r, \phi_r) = \frac{\frac{\delta P_r}{\delta A \cos \theta_r \delta \Omega_r}}{\frac{\delta P_i}{\delta A}} \quad (1b)$$

where δP_i is the power, in watts, incident from the direction (θ_i, ϕ_i) on the small area δA , and δP_r is the resulting power scattered into the small solid angle $\delta \Omega_r$ in the direction (θ_r, ϕ_r) .

When polarization dependence is to be shown, subscripts are appended to the ρ' term. Thus when we write $\rho'_{\alpha_i \alpha_r}$, the leading subscript, α_i , describes the source polarization while the trailing subscript, α_r , describes the receiver polarization. The source polarization, always referred to the plane of incidence, describes the polarization state of the electric field vector. The appended subscript symbols \parallel and \perp indicate whether the source electric vector polarization is parallel to or perpendicular to the incidence plane. The reflected electric field polarization state is specified by the same symbols, but here the reference plane is that reflectance plane defined by the sample normal and the direction to the receiver. (For example, $\rho'_{\perp \parallel}$ represents reflectance measured when source polarization is perpendicular to the incidence plane and receiver polarization is parallel to the reflectance plane.) Notice that when either the source or the receiver, or both, are scanned in angle over the sample, the incidence and reflectance planes change orientation with relation both to the sample and to each other.

Bidirectional reflectance depends on the physical properties of the material as well as on the geometric state of its surface. Different surface states result in different reflectances. Hence, a complete collection of bidirectional reflectance data for any single material would require measurements of a large number of samples of the material, each with a different surface state. Each sample would have to be measured with several source-receiver polarization combinations. Consequently a very large number of source and receiver positions would be

required for each set of polarization states. Finally, the entire procedure would have to be repeated at many different wavelengths. The purpose of modeling is to predict reflectance data from only a limited number of measurements and hence eliminate the need for an otherwise unwieldy measurement program.

3
BACKGROUND INFORMATION

The bidirectional reflectance model is based on observations of polarized bidirectional data from rough, painted surfaces which exhibit a Brewster angle (Fresnel-like behavior in relation to the specular geometry). The degree of depolarization appears slight, and on that basis for the initial modeling work in this program single specular reflection from the rough front surface was assumed to be the dominant reflection mechanism. Multiple front-surface reflections and internal scatterings were observed to be smaller and were initially incorporated into a Lambertian "volume" model to account for the diffuse component.

The assumption that the diffuse component is Lambertian, however, makes it difficult to account for certain anomalies that occur when measured data are compared with the model's output. For example, Fig. 2 is a bidirectional reflectance curve showing the reflectances at the receiver as the receiver scans over zenith angles from 0° to 90° in the $\phi_r = 0^\circ$ and $\phi_r = 180^\circ$ half planes. The source remains fixed at $\theta_i = 40^\circ$ and $\phi_i = 180^\circ$. The upper curve shows reflectances when source and receiver are both linearly polarized at the same polarization angle with respect to the target-incidence and target-receiver planes. (In this case, both are perpendicular-polarized.) The lower curve shows reflectances when source and receiver are cross-polarized with respect to one another. (Source is perpendicular-polarized; receiver is parallel-polarized.) Note the marked angular dependence in the lower curve. If the nonspecular component were truly Lambertian, no such angular dependence would be present.

Also, although radiation sources in this work are all linearly polarized, future work may well involve more general cases. Therefore, the model should account for the most general type of polarization —namely, elliptical.

For the above reasons, and in order to obtain a closer overall correspondence between model prediction and measured data, the model has been extended to account for the following:

- (1) possible non-Lambertian angular dependence of depolarized component
- (2) shadowing and obscuration produced by the roughness of the surface
- (3) elliptical polarization

The model —a phenomenological one in that its use requires a limited number of measurements —is described in the next two sections. Section 4 includes a discussion of specular reflectance from the surface, effects caused by shadowing and obscuration resulting from surface roughness, and polarization effects. Section 5 describes the volume model.

A02018 001

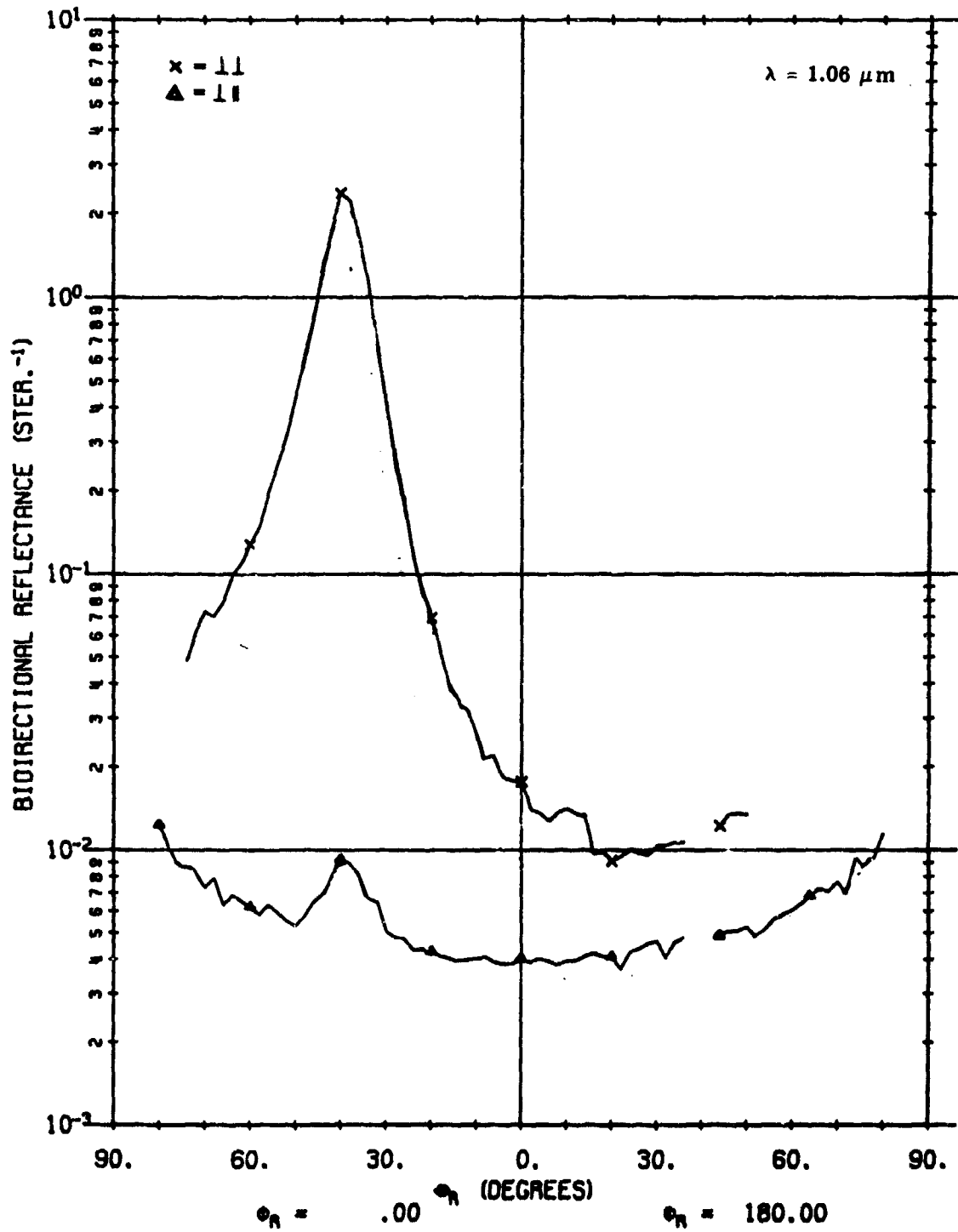


FIGURE 2. EXAMPLE OF ρ' FOR A02018-001. $\theta_i = 40^\circ$, θ_r scanned in plane.

4
SURFACE MODEL

In this section, we review the surface model and also discuss the interference effects that necessitated model modification.

4.1. AVAILABLE AREA

If the rough surface is considered to be made up of small sequins having a distribution of orientations, there will be some specular reflectance at any receiver angle and the extent of that reflectance will be determined in part by the amount of surface oriented for specular reflection at that receiver angle. (The area available for such reflection will also depend on how some sequins shadow or obscure others.) Since measurements do, in fact, show a reflectance distribution over the hemisphere, we assume that the above description is valid and that there is, indeed, a distribution of surface areas which have normals pointing in different directions. Therefore, to establish the distribution of available surface area, we define a density function $\Xi(\theta, \phi)$ which describes the relative density of local surface normals (per steradian) pointing in the direction (θ, ϕ) .

The effect of the distribution of surface normals is measured by a zero bistatic measurement in which $\theta_i = \theta_r$ and $\phi_i = \phi_r$. (Note that we really use a fixed bistatic scan with a small bistatic angle. A true zero bistatic scan would be very difficult to obtain since source and receiver obviously cannot occupy the same position.)

4.2. FRESNEL COEFFICIENTS

Fresnel reflectance coefficients describe the reflectance and polarization of specularly reflected radiation as functions of source and detector positions and of the complex index of refraction. However, since we are trying to find reflectance as a function of source and detector positions only, we must know—or be able to determine—the index of refraction. (As discussed later in this section, we can determine the index by measuring the Brewster angle.) Since, in the surface model, we consider only single, local specular reflections, the Fresnel equations automatically account for polarization.

If the receiver subtends the solid angle $\delta\Omega_r$ from the sample (see Fig. 1) the solid angle $\delta\Omega_{\hat{n}}$ in which local surface normals must lie to permit collection of the local specularly reflected radiation by the receiver is given by:

$$\delta\Omega_{\hat{n}} = \frac{\delta\Omega_r}{4} \cos \beta \quad (2)$$

This solid angle is centered about the direction $\left(\begin{matrix} \theta \\ \hat{n} \end{matrix}, \begin{matrix} \phi \\ \hat{n} \end{matrix} \right)$.

Let δP_i be power incident on area δA . The fraction of surface area, $\delta A \left(\theta_{\hat{n}}, \phi_{\hat{n}} \right)$, which reflects radiation into the receiver is given by

$$\delta A \left(\theta_{\hat{n}}, \phi_{\hat{n}} \right) = \Xi \left(\theta_{\hat{n}}, \phi_{\hat{n}} \right) \delta A \delta \Omega_{\hat{n}} \quad (3)$$

The power incident on $\delta A \left(\theta_{\hat{n}}, \phi_{\hat{n}} \right)$ is

$$\delta P_i \frac{\delta A \left(\theta_{\hat{n}}, \phi_{\hat{n}} \right)}{\delta A} \frac{\cos \beta}{\cos \theta_i} \quad (4)$$

Since the Fresnel reflectance, $R(\beta)$, is just the ratio of reflected power to incident power, then

$$\delta P_r = R(\beta) \delta P_i = \frac{\delta A \left(\theta_{\hat{n}}, \phi_{\hat{n}} \right)}{\delta A} \frac{\cos \beta}{\cos \theta_i} \quad (5)$$

Recall that in Eq. (1b): $\rho'(\theta_i, \phi_i; \theta_r, \phi_r) = \frac{\delta P_r}{\frac{\delta A \cos \theta_r \delta \Omega_r}{\delta P_i}}$. Substituting Eqs. (5), (3) and (2):

$$\rho'(\theta_i, \phi_i; \theta_r, \phi_r) = \frac{R(\beta) \Xi \left(\theta_{\hat{n}}, \phi_{\hat{n}} \right)}{4 \cos \theta_i \cos \theta_r} \quad (6)$$

By considering the case when source and receiver are in the same position, i.e., a zero bistatic ($\beta = 0$) case, $\Xi \left(\theta_{\hat{n}}, \phi_{\hat{n}} \right)$ can be determined. In this situation

$$\rho' \left(\theta_{\hat{n}}, \phi_{\hat{n}}; \theta_{\hat{n}}, \phi_{\hat{n}} \right) = \frac{R(0) \Xi \left(\theta_{\hat{n}}, \phi_{\hat{n}} \right)}{4 \cos^2 \theta_{\hat{n}}} \quad (7)$$

and

$$\Xi(\theta, \phi) = \frac{4 \rho' \left(\theta_{\hat{n}}, \phi_{\hat{n}}; \theta_{\hat{n}}, \phi_{\hat{n}} \right) \cos^2 \theta_{\hat{n}}}{R(0)} \quad (8)$$

Now substitute back into Eq. (6) and

$$\rho'(\theta_i, \phi_i; \theta_r, \phi_r) = \frac{R(\beta)}{R(0)} \frac{\rho' \left(\theta_{\hat{n}}, \phi_{\hat{n}}; \theta_{\hat{n}}, \phi_{\hat{n}} \right) \cos^2 \theta_{\hat{n}}}{\cos \theta_i \cos \theta_r} \quad (9)$$

Equation (9) is an expression for the bidirectional reflectance given in terms of measured data and Fresnel reflectance coefficients. However, to evaluate the Fresnel coefficients so they can be used in Eq. (9) takes a little work. For example, $R(\beta)$ is a function of the real and imaginary parts of the complex index of refraction, $n' = n - ik$ (see Ref. 3 or Appendix III). Therefore, n and k must be found before $R(\beta)$ can be determined.

Moreover, k is taken to be very small* so that n can be determined experimentally by measuring the Brewster angle, θ_B , and then using $n = \tan \theta_B$ to solve for n .

4.3. SHADOWING AND OBSCURATION

Referring to Eq. (9), we can derive a zero bistatic curve, $\rho'(\theta_{\hat{n}}, \phi_{\hat{n}}; \theta_{\hat{n}}, \phi_{\hat{n}})$, from a $\rho'(\theta_i, \phi_i, \theta_r, \phi_r)$ curve with θ_i, ϕ_i fixed and θ_r variable by inverting the equation so that

$$\rho'(\theta_{\hat{n}}, \phi_{\hat{n}}, \theta_{\hat{n}}, \phi_{\hat{n}}) = \frac{R(0)}{R(\beta)} \frac{\rho'(\theta_i, \phi_i, \theta_r, \phi_r) \cos \theta_i \cos \theta_r}{\cos^2 \theta_{\hat{n}}} \quad (10)$$

after doing this for a variety of θ_i 's, we found that the curves obtained differed systematically from those obtained from a fixed bistatic measurement. Apparently, because of surface roughness, some sequins shadow or obscure others; this reduces reflectance everywhere except at a purely back-scattered position. The model must therefore be modified to correct for such interference.

Torrance and Sparrow [4] have developed an analytical function that helps correct the situation; however, we have constructed our own function using empirical considerations only. Our function results in better agreement between measured and derived fixed bistatic curves than does the analytical function of Torrance and Sparrow. The empirical function (SO) is defined as:

$$SO = \frac{1 + \frac{\theta_{\hat{n}}}{\Omega} e^{-2\beta/\tau}}{1 + \frac{\theta_{\hat{n}}}{\Omega}} \left(\frac{1}{1 + \frac{\phi_n}{\Omega} \frac{\theta_i}{\Omega}} \right) \quad (11)$$

where Ω and τ are parameters, and ϕ_n is a factor calculated from the geometry, which adjusts the fall-off rate of the shadowing and obscuration function in the forward-scattered direction.

*For the calculations in this study, results of past measurement programs [1] were used to establish the refractive indices. In those programs, it was determined that the magnitude of the total index of refraction was close to 1.65; that the imaginary part of the index of refraction could be neglected, compared to the real part; and that the index of refraction, for the wavelengths of incident radiation under consideration (1 to 4 μm), did not vary appreciably.

We now modify Eq. (9):

$$\rho'(\theta_{\hat{n}_i}, \phi_{\hat{n}_i}; \theta_{\hat{n}_r}, \phi_{\hat{n}_r}) = \frac{R(\beta)}{R(0)} \frac{\rho'(\theta_{\hat{n}_i}, \phi_{\hat{n}_i}; \theta_{\hat{n}_r}, \phi_{\hat{n}_r}) \cos^2 \theta_{\hat{n}_r}}{\cos \theta_{\hat{n}_i} \cos \theta_{\hat{n}_r}} \quad (\text{SO}) \quad (12)$$

Equation (10) becomes

$$\rho'(\theta_{\hat{n}_i}, \phi_{\hat{n}_i}; \theta_{\hat{n}_r}, \phi_{\hat{n}_r}) = \frac{R(0)}{R(\beta)} \frac{\rho'(\theta_{\hat{n}_i}, \phi_{\hat{n}_i}; \theta_{\hat{n}_r}, \phi_{\hat{n}_r}) \cos \theta_{\hat{n}_i} \cos \theta_{\hat{n}_r}}{(\cos^2 \theta_{\hat{n}_r})} \quad (\text{SO}) \quad (13)$$

The following discussion outlines the reasoning behind the extended portion of the bidirectional reflectance model. (The extended portion is referred to as the "volume" model.)

Different materials with varying degrees of surface roughness and different optical properties show differences in nonspecular reflectance behavior. These differences show up in the extent to which the nonspecular reflectance is dependent upon angular position of the receiver.

To make provision for materials that do exhibit such angular dependence and for those that do not, two volume models are used. The following discussion describes, first, a Lambertian volume model which has no angular dependence, and then a non-Lambertian volume model in which angular dependence is important.

5.1. LAMBERTIAN

In addition to Fresnel reflection from a surface, other effects such as might take place beneath the surface can produce a nonspecular reflectance component everywhere in the hemisphere. If the surface roughness as well as the absorption properties of the surface are right, this volume reflectance may be completely diffuse and uniform over the hemisphere. Moreover, the reflected radiation will be totally depolarized, regardless of the polarization of the source. Thus, if the receiver is polarized in the orthogonal direction to the source polarization, an in-plane measurement will represent the volume component only. However, only half the volume component is actually represented, since there should be an equal diffuse contribution polarized in the same direction as the source.

The Lambertian volume component is one of the input parameters for the model when a target material with Lambertian reflectance properties is considered. A method whereby values for this parameter may be extracted is described in Section 6.

5.2. NON-LAMBERTIAN

On the basis of the Lambertian diffuse model described above, no angular dependence would be expected for the diffuse component. However, for some materials, actual measurements show that there is an angular dependence. To provide for the angular dependence of the diffuse component, the model has been extended by including scattering that takes place beneath the surface.

Assuming an exponential scattering function as the radiation first enters and then leaves the surface, and making reference to Fig. 3, we construct an expression for the volume scattering component of the bidirectional reflectance as follows:

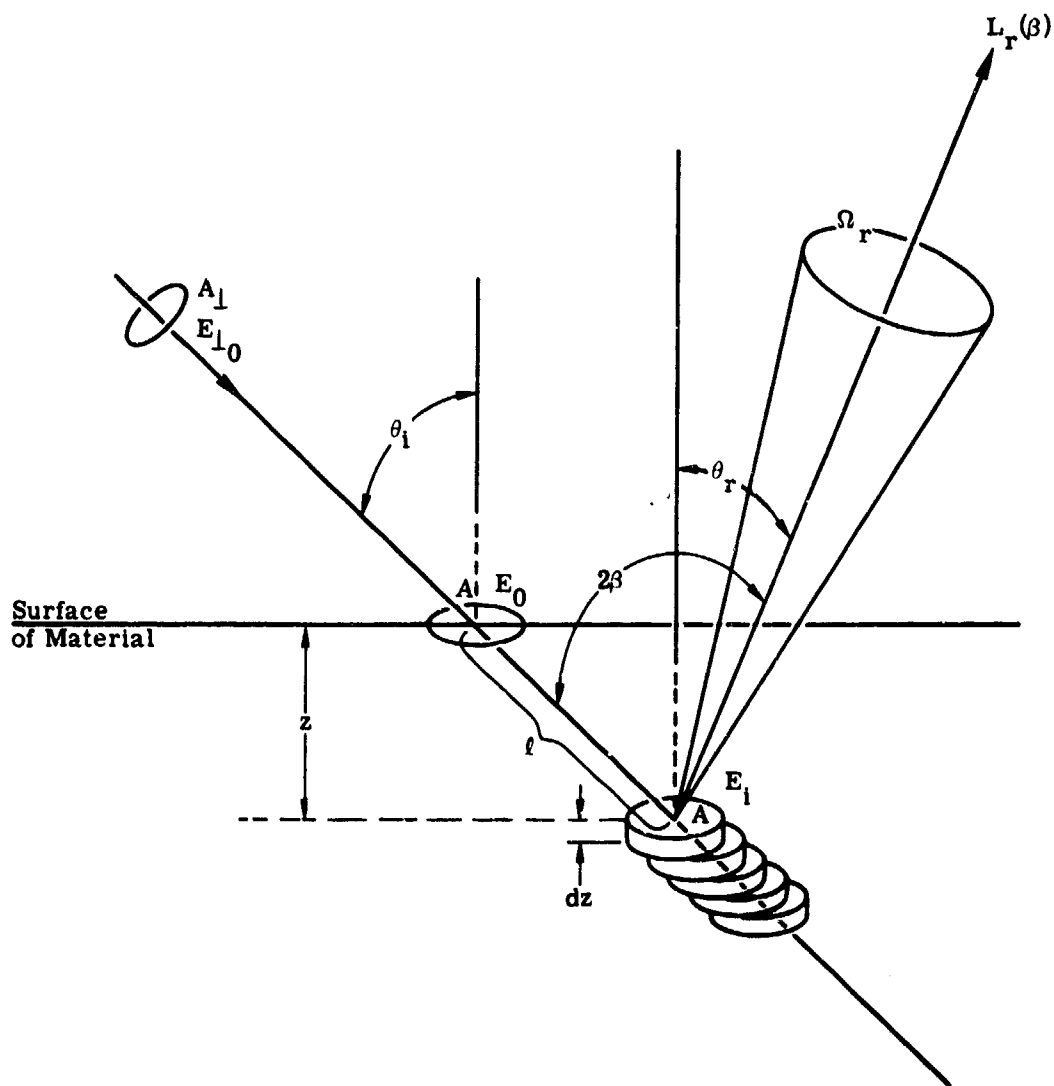


FIGURE 3. VOLUME SCATTERING GEOMETRY AND PARAMETERS

$E_{\perp 0}$ = irradiance at surface of area A_{\perp} , where A_{\perp} is the area of cross section of the collimated beam and is normal to the beam

E_0 = irradiance on surface element of area A

E_i = irradiance on surface of slab or area A at distance z beneath surface

$L_r(\beta)$ = radiance scattered from primary beam through 2β in direction of receiver

β = half of angle between target-to-source and target-to-receiver vectors

σ = total scattering cross section (ignoring absorption)

$\sigma(\beta)$ = differential scattering cross section with respect to β , i.e., $\int \sigma(\beta) d\Omega = \int d\sigma/d\Omega d\Omega = \sigma$

Ω = solid angle subtended at target by receiver, assuming a point target

θ_i = angle of incident beam relative to fixed z axis

θ_r = angle of reflected beam relative to fixed z axis

The objective of the following calculation is to determine that portion of the primary beam scattered from distance z beneath the surface through an angle 2β toward a receiver which subtends solid angle Ω .

First, the bidirectional reflectance defined in Eq. (1) is now $\rho' = L_r/E_0$ with respect to the slab (see Fig. 3). To determine E_0 :

$$A_{\perp} = A \cos \theta_i \quad (14)$$

$$E_0 = \frac{P}{A} = \frac{P}{A_{\perp}/\cos \theta_i} = \frac{P \cos \theta_i}{A_{\perp}} = E_{\perp 0} \cos \theta_i \quad (15)$$

where P is the power at surface of area A .

The irradiance incident on the slab at distance z beneath its surface is:

$$E_i = E_0 e^{-\sigma l} = E_0 e^{-\sigma z / \cos \theta_i} \quad (16)$$

where $l = z / \cos \theta_i$. Hence

$$E_i = E_{\perp 0} \cos \theta_i e^{-\sigma z \cos \theta_i} \quad (17)$$

and

$$dE_i = -E_{\perp 0} \sigma e^{-\sigma z \cos \theta_i} dz \quad (18)$$

where dE_i is the amount by which irradiance decreases in going from distance z to distance $z + dz$ beneath surface. Note also that $e^{-\sigma z \cos \theta_i}$ and $e^{-\sigma z / \cos \theta_r}$ represent the scattering loss from the beam on the way in and on the way out of the material, respectively. To determine L_r ,

$$P_r = L_r A \Omega_r \cos \theta_r = \text{power at the receiver} \quad (19)$$

$$dL_r = \text{radiance scattered, in direction of receiver, from one small slab} \quad (20)$$

of thickness dz

Radiance from slab in direction θ_r (or β) can be written:

$$dL_r = -dE_i \sigma(\beta) \quad (21)$$

since $\sigma(\beta)$ is, by definition the fraction of beam scattered into 2β . Note that (since we are ignoring absorption) irradiance lost from the incident beam is the radiance of the scattered beam; therefore a minus sign precedes dE_i . Hence, if there is no further power loss

$$dP_r = -A \Omega_r dE_i \sigma(\beta) \quad (22)$$

However, power loss caused by beam scattering occurs on the way out as well as the way in; the loss is represented by $\left(e^{-\sigma z / \cos \theta_r} \right)$ on the way out.

Therefore

$$dP_r = \left(-A \Omega_r \sigma(\beta) e^{-\sigma z / \cos \theta_r} dE_i \right) = -\frac{A_{\perp}}{\cos \theta_i} \Omega_r \sigma(\beta) e^{-\sigma z / \cos \theta_r} dE_i \quad (23)$$

Substituting the expression for dE_i , Eq. (18), into Eq. (23), we obtain:

$$dP_r = E_{\perp 0} \sigma e^{-\sigma z / \cos \theta_i} \left(\frac{A_{\perp} \sigma(\beta) e^{-\sigma z / \cos \theta_r}}{\cos \theta_i} \right) \Omega_r dz \quad (24)$$

$$P_r = \int_0^{\infty} dP_r = \frac{E_{\perp 0} A_{\perp} \Omega_r}{\cos \theta_i} \cdot \frac{\sigma(\beta)}{\left(\frac{1}{\cos \theta_i} + \frac{1}{\cos \theta_r} \right)} \quad (25)$$

where the integration from 0 to ∞ assumes no transmission of power through the material, i.e., the material has effectively an infinite thickness with respect to transmission. Therefore

$$L_r = \frac{P_r}{A \cos \theta_r \Omega_r} = \frac{E_{\perp 0} \sigma(\beta)}{\cos \theta_r \left(\frac{1}{\cos \theta_i} + \frac{1}{\cos \theta_r} \right)} \quad (26)$$

and

$$\rho' = \frac{L_r}{E_0} = \frac{\sigma(\beta)}{\cos \theta_i \cos \theta_r \left(\frac{1}{\cos \theta_i} + \frac{1}{\cos \theta_r} \right)} = \frac{\sigma(\beta)}{(\cos \theta_i + \cos \theta_r)} \quad (27)$$

In ignoring the finite thickness of the layer of material, we have also ignored the possible specular reflectance of the bottom surface. To account for the possibility of specular reflection from the bottom layer, it may be useful to provide a parameter function peaked near $\theta_{\hat{n}} = 0$. Therefore, we include all β dependence in a function $f(\beta)$, and all $\theta_{\hat{n}}$ dependence in a function $g(\theta_{\hat{n}})$, and write

$$\rho' = 2 \frac{\rho_V f(\beta) g(\theta_{\hat{n}})}{\cos \theta_i + \cos \theta_r} \quad (28)$$

where $f(\beta)$ and $g(\theta_{\hat{n}})$ provide freedom for empirical adjustment. The constant, ρ_V , represents the value of ρ' when $\theta_i = \theta_r = 0$ and $f(\beta) = g(\theta_{\hat{n}}) = 1$.

6
MODEL VALIDATION

Use of the bidirectional reflectance model requires a limited amount of measured data (namely the zero bistatic measurement) from which complete sets of reflectances can be calculated. The results of these model-calculated bidirectional reflectances can then be compared to corresponding results of actual measurements. This was the procedure we followed to validate the model.

Model calculations and measured data were compared in terms of ρ' (the reflectance), α or ψ_r (the angle of polarization for the beam after reflection from the target), and P (the percentage of polarization of the reflected beam).

Measured data for materials of different properties (color and roughness) were used to demonstrate the model's performance. The materials are designated as A02018-001, A02018-002, and A02100. Material A02018-001 is a green paint and material A02018-002 is a tan paint. These materials were supplied by the Army Ballistic Research Laboratories for the purpose of developing the non-Lambertian diffuse component of the model.

Measured data for materials A02018-001 and A02018-002 were used for the fitting since it was felt that two surfaces of extremely different properties (color and roughness) would be necessary to demonstrate the performance of the model. Measurements on material A02017-001 show that the bidirectional reflectance very closely resembles that of material A02018-001. Therefore, sufficient information was developed in validating the model with material A02018-001 to permit assignment of parameters to material A02017-001 as well. Additional validation was performed with respect to A02100 (soil) and discussion is included. Model parameters are listed in Table I. (See Section 7 for definitions of model parameters.) The overall discussion of the model fitting is divided into five parts:

- (1) ρ' for A02018-001
- (2) ρ' for A02018-002
- (3) polarization angle (α or ψ_r) for A02018-001
- (4) percent polarization (P) for A02018-001 and A02018-002
- (5) ρ' for A02100

In what follows, the orientation of the source polarizer in the measurements of materials A02018-001 and A02018-002 was not actually perpendicular, parallel, nor at 45° to the plane of incidence but instead was offset by 5° in each case. Specifically, the appropriate correspondences, shown in Table II, should be recognized. These shifts were taken into account when the validation calculations were made on the computer; however, we continue to refer to "perpendicular," "parallel," and " 45° ."

TABLE I. MODEL PARAMETERS FOR SAMPLE PAINTS

Parameter	Material		
	A02017-001	A02018-001	A02018-002
n	1.65	1.65	1.65
k	0	0	0
$\rho_{\chi 1}$	---	---	0.044
$\rho_{\chi 2}$	---	---	0.044
ρ_V	.0064	0.007	0.05**
τ	15	15	15
Ω	40	40	40
$f(\beta)$	1	1	1
$g(\theta_{\hat{n}})$	1	1	1
$\rho'(\theta_{\hat{n}}, \theta_{\hat{n}}; \theta_{\hat{n}}, \theta_{\hat{n}}) \cos^2 \theta_{\hat{n}}$	---	---	---
λ	1.06 μm	1.06 μm	1.06 μm

*This material is run with the non-Lambertian volume model; therefore ρ_{χ} values are not necessary.

**Material 2018-002 was run with the Lambertian volume model; therefore ρ_V should not be used.

TABLE II. TRUE SOURCE POLARIZATION ANGLES

Receiver Azimuth Plane	Nominal Angles			
	$1(0^\circ)$	$11(90^\circ)$	$+45^\circ$	-45°
$0^\circ - 180^\circ$				
$30^\circ - 210^\circ$	5°	-85°		-40°
$60^\circ - 240^\circ$				
$90^\circ - 270^\circ$	5°	$+95^\circ$	$+50^\circ$	
Fixed Bistatic	5°	$+95^\circ$	$+50^\circ$	

6.1. REFLECTANCE FOR SAMPLE MATERIAL A02018-001

Material A02018-001 is a green painted surface. The zero bistatic measurement with 5° polarization angle (i.e., almost perpendicular polarization) is shown in Fig. 4. (The zero bistatic data with parallel-polarized source, although not shown, have identical characteristics.) The zero bistatic plot is sharply peaked at 0° , falling off rapidly to a constant value at about

A02018 001

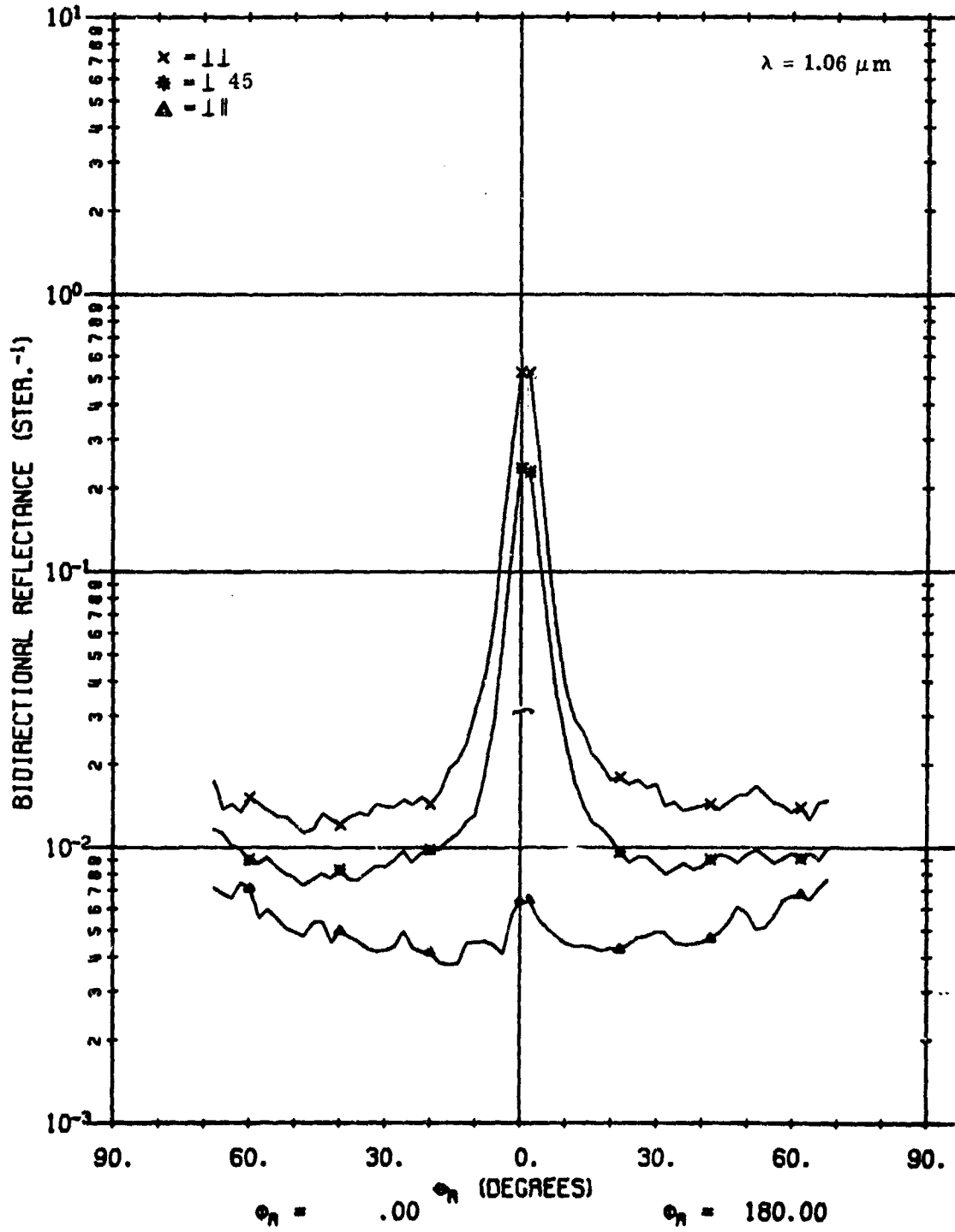


FIGURE 4. FIXED BISTATIC ρ' FOR A02018-001

20°. In all receiver polarizations, ρ' shows an angular dependence clearly departing from Lambertian behavior. The table of values for $\rho'(\theta_{\hat{n}}, \phi_{\hat{n}}; \theta_{\hat{n}}, \phi_{\hat{n}}) \cos^2 \theta_{\hat{n}}$ used in the model was obtained from this measurement by reading off $\rho'_{\perp\perp}$ and $\rho'_{\perp\parallel}$ at each angle and then calculating $(\rho'_{\perp\perp} - \rho'_{\perp\parallel}) \cos^2 \theta_{\hat{n}}$ where $\theta_{\hat{n}}$ is the angle that the normal to the reflecting facet makes with the fixed z-axis. In zero bistatic scans, $\theta_i = \theta_r = \theta_{\hat{n}}$ (see Fig. 1). (Physically the source and receiver were separated by 1.8°. Thus, both were 0.9° from the true $\theta_{\hat{n}}$. In the calculations, the axis was translated to bring the x-axis into correspondence with $\theta_{\hat{n}} = 0$.) The subtraction, $\rho'_{\perp\perp} - \rho'_{\perp\parallel}$ eliminates the diffuse contribution which would distort the value for $\rho'(\theta_{\hat{n}}, \phi_{\hat{n}}; \theta_{\hat{n}}, \phi_{\hat{n}})$ which is what must be measured (recall Eq. 9).

In Figs. 5, 7, 9 and 11,* plots of measured data are shown for $\theta_i = 40^\circ$, $\phi_i = 180^\circ$ and where θ_r is scanned in azimuth planes represented by $\phi_r = 0^\circ, 180^\circ; 90^\circ, 270^\circ; 30^\circ, 210^\circ; 60^\circ, 240^\circ$. Each measurement plot is followed by plots of data generated, respectively, by the Lambertian model with no shadowing and obscuration factor, by the non-Lambertian model with no shadowing and obscuration factor, and by the non-Lambertian model with the shadowing and obscuration factor. For example, Fig. 6 shows the calculated ρ' data for $\theta_i = 40^\circ$ and θ_r as scanned in the 0° and 180° azimuth planes for the above variations of the model. The simulated source is taken to have a "perpendicular" polarization angle. In these in-plane scans ($\phi_r = 0^\circ, 180^\circ$), the main peak is in the 0° azimuth plane which is the forward direction for the source angle of $\phi_i = +180^\circ$. Note the rise (in the plot of measured data) at large zenith angles for the cross-polarized component. This is a characteristic which suggests the need for the non-Lambertian volume model.

Surface Plus Lambertian Volume Model with No Shadowing and Obscuration Correction.

Figure 6 plots (in solid lines) the model calculation using the surface model plus the Lambertian volume model with no correction for shadowing and obscuration. The following characteristics should be noted:

- (1) In the $\phi_r = 0$ (forward scattering) azimuth plane, the model fits the measured data very well between $\theta_r = 0$ and $\theta_r \approx 50^\circ$ for matched polarization of source and receiver. At $\theta_r = 60^\circ$, the calculated curve suddenly diverges. This is thought to be the result of the failure to account for shadowing and obscuration as discussed earlier. At $\theta_r = 0^\circ$ and on into the backscattered ($\phi_r = 180^\circ$) direction, the calculated values lie above the measured values and this, too, is believed to be the result of the lack of a shadowing and obscuration correction.
- (2) In the cross-polarization component ($\perp\parallel$), the model predicts a flat response except for a slight hump under the specular peak. The measured data, however, show a clear angular dependence on θ_r .

*Note: On all reprints of original computer plots, the symbols θ_r and ϕ_r are represented by Θ_R and Φ_R respectively.

A02018 001

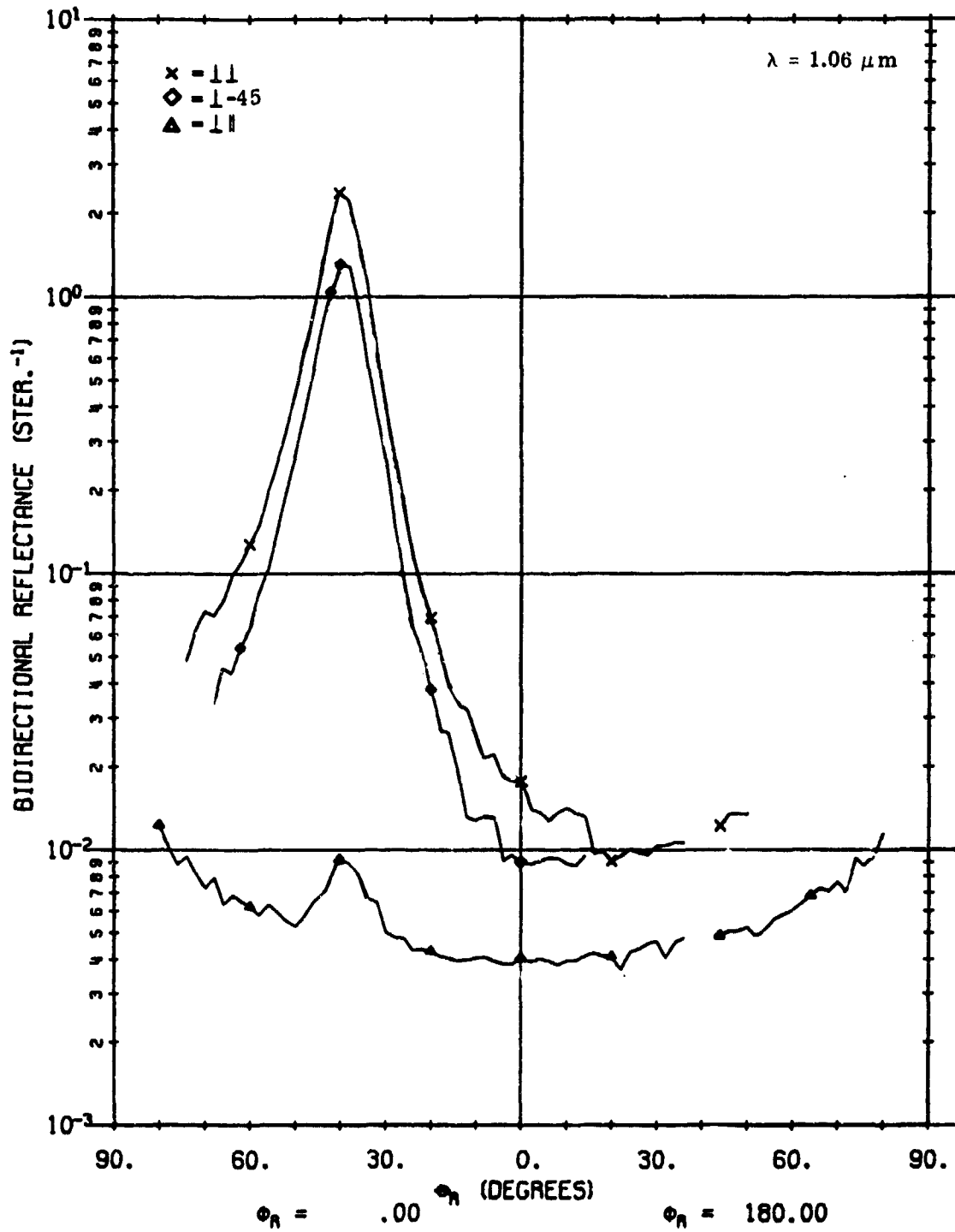


FIGURE 5. MEASURED ρ' FOR A02018-001. $\theta_i = 40^\circ$, $\phi_r = 0, 180^\circ$.

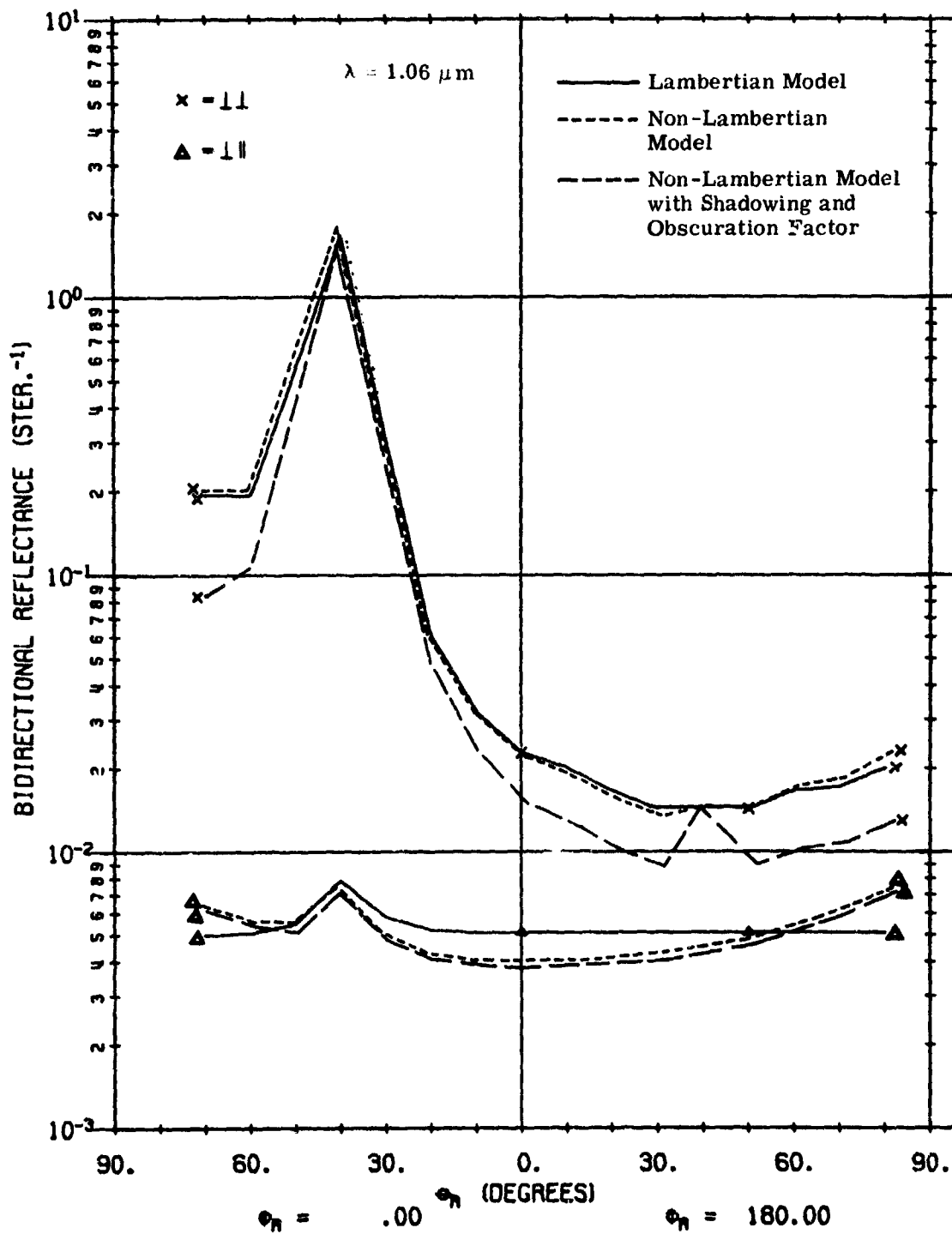


FIGURE 6. CALCULATED ρ' FOR A02018-001 USING LAMBERTIAN VOLUME MODEL AND NON-LAMBERTIAN MODEL WITH AND WITHOUT SHADOWING AND OBSCURATION FACTOR.

$\theta_i = 40^\circ, \phi_r = 0^\circ, 180^\circ.$

With the exception of these two characteristics, however, the surface plus Lambertian volume model with no shadowing and obscuration correction fits the measured data fairly well.

Non-Lambertian Volume Model with No Shadowing and Obscuration Correction. The dotted lines in Fig. 6 show a model plot using the same parameters, except that the non-Lambertian volume model is now used. Keep in mind that one may use the non-Lambertian volume scattering as a model by itself or in conjunction with a specular component. The latter is used here. In the like-polarized component, nothing has changed from the previous case. However, the cross-polarized component now fits the measured data much more closely. It rises steadily at large angles, both in the back-scattered and forward-scattered directions—a result of $1/(\cos \theta_i + \cos \theta_r)$ dependence shown in Eq. (28) for the volume model. However, the response for the like-polarized component does not drop sharply enough at either side of the peak, and at high angles in the forward-scattered direction, the awkward divergence still appears at 60° .

Thus, the non-Lambertian volume model improves the cross-polarized fit (with respect to material A02018-001) over that of the Lambertian volume model and, apart from anomalies at high angles and near 0° , provides a reasonable fit to the measurements.

Non-Lambertian Volume Model with Shadowing and Obscuration Correction. The dashed-line curves in Fig. 6 show results with the shadowing and obscuration correction applied to the non-Lambertian volume model calculation. The cross-polarized component is unaffected. The net effect on the match-polarized component is to reduce the reflectance everywhere except at the specular peak and at the direct backscattering peak (i.e., at $\beta = 0$). In particular, it lowers the forward-scatter contributions beyond 50° , bringing the model closer to measured data in this region. Overall, the fit obtained using the volume model with a shadowing and obscuration correction agrees closely with measurements.

The foregoing discussion applies to "in plane" receiver scans—those in the $\phi_r = 0$ and $\phi_r = 180^\circ$ azimuth planes. The azimuth plane perpendicular to the $0^\circ, 180^\circ$ plane is the $90^\circ, 270^\circ$ plane and is referred to as "out-of-plane". The plane we are in or out of is the plane of incident beam and target normal, or the target incidence plane. (See Fig. 1.)

In Fig. 7 we have the plot of measured data for the out-of-plane situation with perpendicular-polarized source again. In this case, however, the incidence plane is perpendicular to the reflection plane. At $\theta_i = 0$, therefore, $\rho'_{\perp\perp}$ in plane is the same as $\rho'_{\perp\parallel}$ out of plane. For this reason, the reflectances of match-polarized and cross-polarized components seem to exchange behaviors in the out-of-plane configuration, as is verified by the plotted measurements as well as by the model calculations. Figure 8 presents plots of a Lambertian model without the shadowing and obscuration factor, a surface plus non-Lambertian volume model without the shadowing and obscuration factor, and the surface plus non-Lambertian volume model with the shadowing and obscuration factor. As before, it is apparent that the use of the non-Lambertian volume model plus the shadowing and obscuration factor improves agreement between model and measurements so that, apart from a possible overall scale factor, the agreement is within measurement fluctuation.

A02018 001

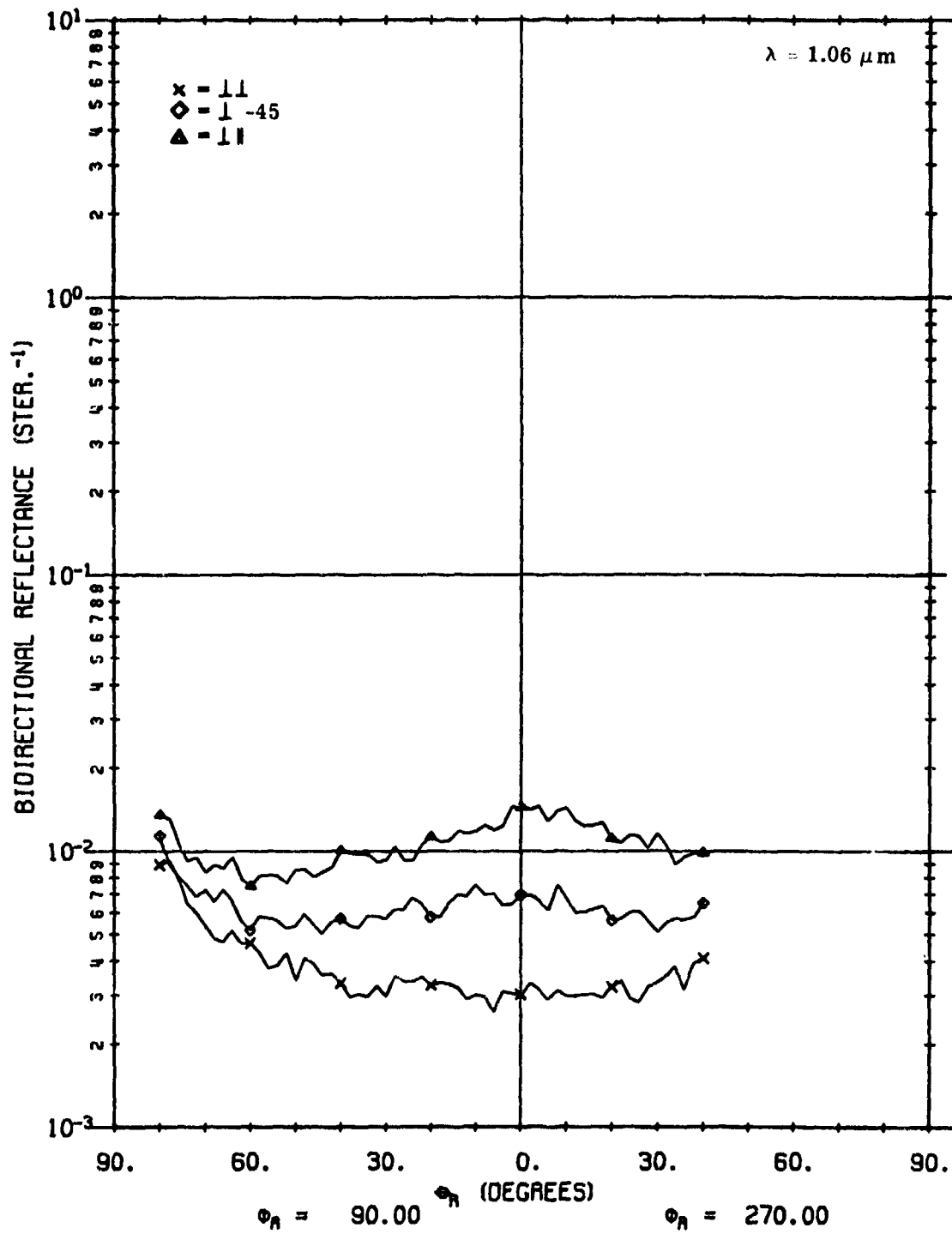


FIGURE 7. MEASURED ρ' FOR A02018-001. $\theta_i = 40^\circ$, $\phi_i = 180^\circ$, $\phi_r = 90^\circ, 270^\circ$.

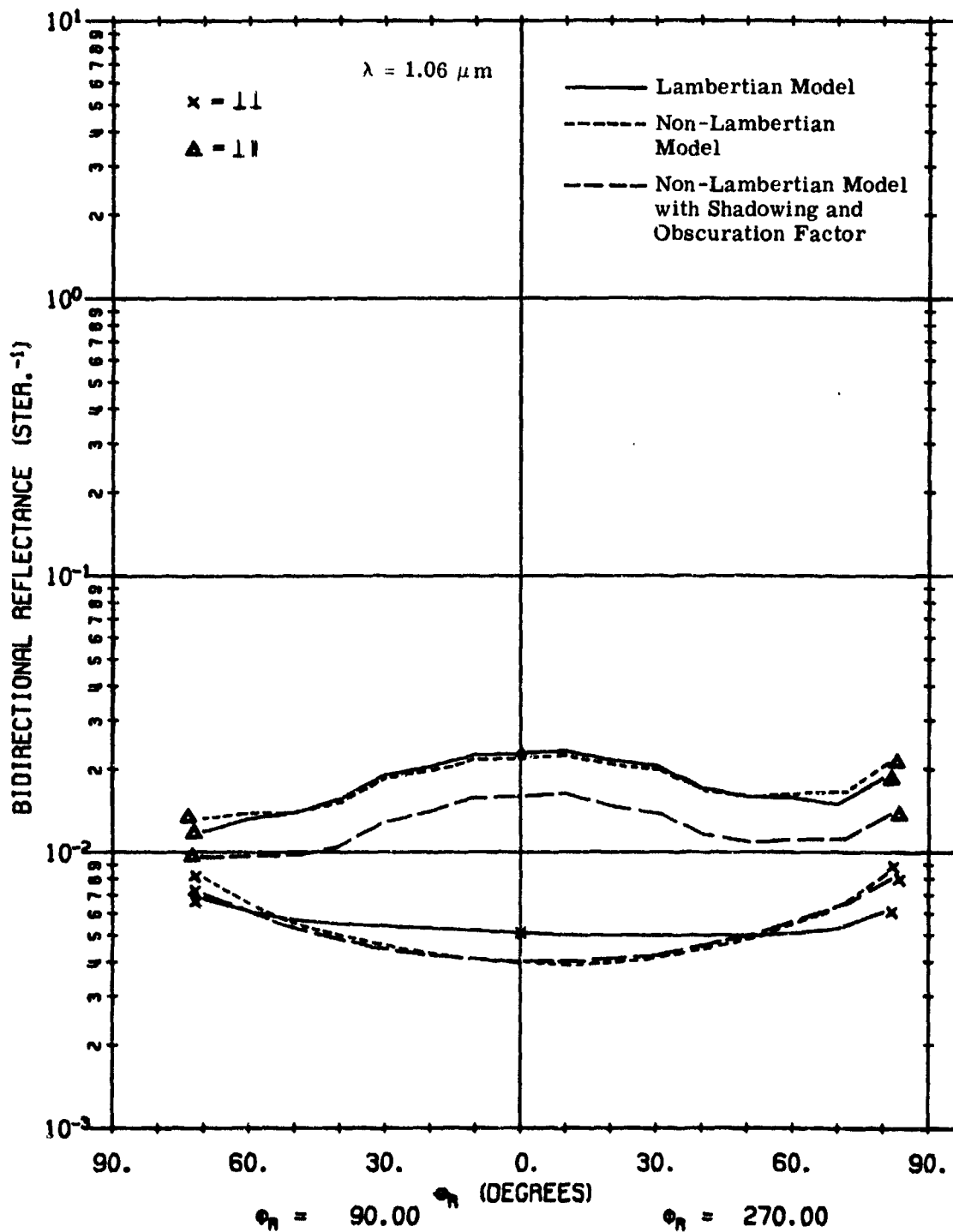


FIGURE 8. CALCULATED ρ' FOR A02018-001 USING LAMBERTIAN VOLUME MODEL AND NON-LAMBERTIAN VOLUME MODEL WITH AND WITHOUT SHADOWING AND OBSCURATION FACTOR. $\theta_i = 40^\circ$, $\phi_i = 180^\circ$; $\phi_r = 90^\circ, 270^\circ$.

For additional validation, plots are shown for the 30° , 210° azimuth planes (Figs. 9 and 10) and for the 60° , 240° azimuth planes (Figs. 11 and 12). The characteristics of calculated and measured curves, apart from a scale factor, are in excellent agreement. Figures 13 through 20 represent similar comparisons for the case when the source polarizer is set for -45° (in the 0° , 180° azimuth plane) and set parallel (in the 30° , 210° ; 60° , 240° ; and 90° , 270° planes). Measured plots are presented with the calculated plot to represent the surface plus non-Lambertian volume model and to include the shadowing and obscuration factor.

6.2. REFLECTANCE FOR SAMPLE MATERIAL A02018-002

Material A02018-002 consists of a tan painted surface.

Based on the zero bistatic scan, Fig. 21, material A02018-002 appears to be somewhat brighter than material A02018-001. Whereas the non-Lambertian volume model was clearly the best choice for material A02018-001, it is not in the case of A02018-002. In this latter case, the best choice is the Lambertian model.

The lack of angular dependence in the reflectance of the cross-polarized component could have a number of explanations. Multiple scattering increases for rougher surfaces. Since such scattering may not be angular dependent, it could become a large enough factor to swamp the angular dependence which is otherwise present. Moreover, the difference in color between the green and tan certainly alters the absorption and, consequently, can alter the angular dependence as well.

In any case, the appropriate model to use can be determined by looking at the cross-polarized component of the fixed bistatic scan. If a clear angular dependence is present, the non-Lambertian model should be used. But if there is little or no apparent angular dependence, as with material A02018-002, then the Lambertian model is more appropriate.

In Figs. 22 through 29, plots are provided for different azimuth planes, beginning with the plot for measured data, followed immediately by the corresponding plot from model calculations. In this group of illustrations, Figs. 22 through 25 represent perpendicular source polarization, while Figs. 26 through 29 represent a source parallel polarization for the 0° , 180° azimuth plane and for the 90° , 270° azimuth plane.

In all cases the fit appears to be excellent, except for occasional anomalies at large azimuth angles. Further modification of the shadowing and obscuration factor should decrease these present anomalies.

6.3. POLARIZATION ANGLE (ψ_p) FOR SAMPLE MATERIAL A02018-001

The reflectances of the perpendicular and parallel components of a linearly polarized beam vary as functions of the source-receiver angles and the index of refraction of the target material. (See, for example, the Fresnel equations, Ref. 3.) Based on observations, the index of refraction varies little over a wide range of paint surfaces. For the particular materials

A02018 001

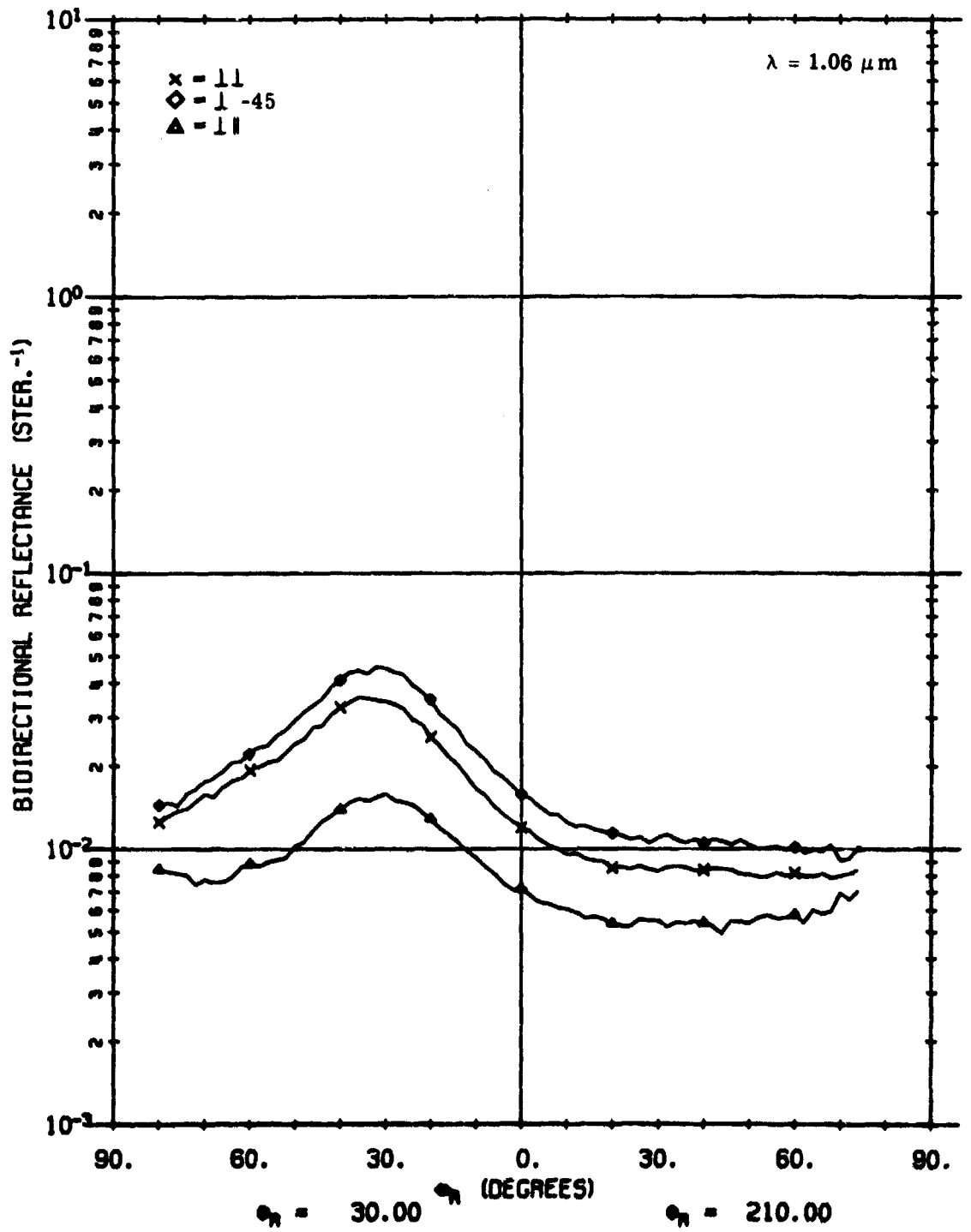


FIGURE 9. MEASURED ρ' FOR A02018-001. $\theta_i = 40^\circ$, $\phi_i = 180^\circ$, $\phi_r = 30^\circ, 210^\circ$.

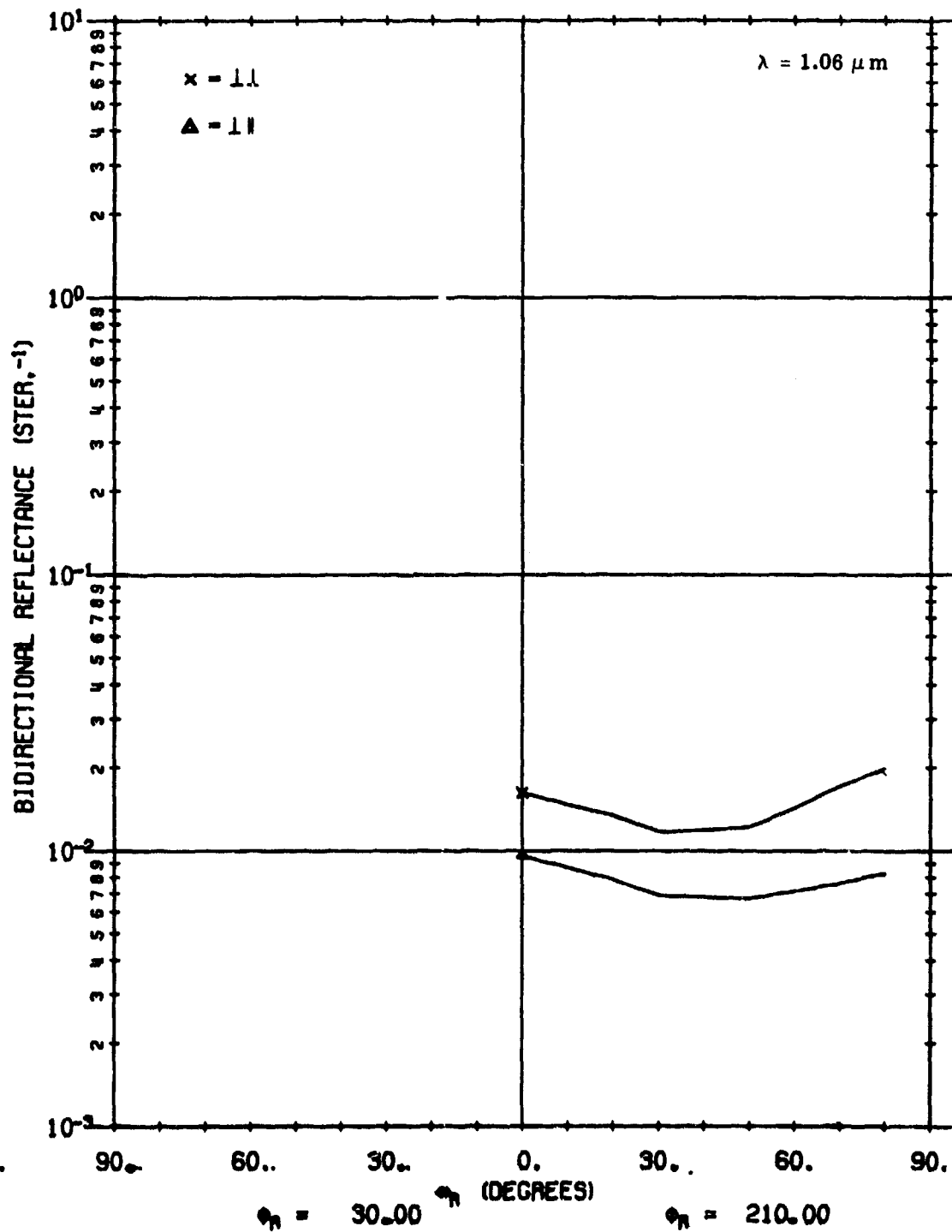


FIGURE 10. CALCULATED ρ' FOR A02018-001 USING NON-LAMBERTIAN VOLUME MODEL WITH SHADOWING AND OBSCURATION FACTOR. $\theta_i = 40^\circ$, $\phi_i = 180^\circ$, $\phi_r = 30^\circ, 210^\circ$.

A02018 001

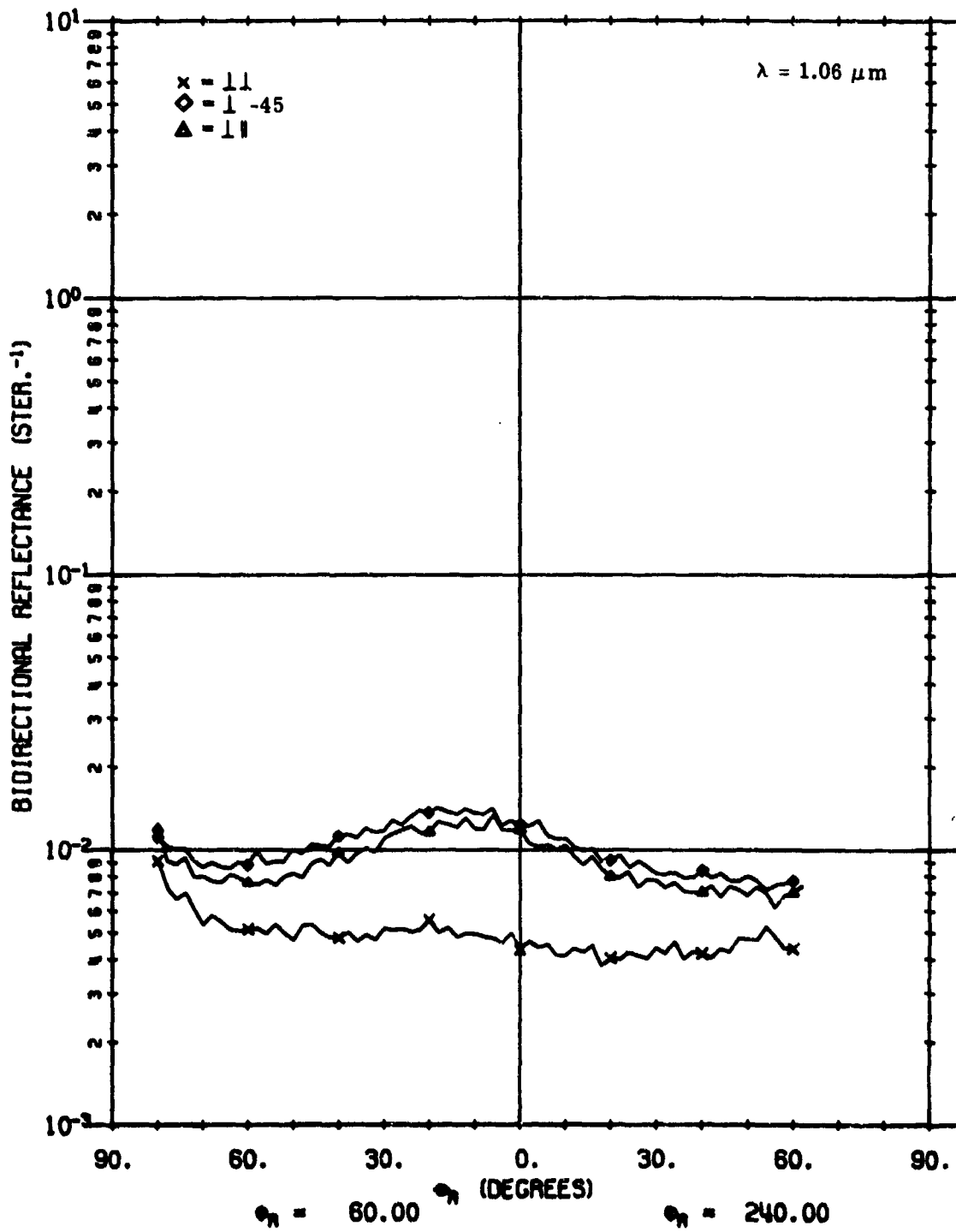


FIGURE 11. MEASURED ρ' FOR A02018-001. $\theta_i = 40^\circ$, $\phi_i = 180^\circ$, $\phi_r = 60^\circ, 240^\circ$.

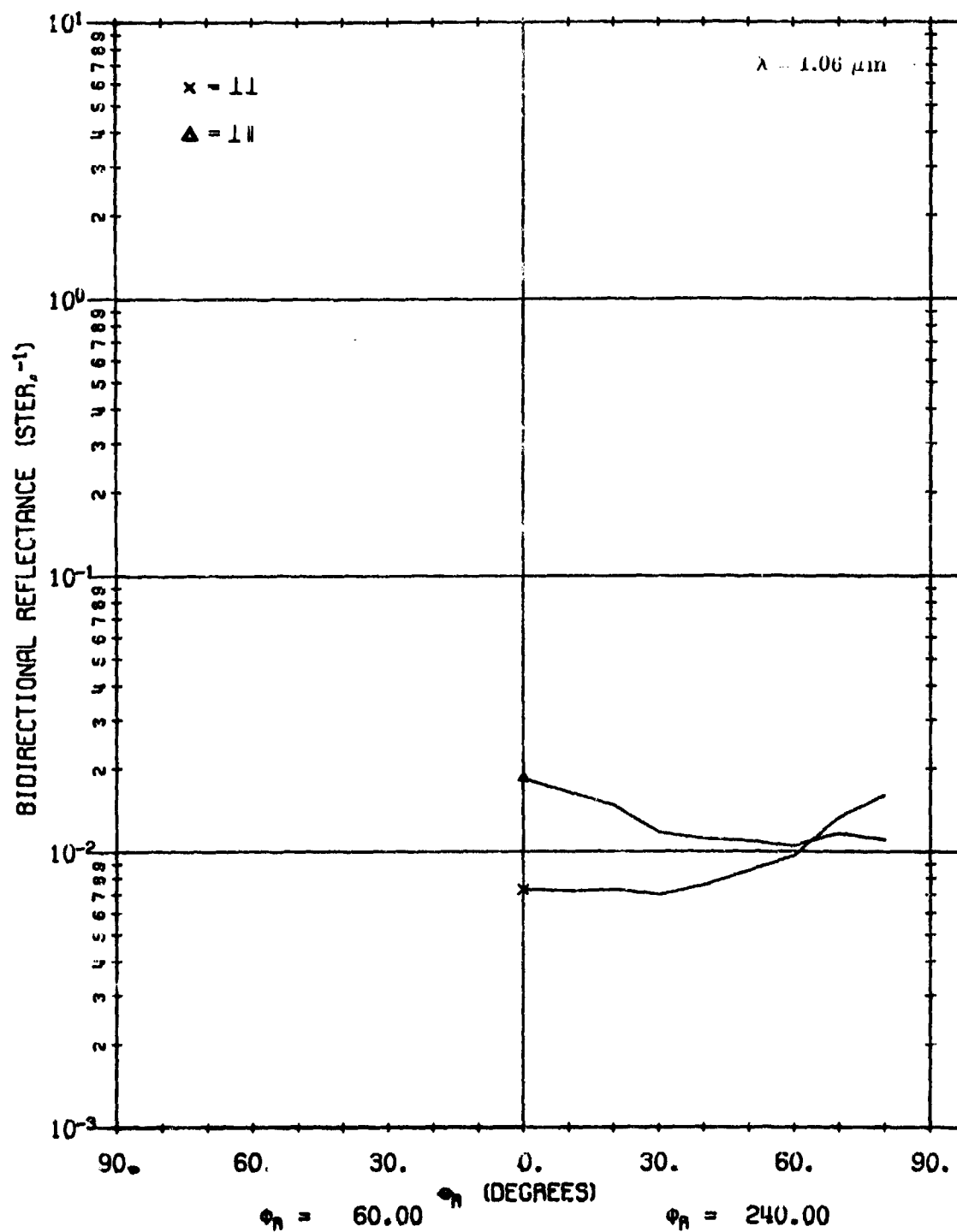


FIGURE 12. CALCULATED ρ' FOR A02018-001 USING NON-LAMBERTIAN VOLUME MODEL WITH SHADOWING AND OBSCURATION FACTOR. $\theta_i = 40^\circ$, $\phi_i = 180^\circ$, $\phi_r = 60^\circ, 240^\circ$.

A02018 001

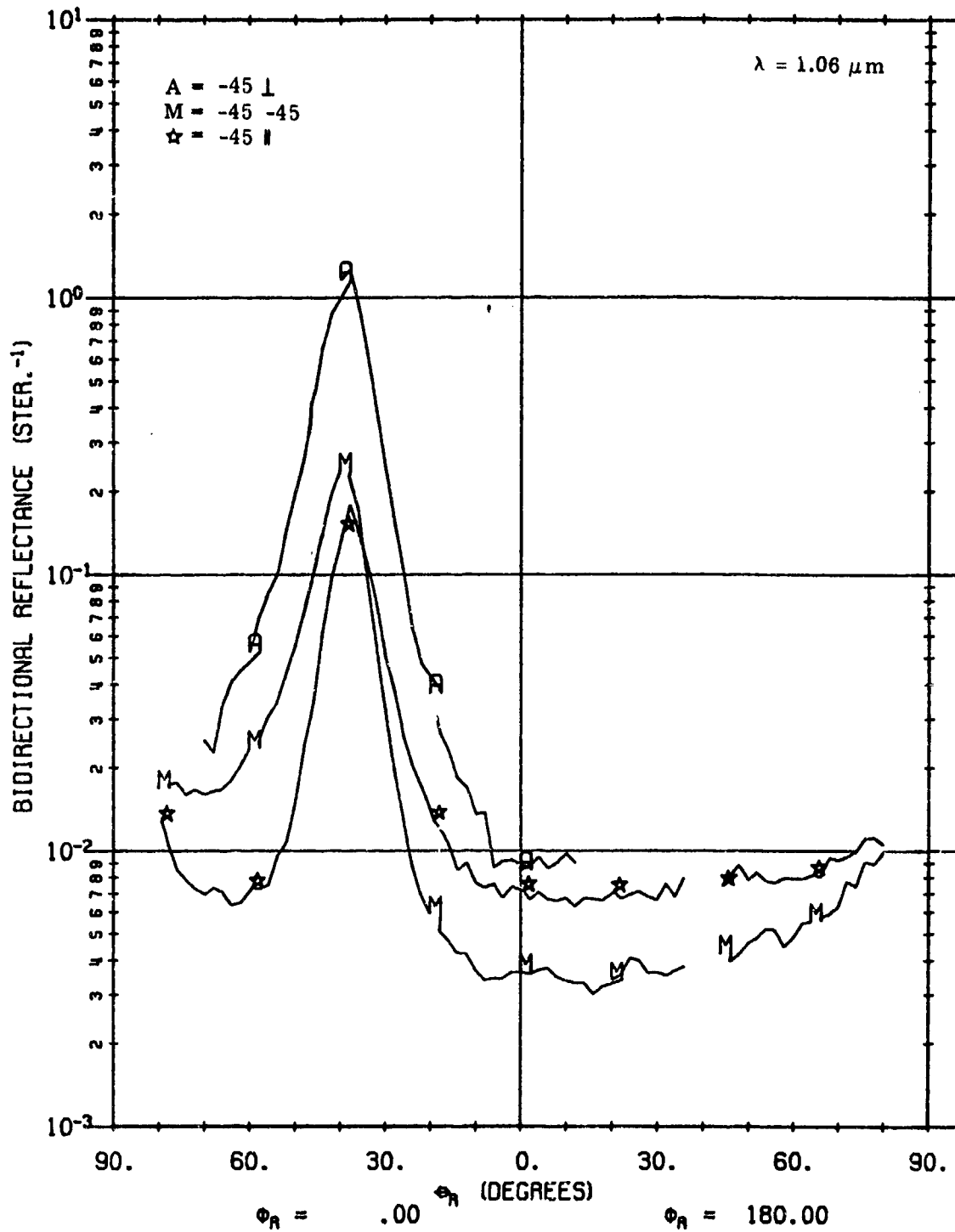


FIGURE 13. MEASURED ρ' FOR A02018-001. $\theta_i = 40^\circ$, $\phi_i = 180^\circ$, $\phi_r = 0^\circ, 180^\circ$.

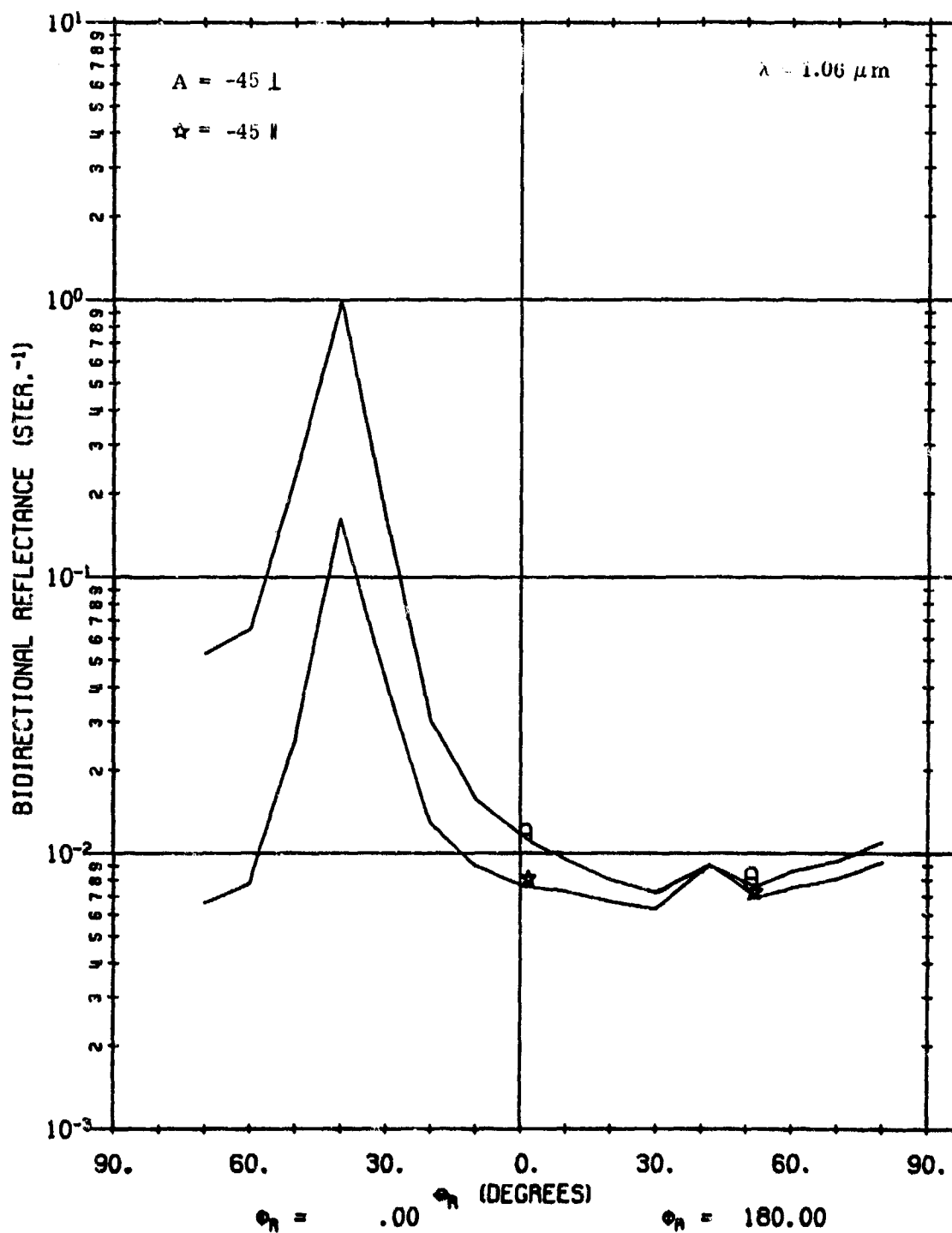


FIGURE 14. CALCULATED ρ' FOR A02018-001 USING NON-LAMBERTIAN VOLUME MODEL WITH SHADOWING AND OBSCURATION FACTOR. $\theta_i = 40^\circ$, $\phi_i = 180^\circ$, $\phi_r = 0^\circ, 180^\circ$.

A02018 001

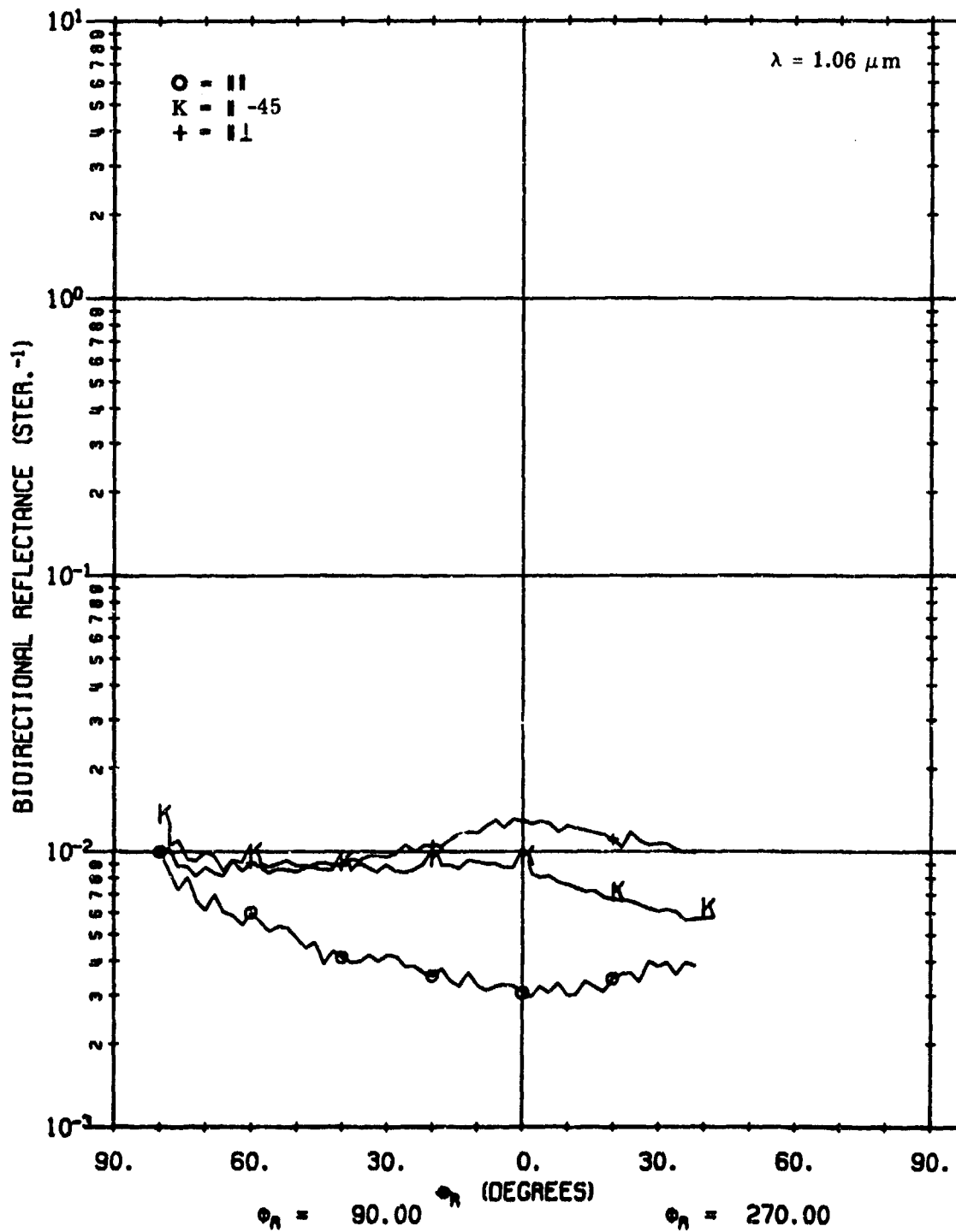


FIGURE 15. MEASURED ρ' FOR A02018-001. $\theta_i = 40^\circ$, $\phi_i = 180^\circ$, $\phi_r = 90^\circ, 270^\circ$.

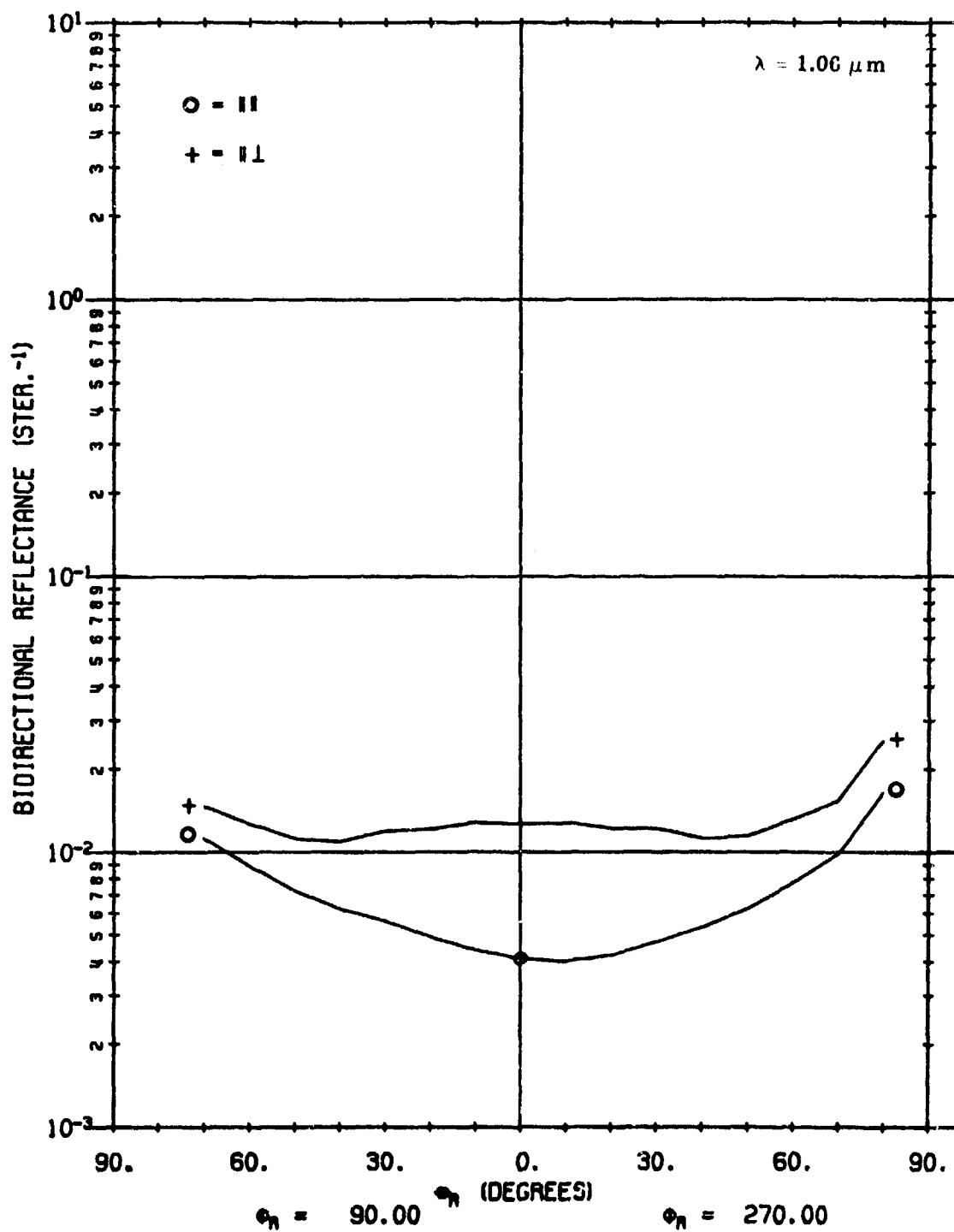


FIGURE 16. CALCULATED ρ' FOR A02018-001 USING NON-LAMBERTIAN VOLUME MODEL WITH SHADOWING AND OBSCURATION FACTOR. $\theta_i = 40^\circ$, $\phi_i = 180^\circ$, $\phi_r = 90^\circ, 270^\circ$.

A02018 001

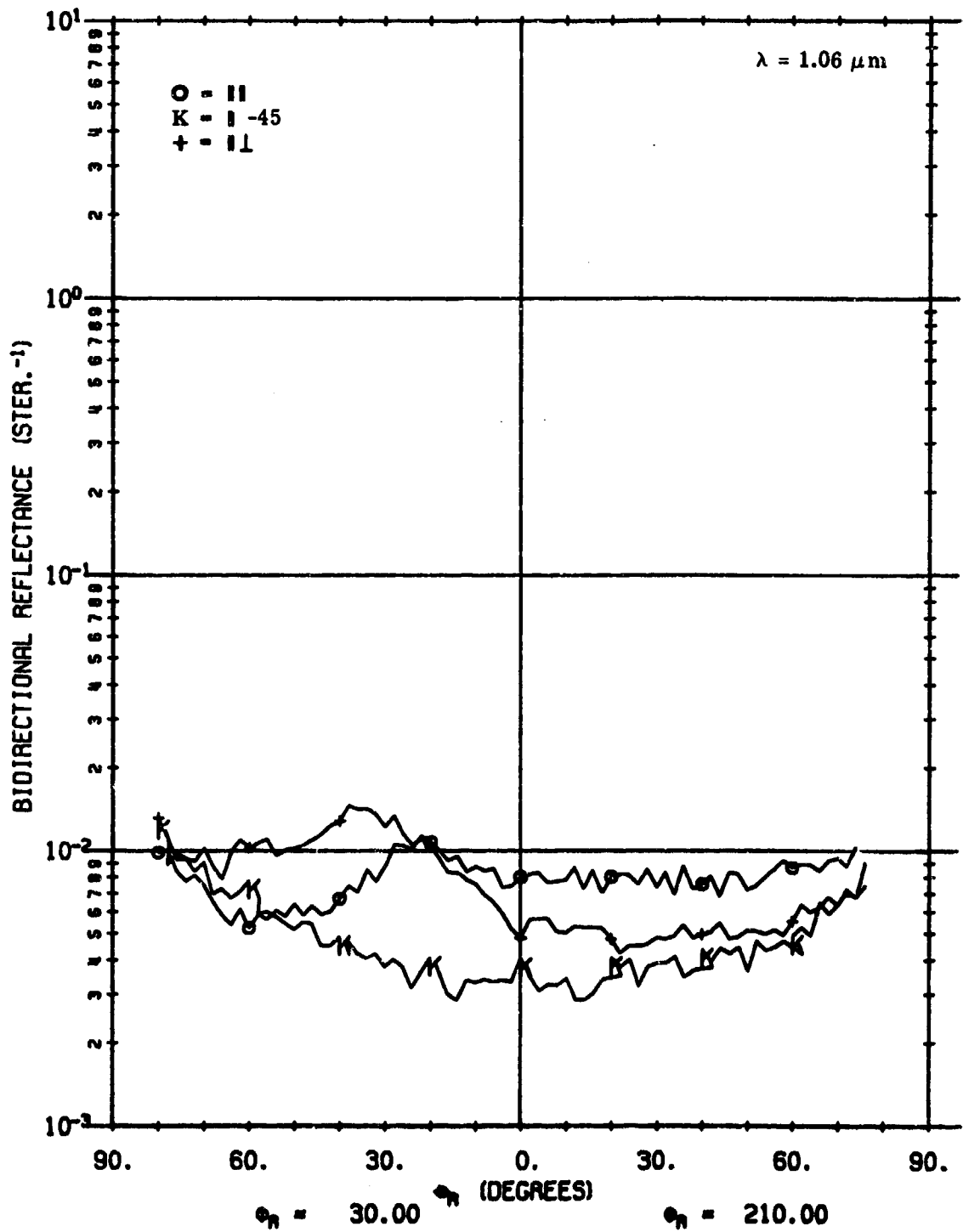


FIGURE 17. MEASURED ρ' FOR A02018-001. $\theta_i = 40^\circ$, $\phi_i = 180^\circ$, $\phi_r = 30, 210^\circ$.

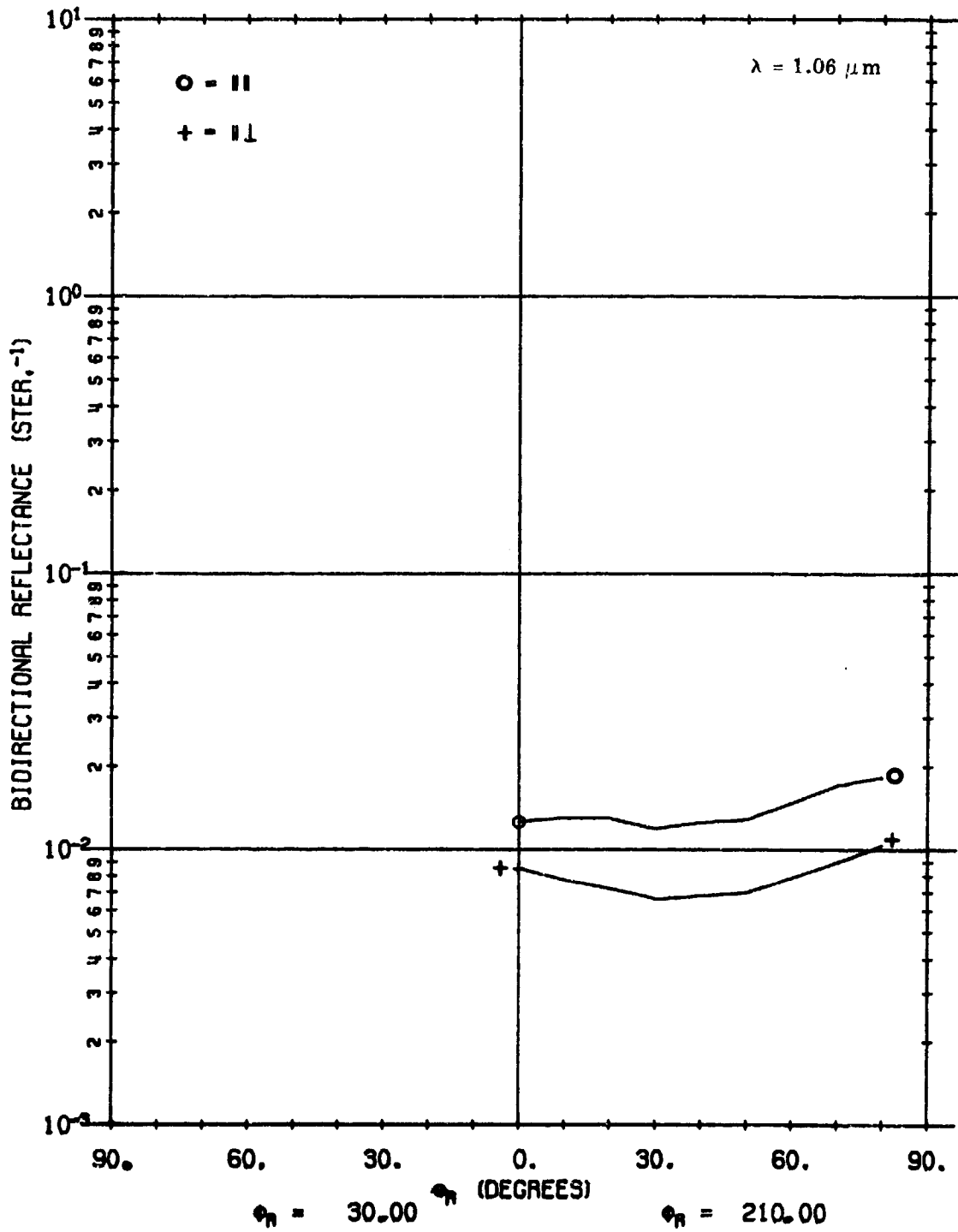


FIGURE 18. CALCULATED ρ' FOR A02018-001 USING NON-LAMBERTIAN VOLUME MODEL WITH SHADOWING AND OBSCURATION FACTOR. $\theta_i = 40^\circ$, $\phi_i = 180^\circ$, $\phi_r = 30^\circ, 210^\circ$.

A02018 001

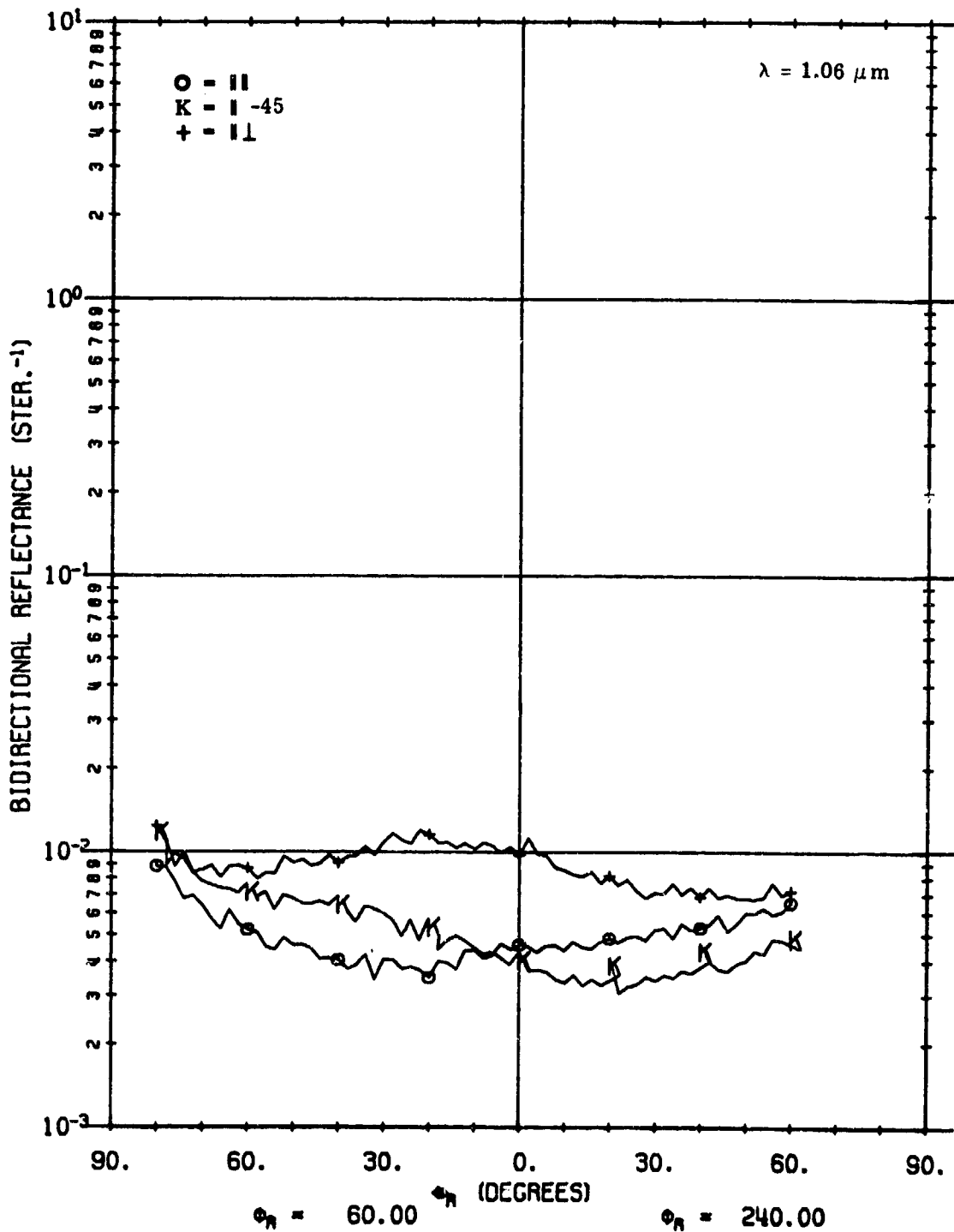


FIGURE 19. MEASURED ρ' FOR A02018-001. $\theta_i = 40^\circ$, $\phi_i = 180^\circ$, $\phi_r = 60^\circ, 240^\circ$.

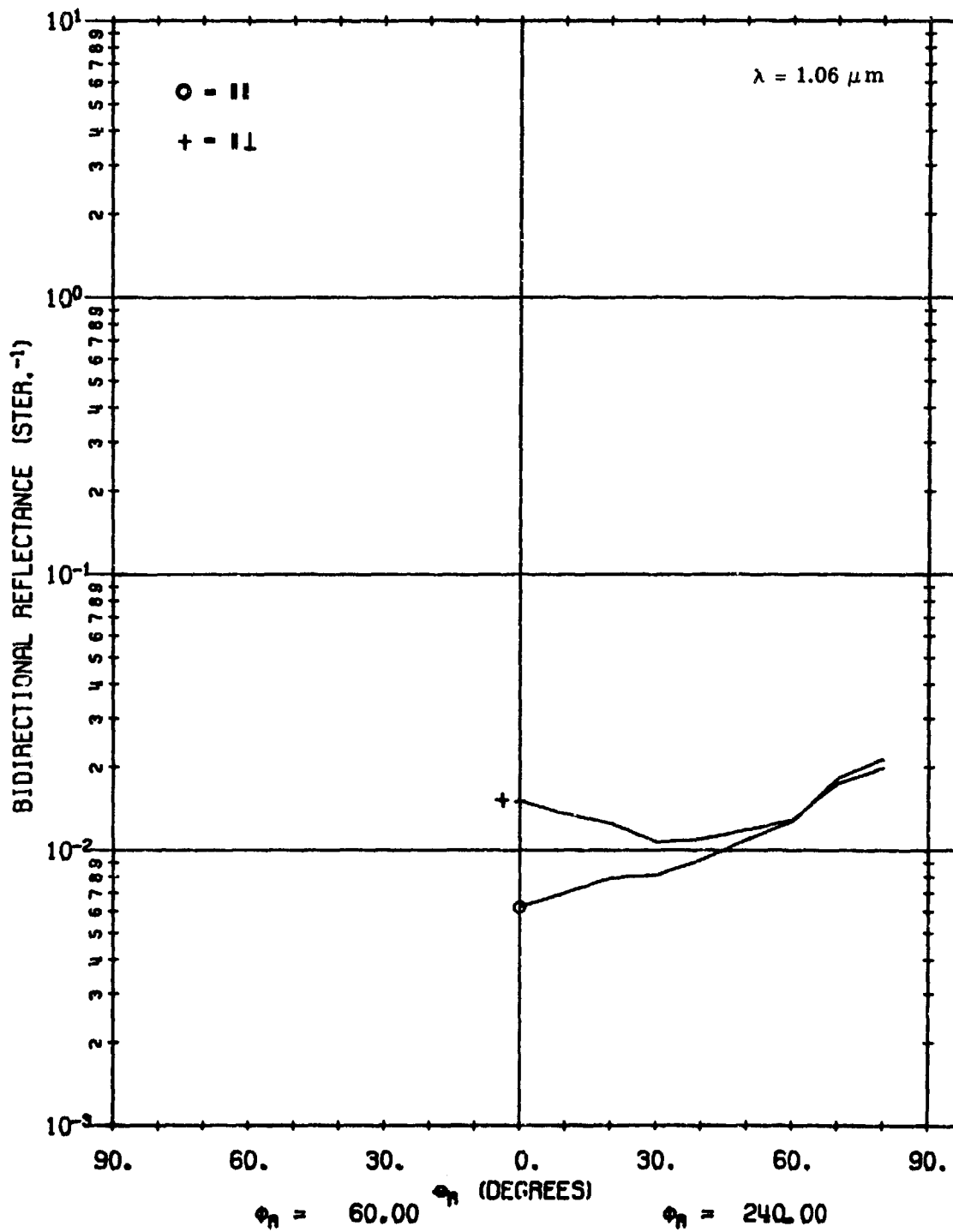


FIGURE 20. CALCULATED ρ' FOR A02018-001 USING NON-LAMBERTIAN VOLUME MODEL WITH SHADOWING AND OBSCURATION FACTOR. $\theta_i = 40^\circ$, $\phi_i = 180^\circ$, $\phi_r = 60^\circ, 240^\circ$.

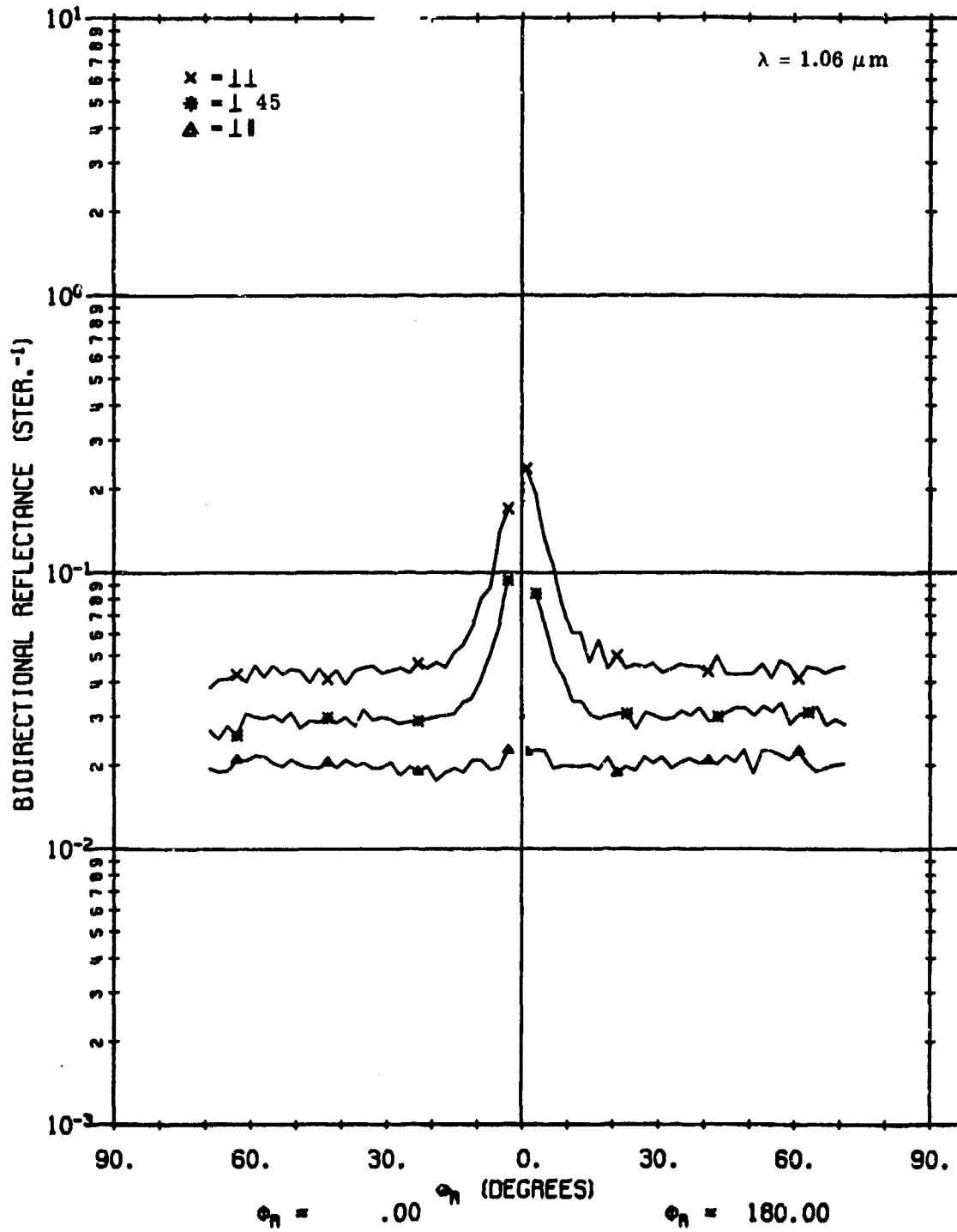


FIGURE 21. FIXED-BISTATIC ρ' FOR A02018-002

A02018 002

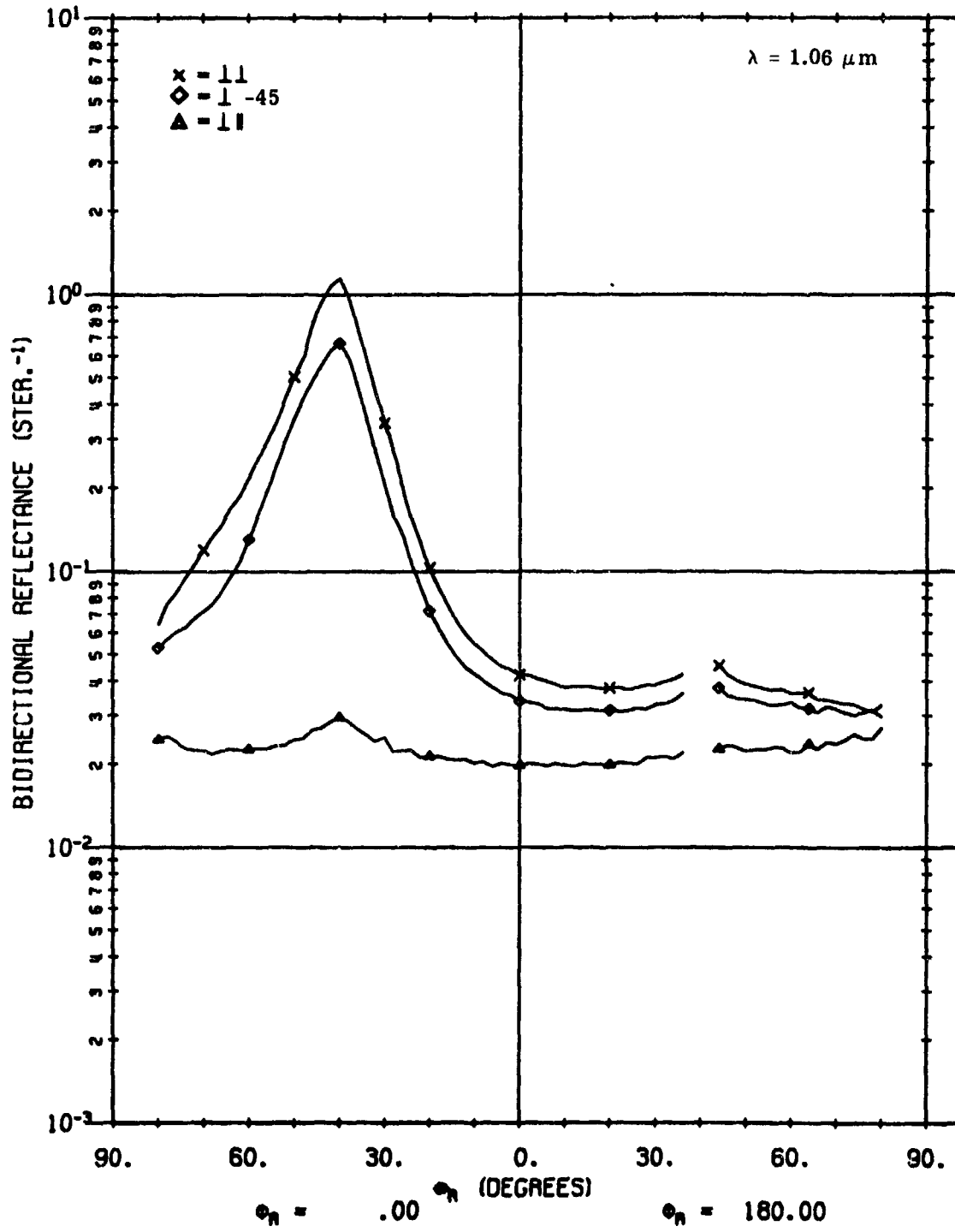


FIGURE 22. MEASURED ρ' FOR A02018-002. $\theta_i = 40^\circ$, $\phi_i = 180^\circ$, $\phi_r = 0^\circ, 180^\circ$.

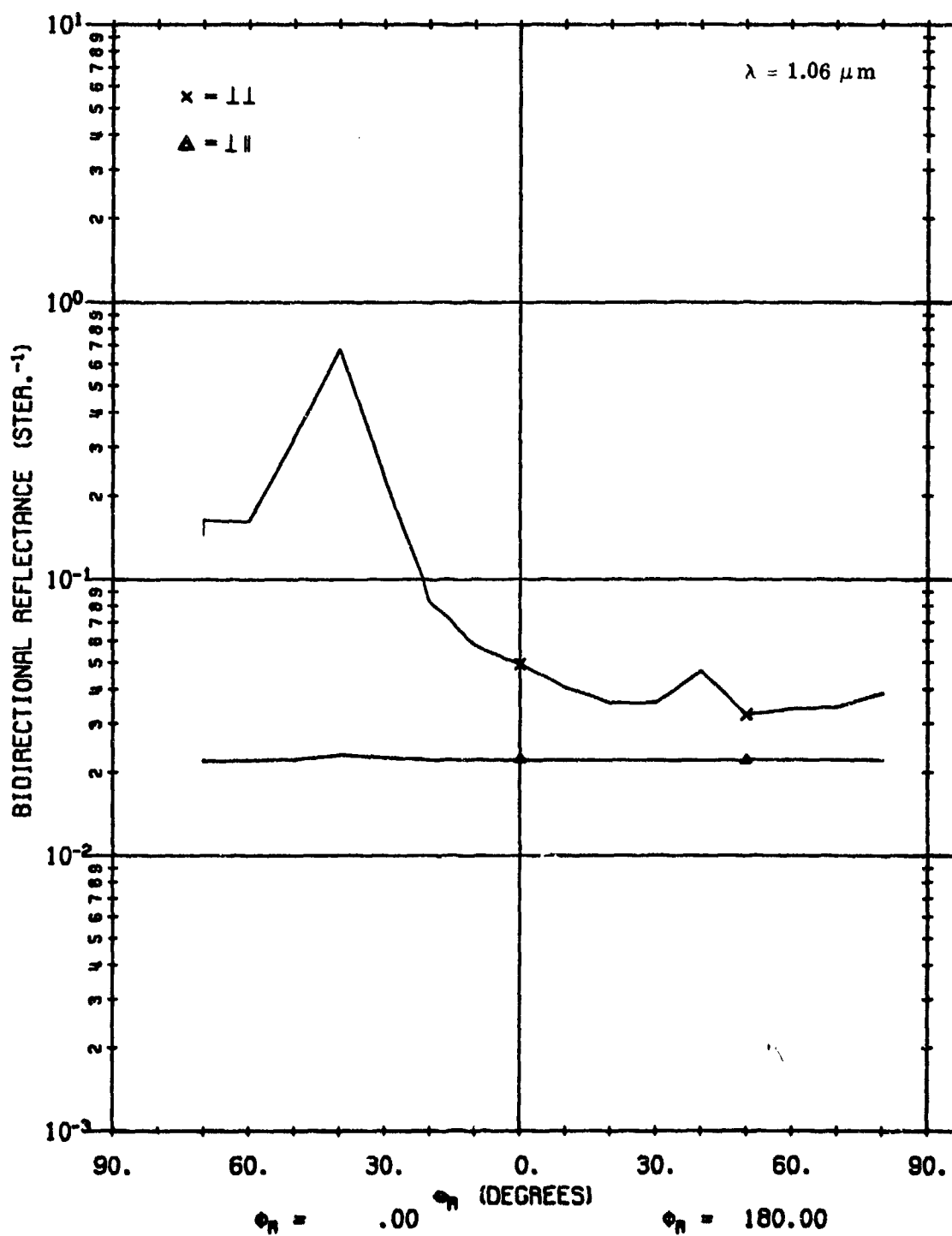


FIGURE 23. CALCULATED ρ' FOR A02018-002 USING LAMBERTIAN VOLUME MODEL.
 $\theta_i = 40^\circ$, $\phi_i = 180^\circ$, $\phi_r = 0^\circ, 180^\circ$.

A02018 002

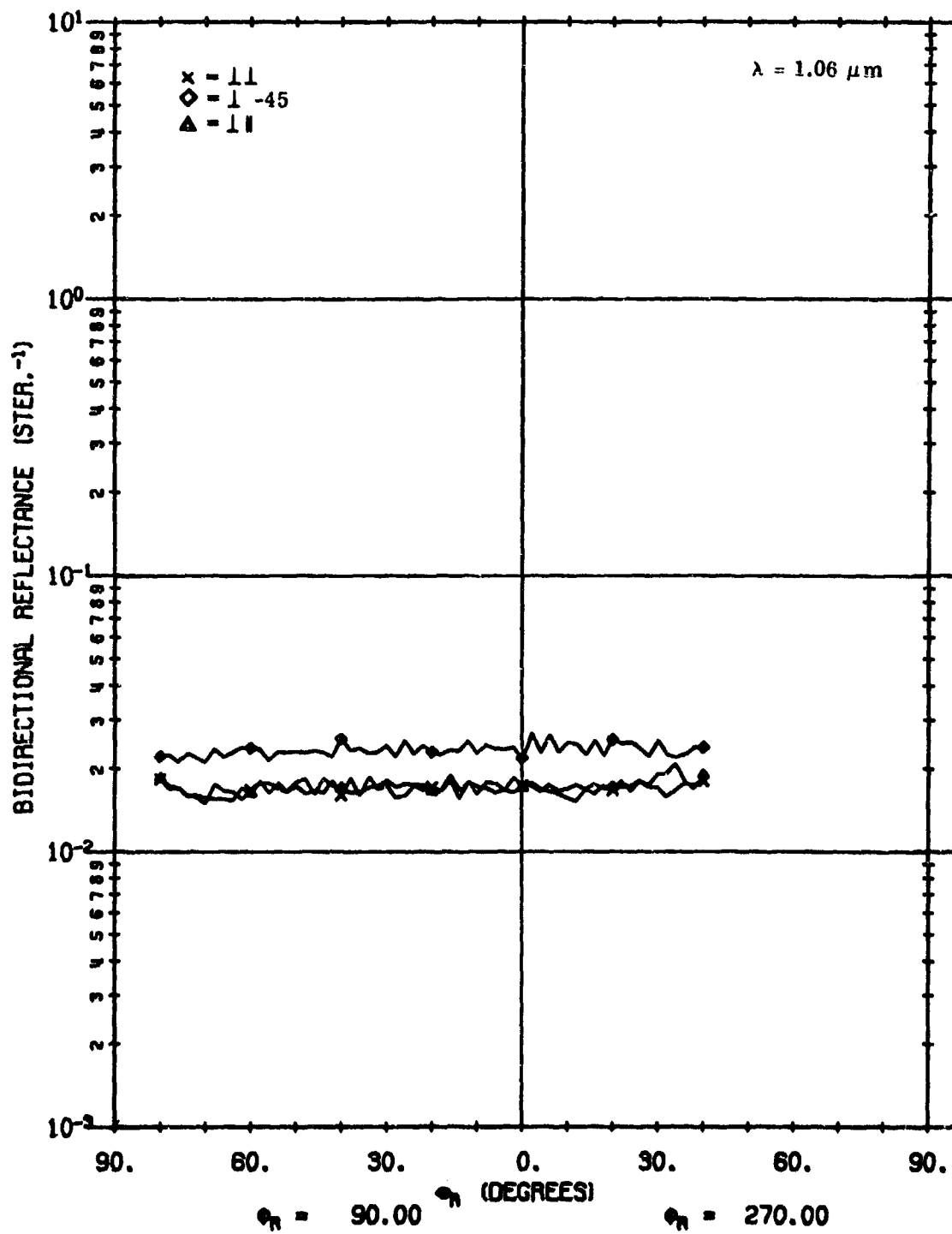


FIGURE 24. MEASURED ρ' FOR A02018-002. $\theta_i = 40^\circ$, $\phi_i = 180^\circ$, $\phi_r = 90^\circ, 270^\circ$.

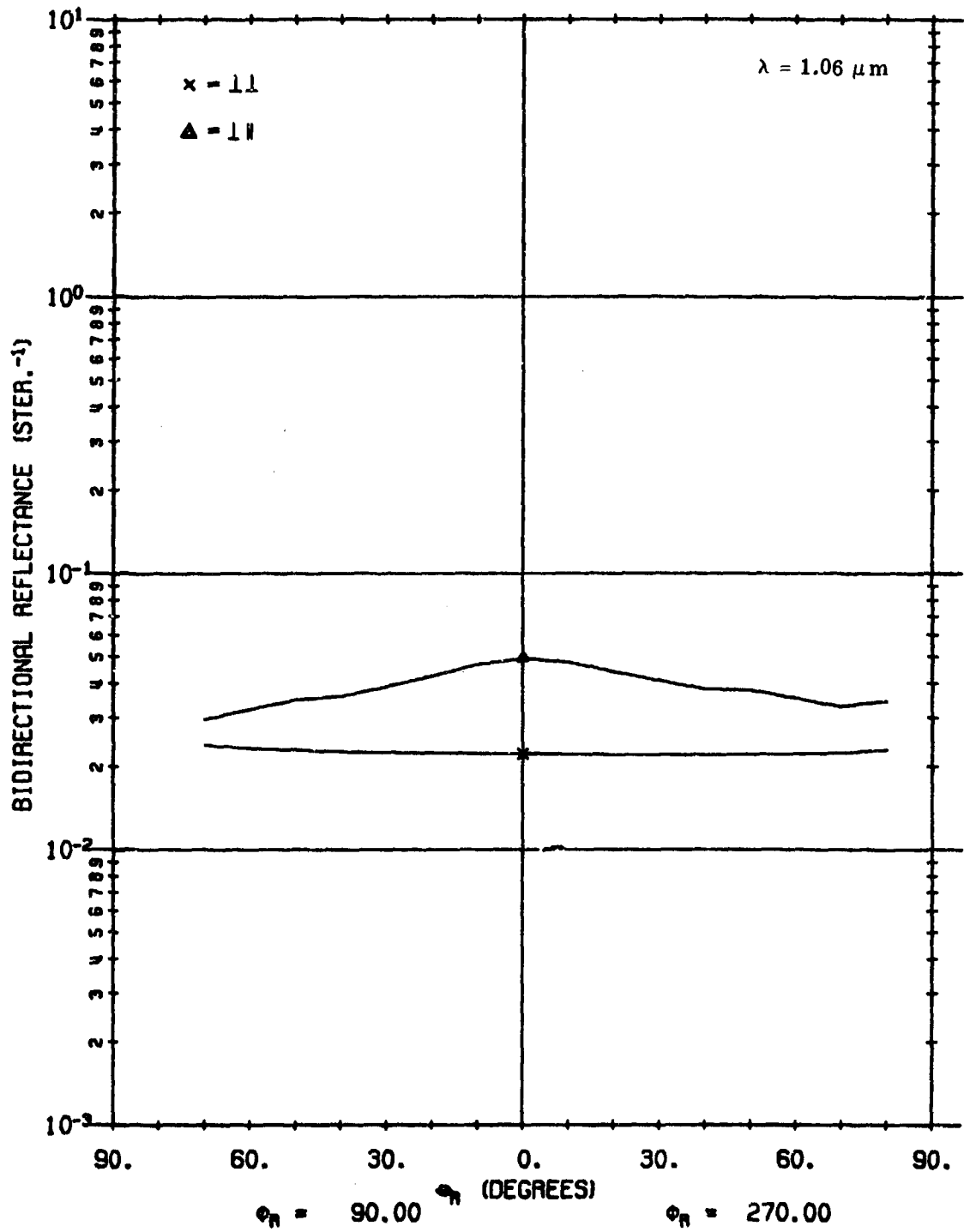


FIGURE 25. CALCULATED ρ' FOR A02018-002 USING LAMBERTIAN VOLUME MODEL.
 $\theta_i = 40^\circ$, $\phi_i = 180^\circ$, $\phi_r = 90^\circ, 270^\circ$.

A02018 002

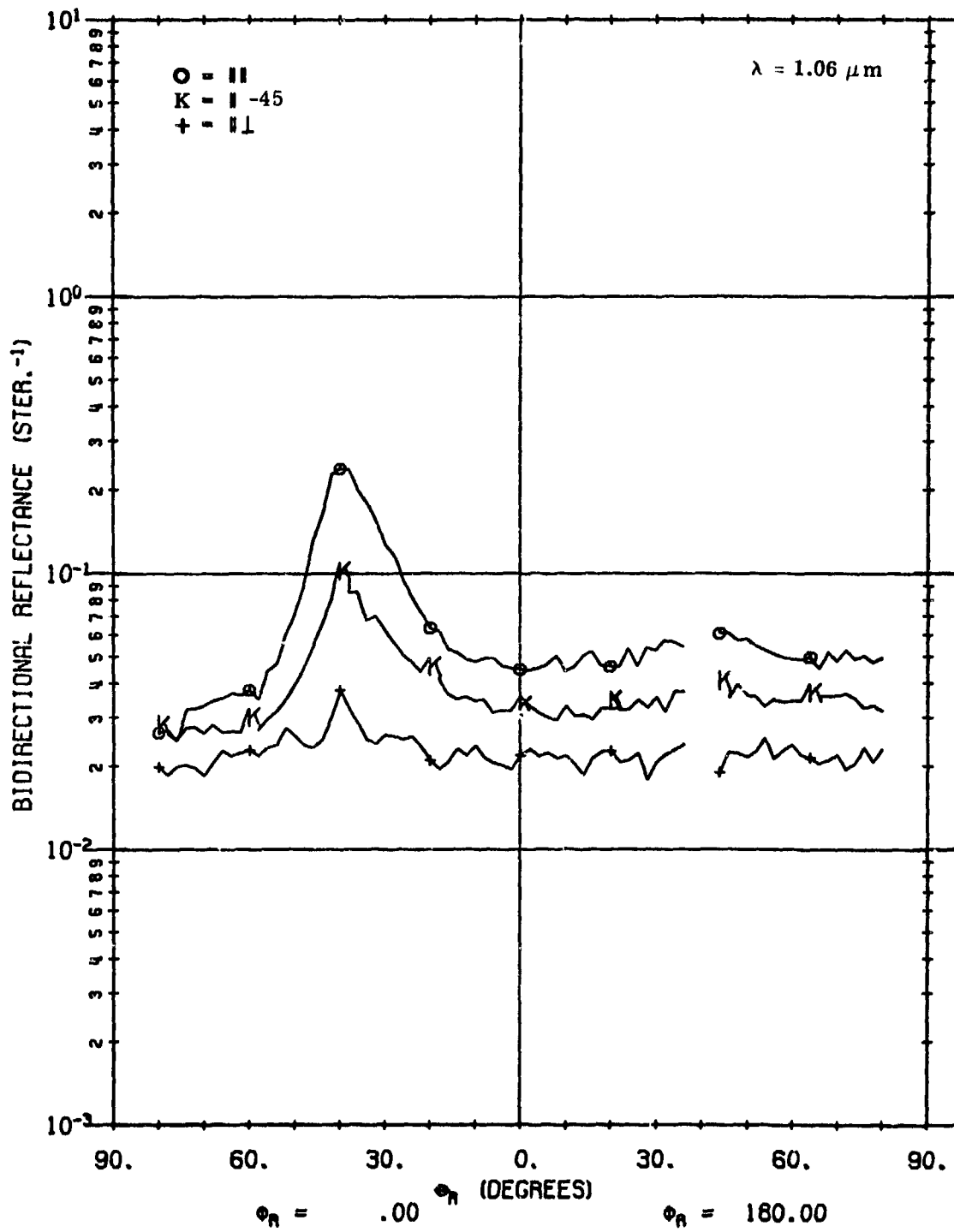


FIGURE 26. MEASURED ρ' FOR A02018-002. $\theta_i = 40^\circ$, $\phi_i = 180^\circ$, $\phi_r = 0^\circ, 180^\circ$.

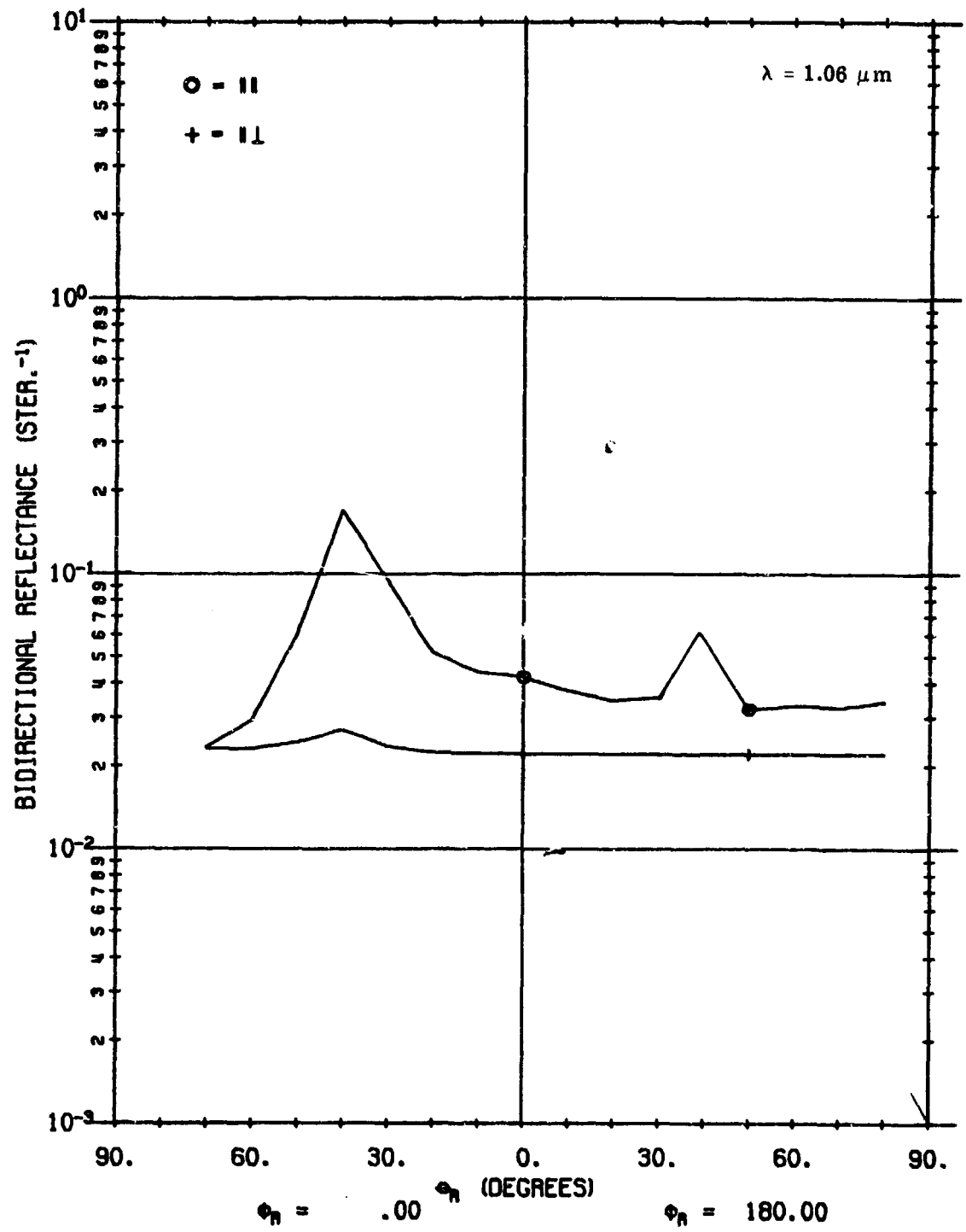


FIGURE 27. CALCULATED ρ' FOR A02018-002. $\theta_i = 40^\circ$, $\phi_i = 180^\circ$, $\phi_r = 0^\circ, 180^\circ$.

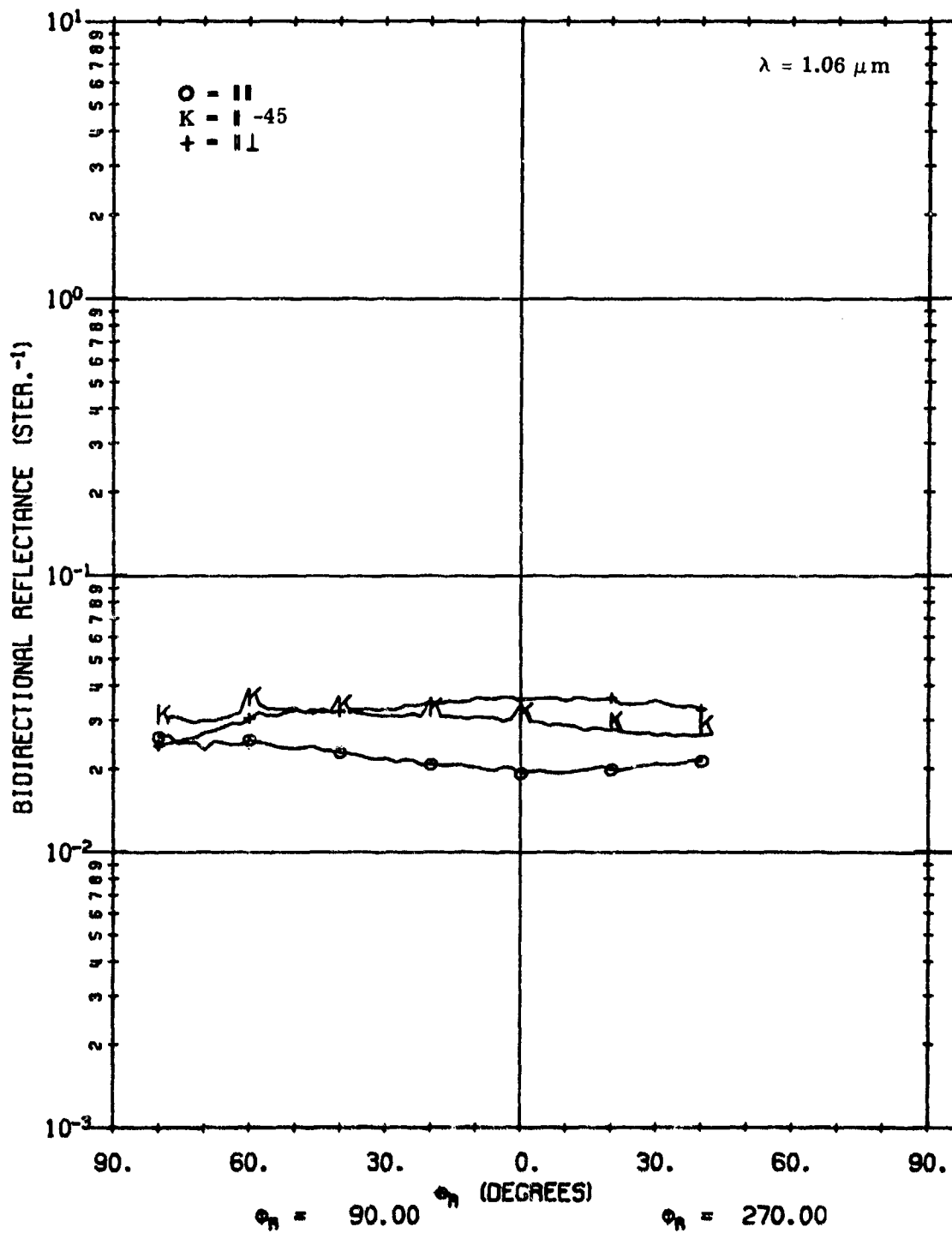


FIGURE 28. MEASURED ρ' FOR A02018-002. $\theta_i = 40^\circ$, $\phi_i = 180^\circ$, $\phi_r = 90^\circ, 270^\circ$.

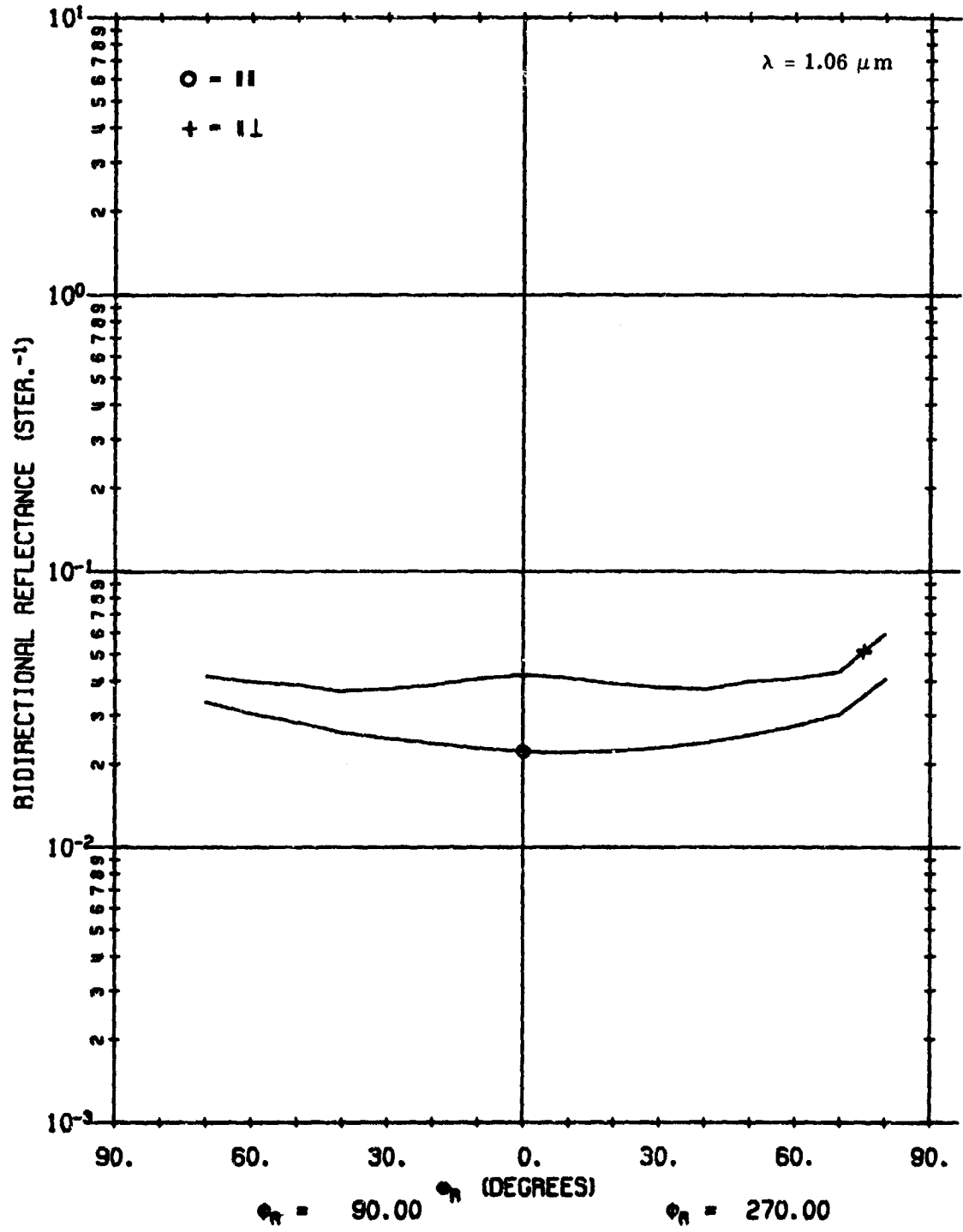


FIGURE 29. CALCULATED ρ' FOR A02018-002 USING LAMBERTIAN VOLUME MODEL.
 $\theta_i = 40^\circ, \phi_i = 180^\circ, \phi_r = 90^\circ, 270^\circ.$

covered in this report, the variation is considered to be zero. Therefore, for these surfaces, polarization angle is essentially a function only of source-receiver positions.

As additional validation for the model, predicted polarization angles are compared with polarization angles extracted from the measured data. Figures 30 through 33 show plots obtained for the 0° , 180° ; 90° , 270° ; 30° , 210° ; and 60° , 240° azimuth planes. Measured data represent material A02018-001. In all cases, agreement between measurements and calculations is excellent, with the average disparity not more than 10%. In particular, the dramatic agreement between measurements and model in the 30° , 210° and 60° , 240° azimuth planes constitutes powerful verification of the model and affirms its usefulness in arbitrary source-receiver positions.

6.4. PERCENT POLARIZATION FOR SAMPLE MATERIALS A02018-001 AND A02018-002

Percent polarization (P) validates the ratio of surface-to-volume contributions to reflectance. Percent polarization depends on both polarized reflectance and angle of polarization, both validated in earlier sections of this report. In this section, we compare model predictions with percent polarization values extracted from measured data.

Figures 34 and 35 illustrate degree of polarization for scans of material A02018-002, for perpendicular and parallel sources, respectively. The validity of the model is supported by the close correlation between the behavior of values extracted from measured data and those calculated with the model.

Additional confirmation of the model is provided in Figs. 36 through 38 where percent polarization plots are given for material A02018-001 in the 0° , 180° and 90° , 270° azimuth angle planes.

6.5. REFLECTANCE FOR SAMPLE MATERIAL A02100

Here the material was a soil specimen. The fixed-bistatic scan (see Fig. 39) indicates a strong angular dependence in both the like-polarized and the cross-polarized components and no specularity. Moreover, the angular dependence in the fixed-bistatic scan looks very much like the $\frac{1}{\cos \theta_i + \cos \theta_r}$ dependence in the non-Lambertian volume model. However, in the θ_r scans with θ_i held fixed, the angular dependence is no longer typical (see Figs. 40, 43, and 46).

Since there is no apparent specularity in the measurement data, the model was run so as to consider only Lambertian or non-Lambertian components, with no specular component. Our validation was done with a perpendicular-polarized source for $\theta_i = 0^\circ$, 20° , and 40° , respectively, and θ_r scanned in-plane. For each θ_i , the measurement graph is given first, followed by the graphs of the non-Lambertian model and the Lambertian model. Note that in selecting ρ_λ value for the Lambertian model, we must take an average of the cross-polarized part of the fixed-bistatic. Therefore, this value is slightly higher than the ρ_V used in the non-Lambertian model. (Section 7 describes how to select parameters.)

For the $\theta_i = 0^\circ$ case, note that the measured data (see Fig. 40) lacks the characteristic angular dependence of the non-Lambertian model (see Fig. 41) — in fact, the graph falls off below the Lambertian graph (see Fig. 42).

For the $\theta_i = 20^\circ$ case, the measured data (see Fig. 43) shows an upturn at higher θ_r values, which is more consistent with the non-Lambertian model. In fact, the non-Lambertian model prediction (see Fig. 44) shows much closer agreement than in the $\theta_i = 0^\circ$ case. The Lambertian calculation (see Fig. 45) once again appears to be taking a rough average. The situation for $\theta_i = 40^\circ$ (see Figs. 46-48) is very similar to that for $\theta_i = 20^\circ$.

Behavior of the fixed-bistatic measurement data indicates that the non-Lambertian component should dominate. However, at small values of θ_i the accuracy is not good. It is not absolutely clear where the difficulty lies. One should note, however, that we took the depolarization to be identically equal to 1. Further modeling to determine the depolarization dependence more accurately may well resolve the problem.

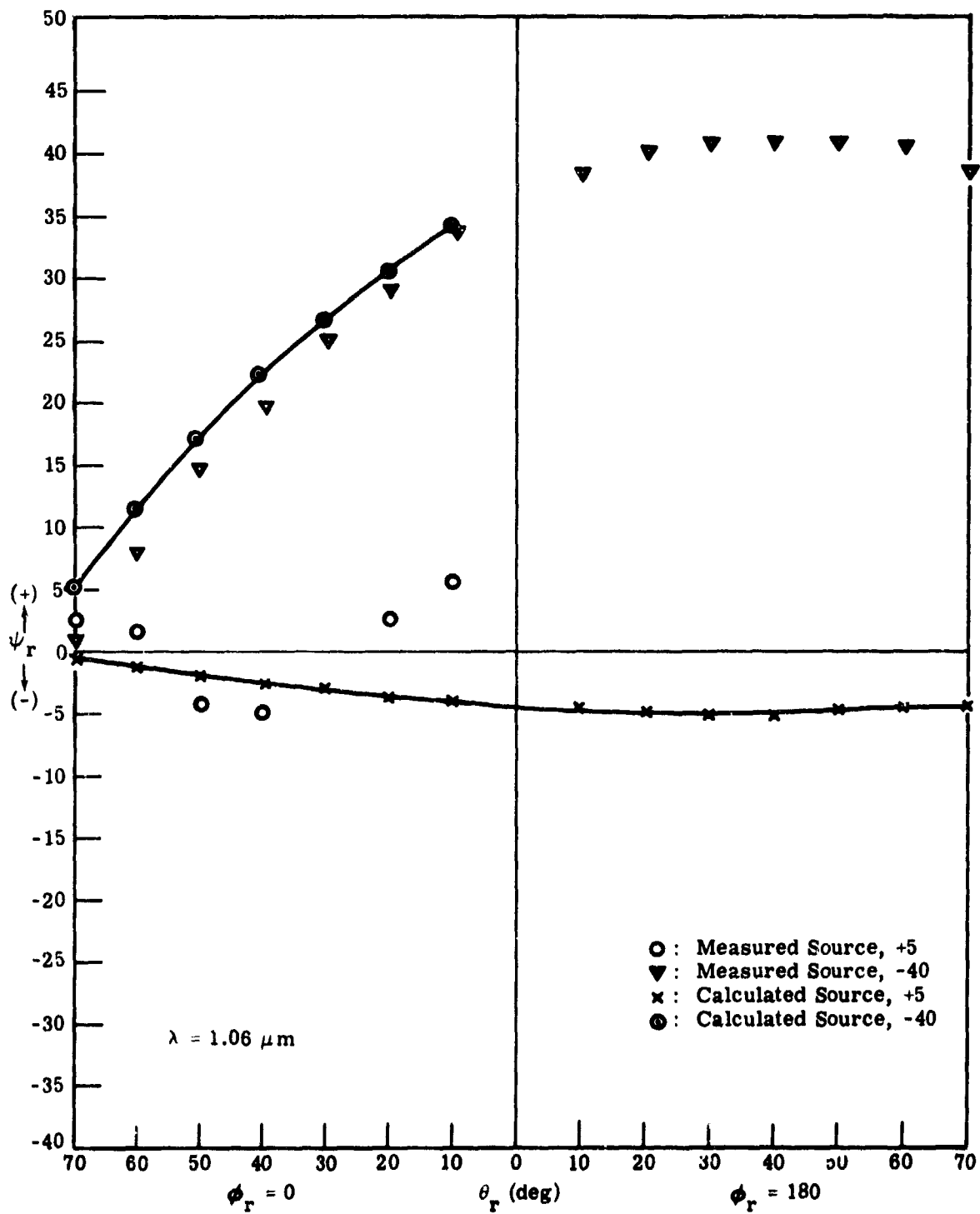


FIGURE 30. VARIATION OF POLARIZATION ANGLE OF REFLECTED RADIANCE AS FUNCTION OF SOURCE-RECEIVER POSITION. $\theta_i = 40^\circ$, $\phi_i = 180^\circ$, $\phi_r = 0^\circ, 180^\circ$.

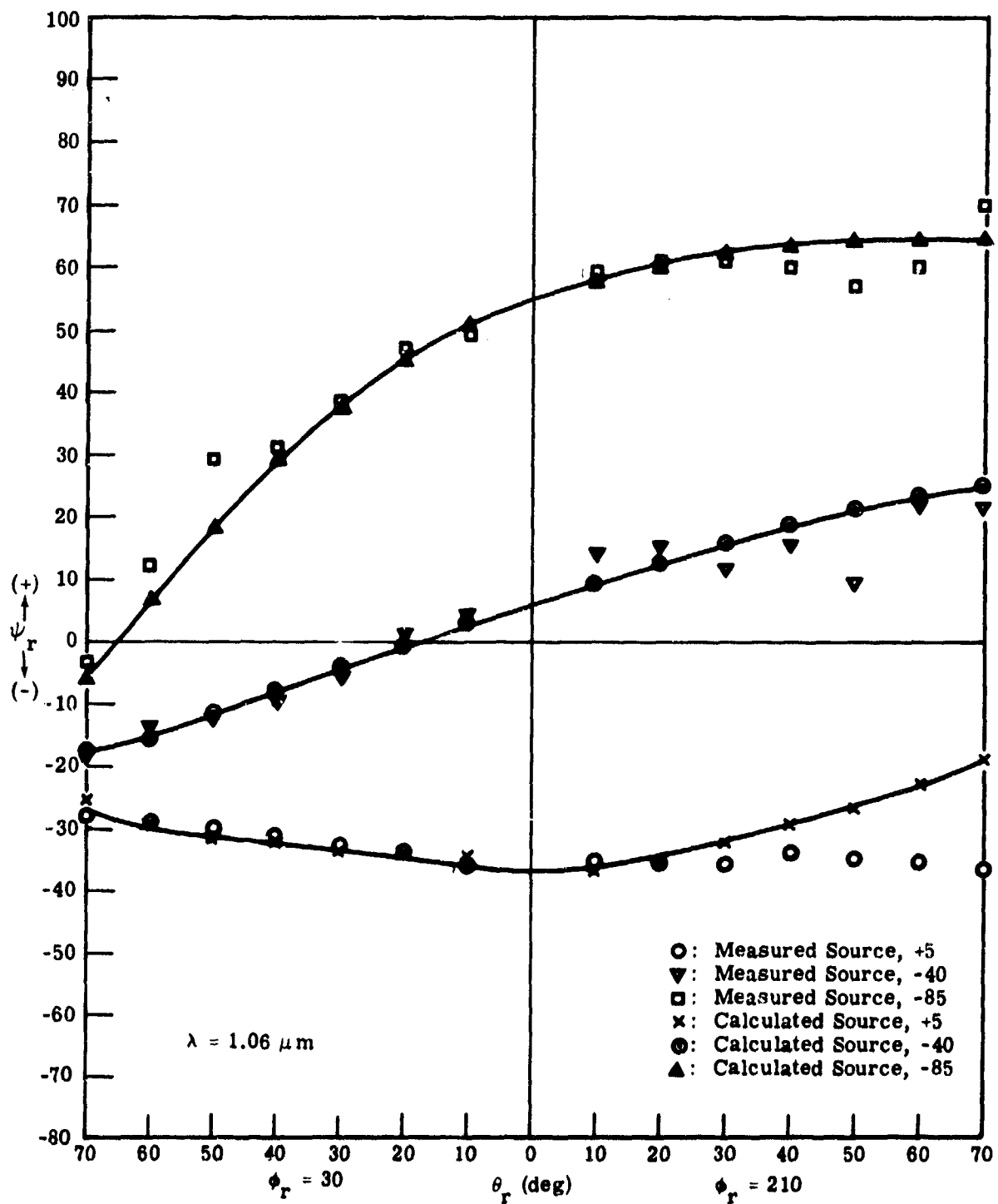


FIGURE 31. VARIATION OF POLARIZATION ANGLE OF REFLECTED RADIANCE AS FUNCTION OF SOURCE-RECEIVER POSITION. $\theta_i = 40^\circ$, $\psi_i = 180^\circ$, $\phi_r = 30^\circ, 210^\circ$.

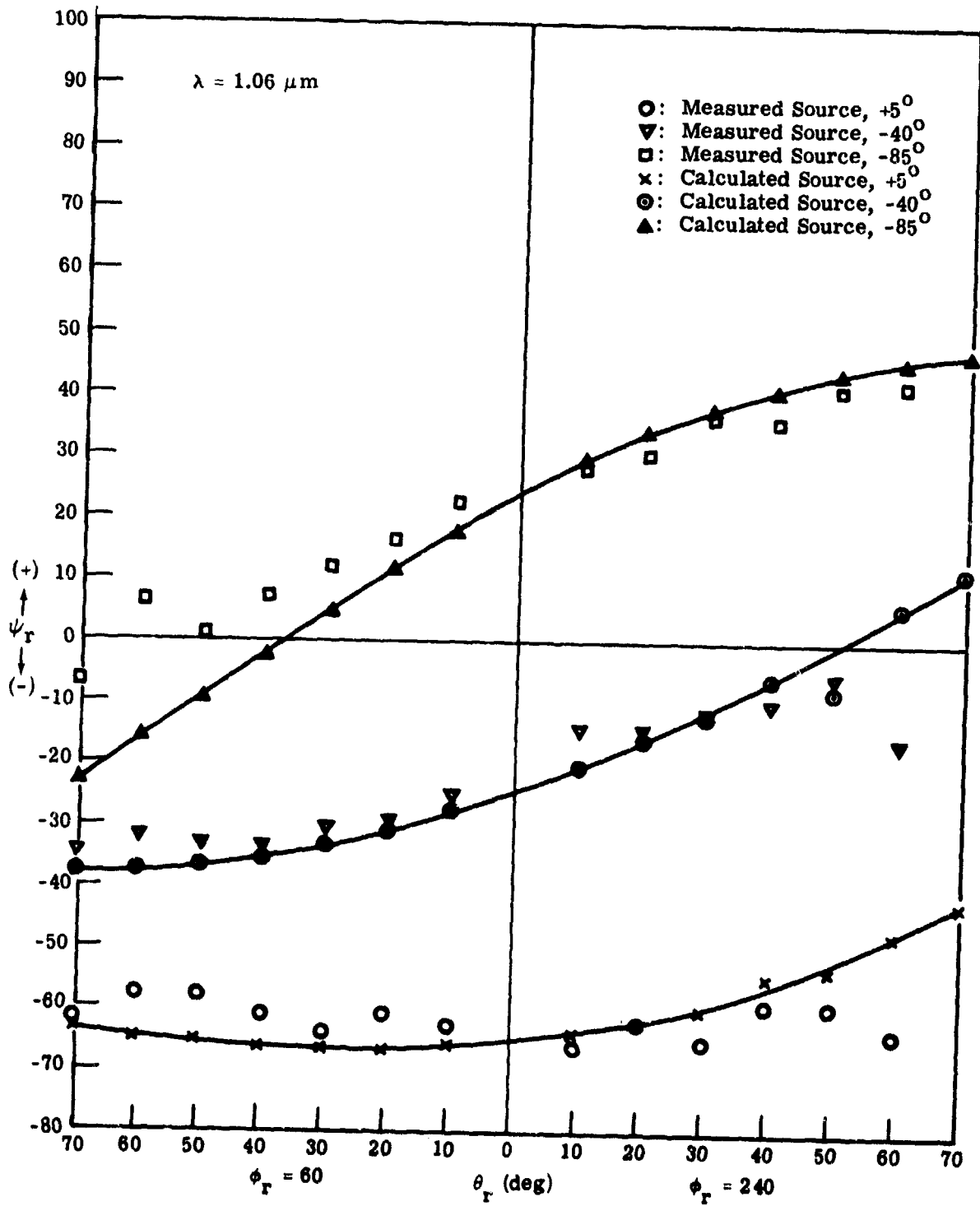


FIGURE 32. VARIATION OF POLARIZATION ANGLE OF REFLECTED RADIANCE AS FUNCTION OF SOURCE-RECEIVER POSITION. $\theta_i = 40^\circ$, $\phi_i = 180^\circ$, $\phi_r = 60^\circ, 240^\circ$.

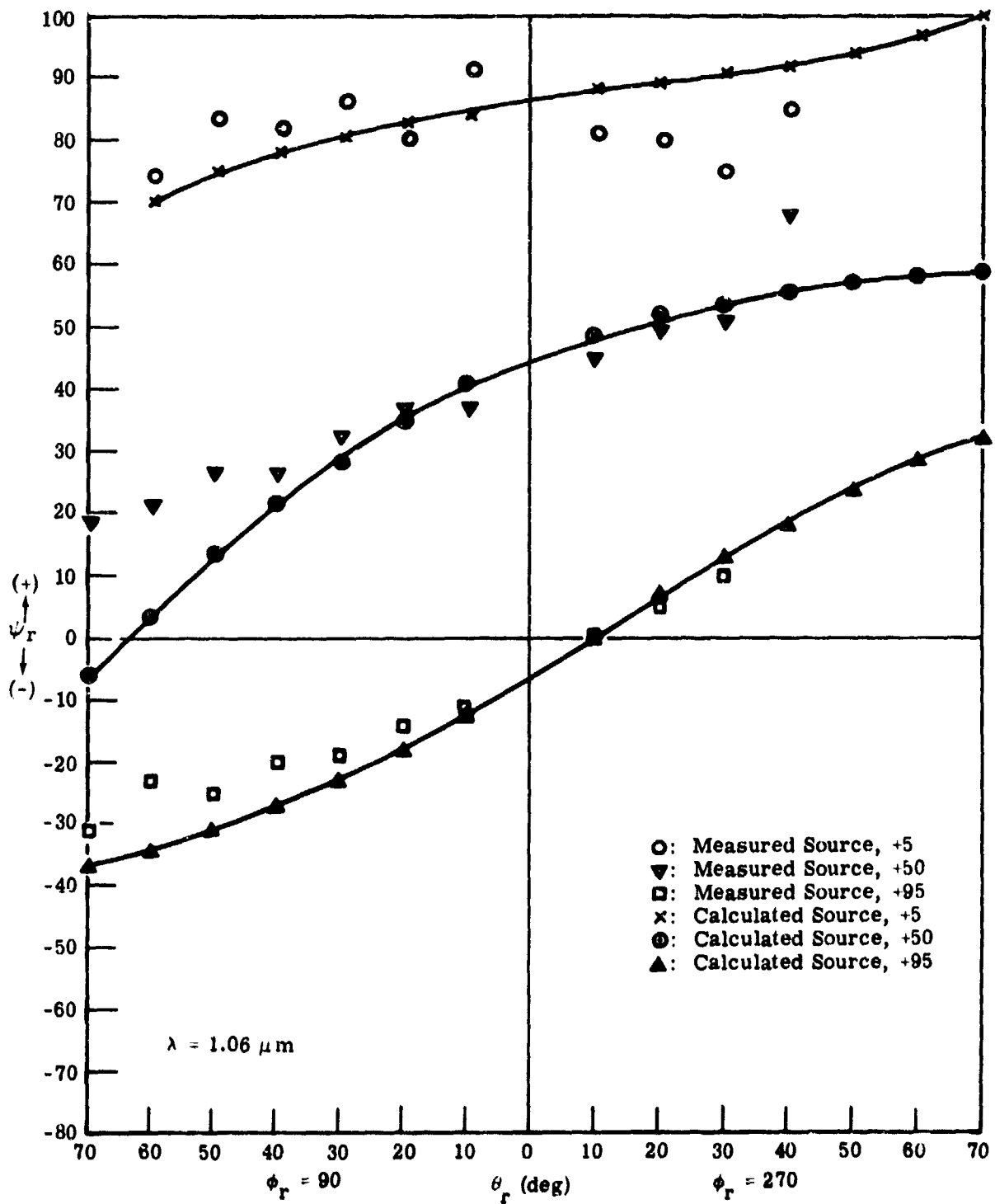


FIGURE 33. VARIATION OF POLARIZATION ANGLE OF REFLECTED RADIANCE AS FUNCTION OF SOURCE-RECEIVER POSITION. $\theta_i = 40^\circ$, $\phi_i = 180^\circ$, $\phi_r = 90^\circ$, 270° .

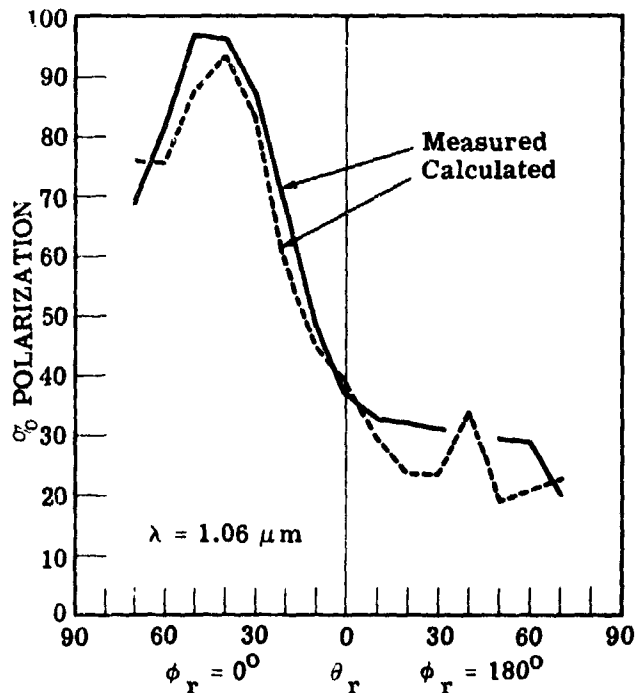


FIGURE 34. PERCENT POLARIZATION VARIATION FOR A02018-002 AS FUNCTION OF SOURCE-RECEIVER POSITION. $\theta_i = 40^\circ$, $\phi_i = 180^\circ$, $\phi_r = 0^\circ, 180^\circ$; perpendicular source.

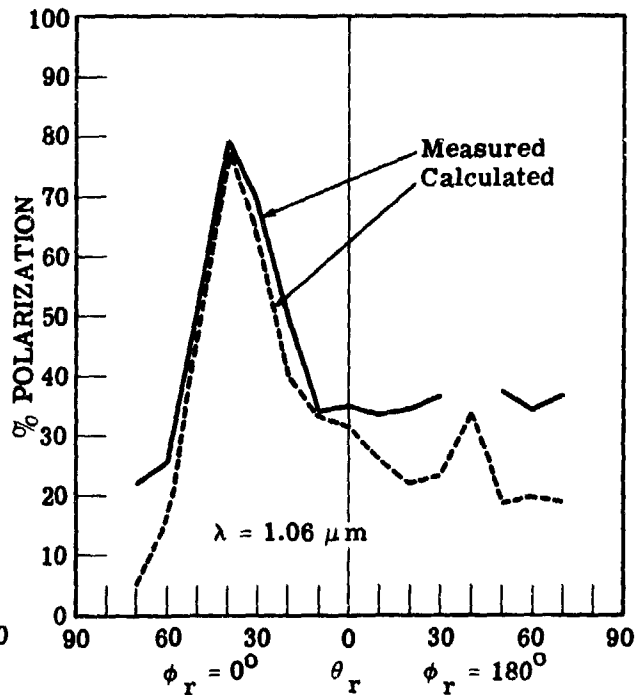


FIGURE 35. PERCENT POLARIZATION VARIATION FOR A02018-002 AS FUNCTION OF SOURCE-RECEIVER POSITION. $\theta_i = 40^\circ$, $\phi_i = 180^\circ$, $\phi_r = 0^\circ, 180^\circ$; parallel source.

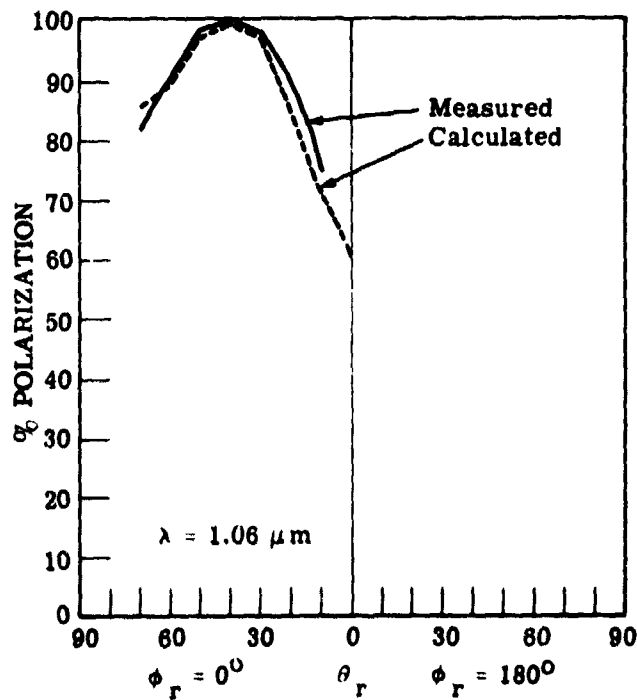


FIGURE 36. PERCENT POLARIZATION VARIATION FOR A02018-001 AS FUNCTION OF SOURCE-RECEIVER POSITION. $\theta_i = 40^\circ$, $\phi_i = 180^\circ$, $\phi_r = 0^\circ, 180^\circ$; perpendicular source.

perpendicular source.

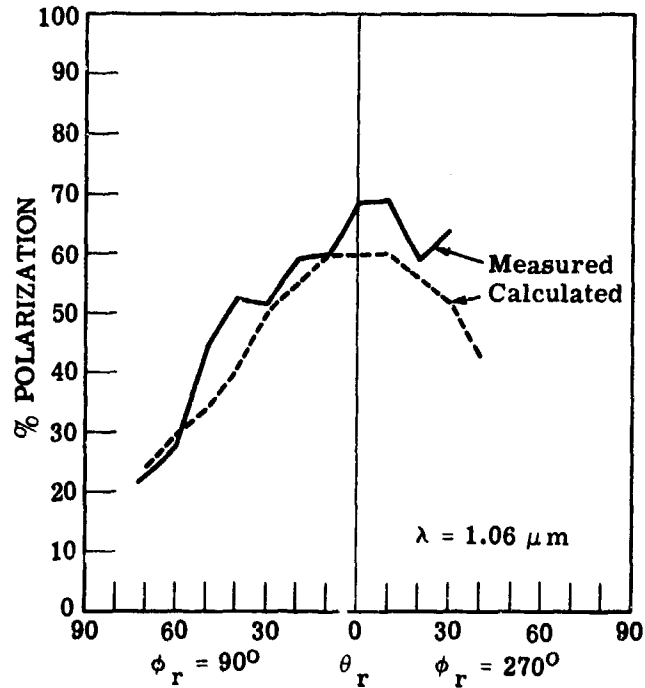


FIGURE 37. PERCENT POLARIZATION VARIATION FOR A02018-001 AS FUNCTION OF SOURCE-RECEIVER POSITION. $\theta_i = 40^\circ$, $\phi_i = 180^\circ$, $\phi_r = 90^\circ, 270^\circ$.

parallel source.

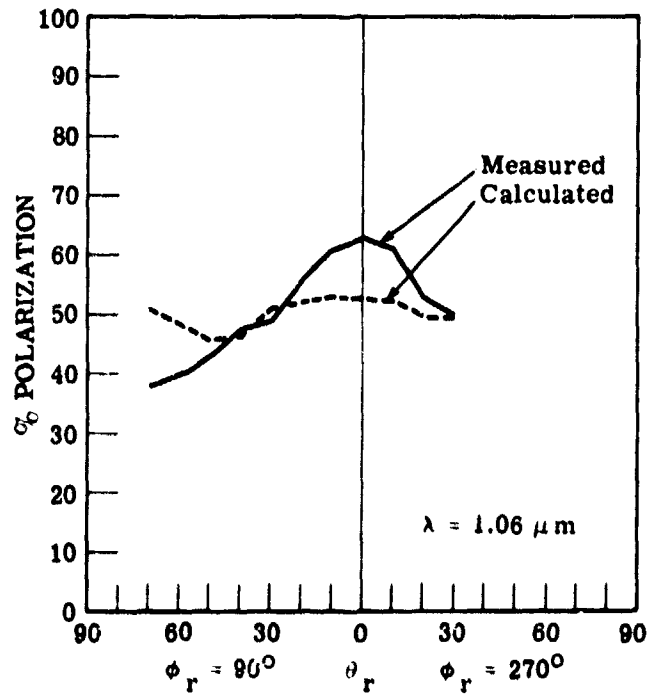


FIGURE 38. PERCENT POLARIZATION VARIATION FOR A02018-001 AS FUNCTION OF SOURCE-RECEIVER POSITION. $\theta_i = 40^\circ$, $\phi_i = 180^\circ$, $\phi_r = 90^\circ, 270^\circ$.

A02100 101

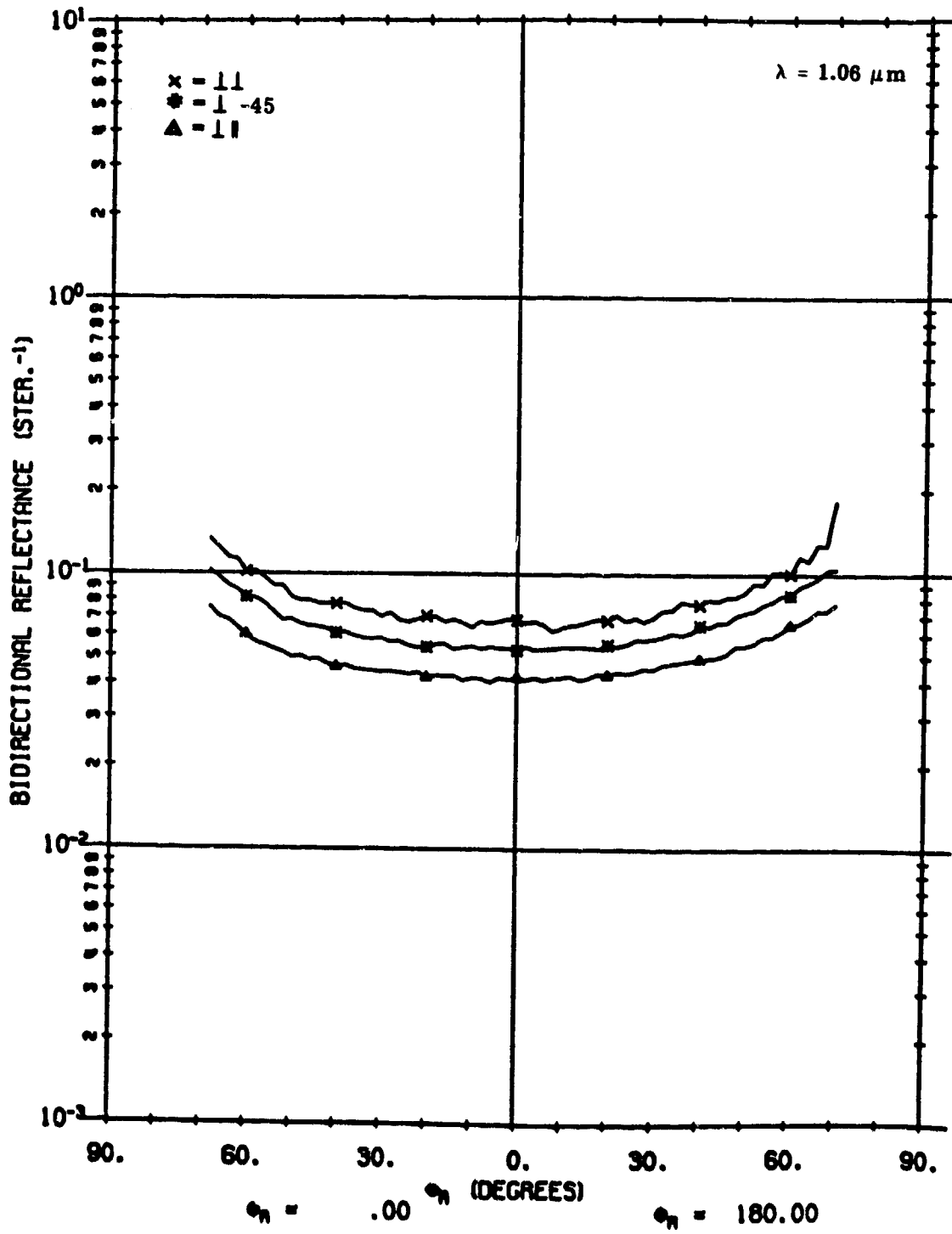


FIGURE 39. FIXED BISTATIC ρ' FOR A02100

A02100 101

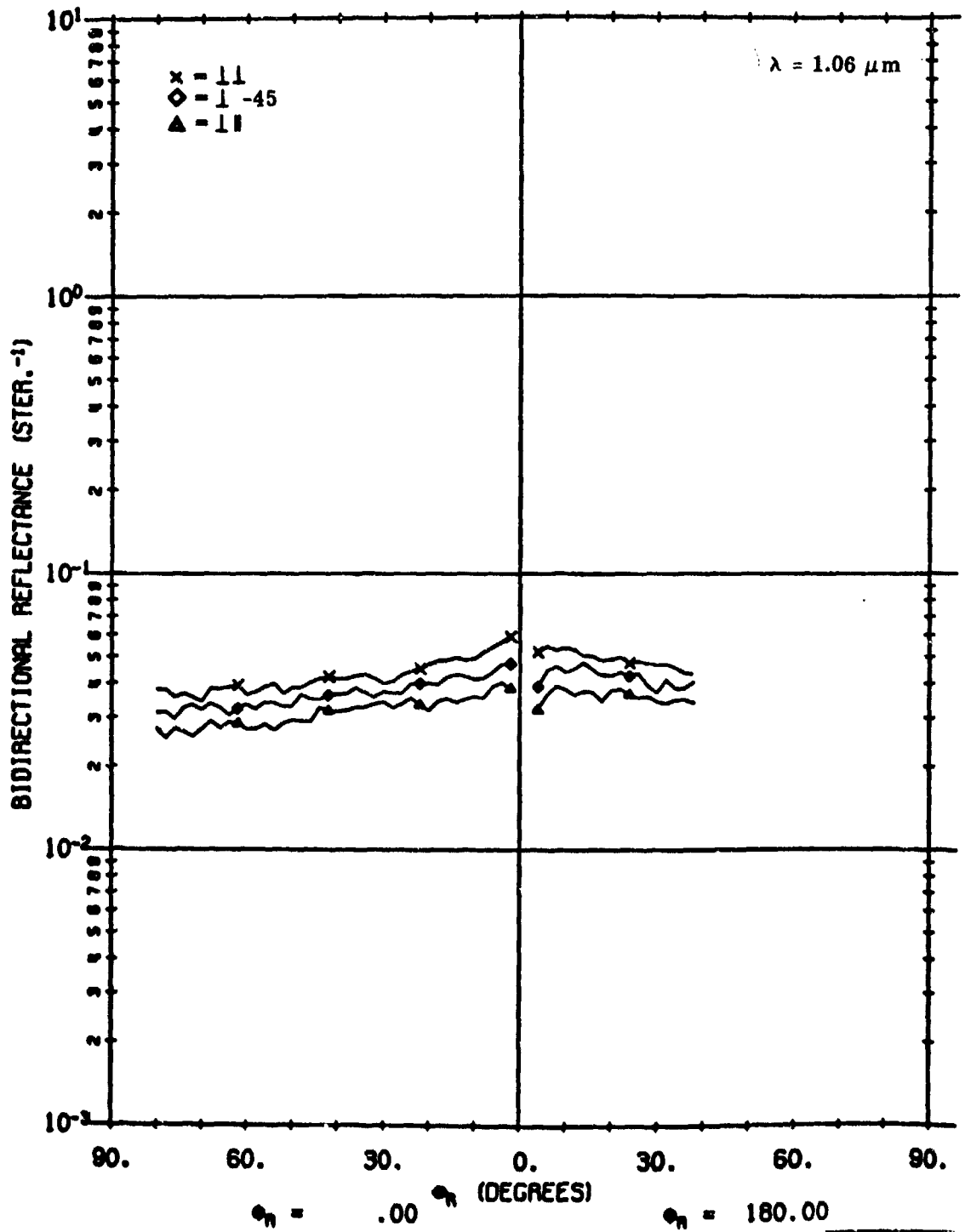


FIGURE 40. MEASURED ρ' FOR A02100. $\theta_i = 0^\circ$, $\phi_i = 0^\circ$, $\phi_r = 0^\circ, 180^\circ$.

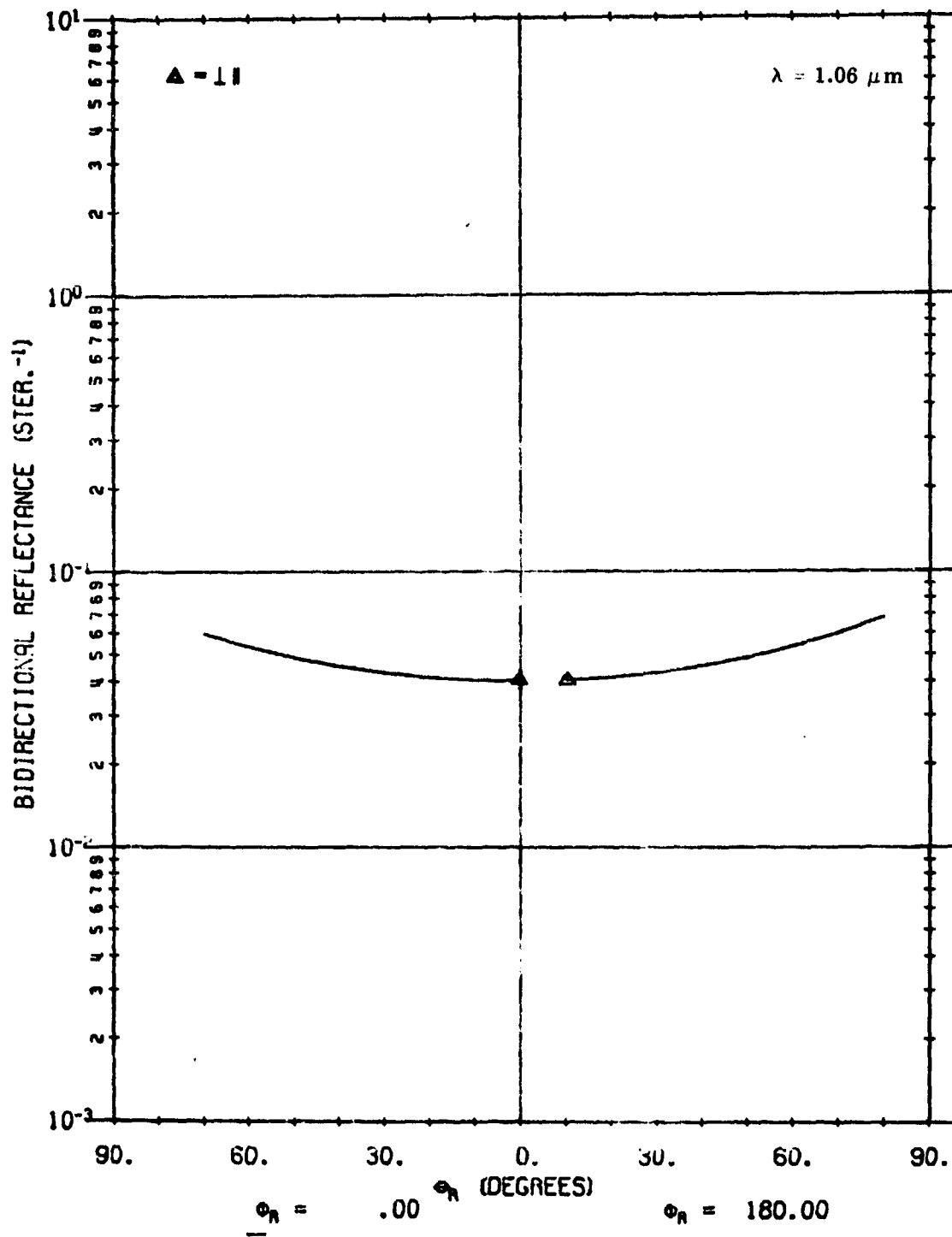


FIGURE 41. CALCULATED ρ^0 FOR A02100 USING NON-LAMBERTIAN VOLUME MODEL. $\phi_1 = 0^\circ, \phi_2 = 180^\circ, \phi_3 = 0^\circ, 180^\circ$.

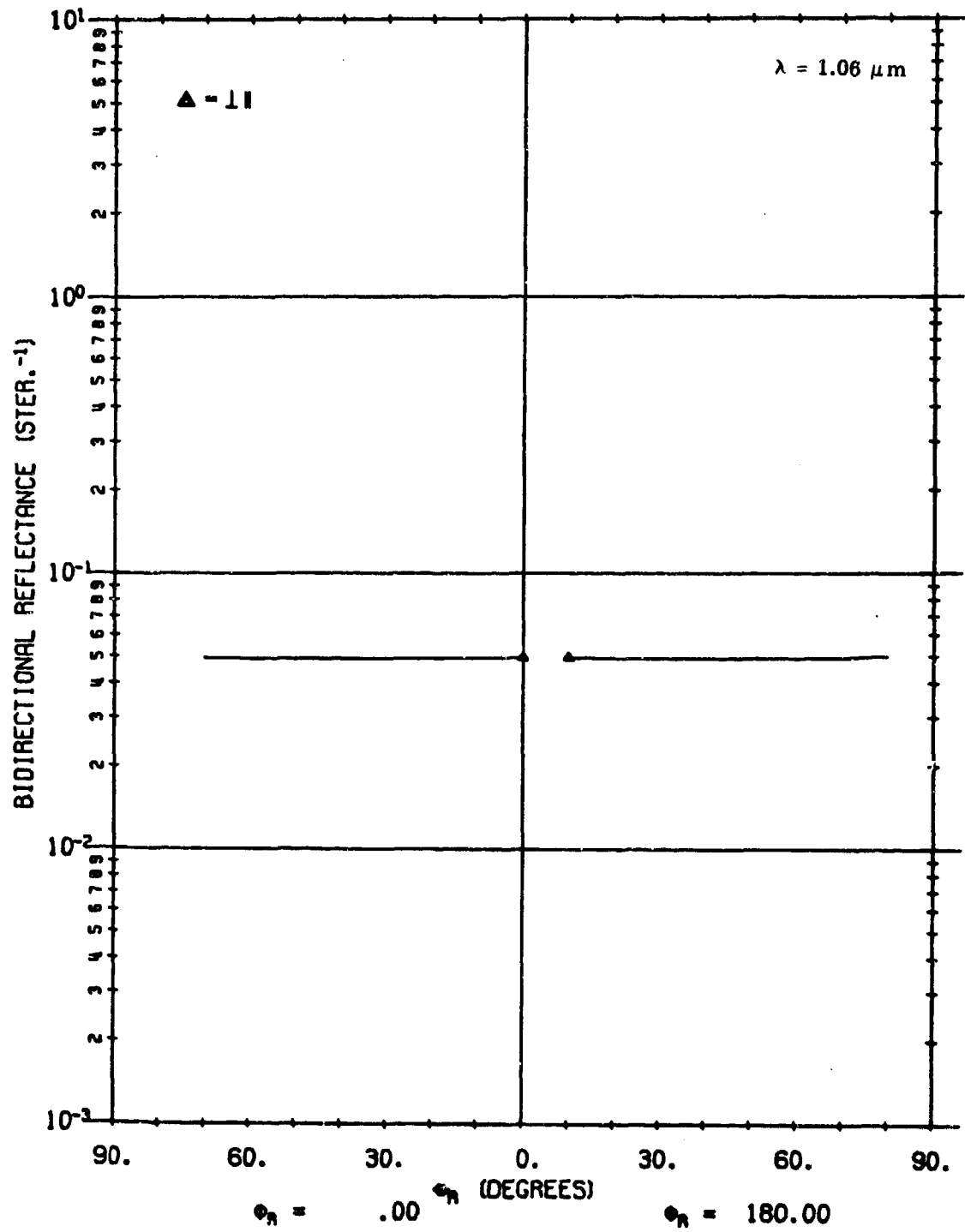


FIGURE 2. CALCULATED ρ' FOR A02100 USING LAMBERTIAN VOLUME MODEL.

$$\theta_i = 0^\circ, \phi_i = 180^\circ, \phi_r = 0^\circ, 180^\circ.$$

A02100 101

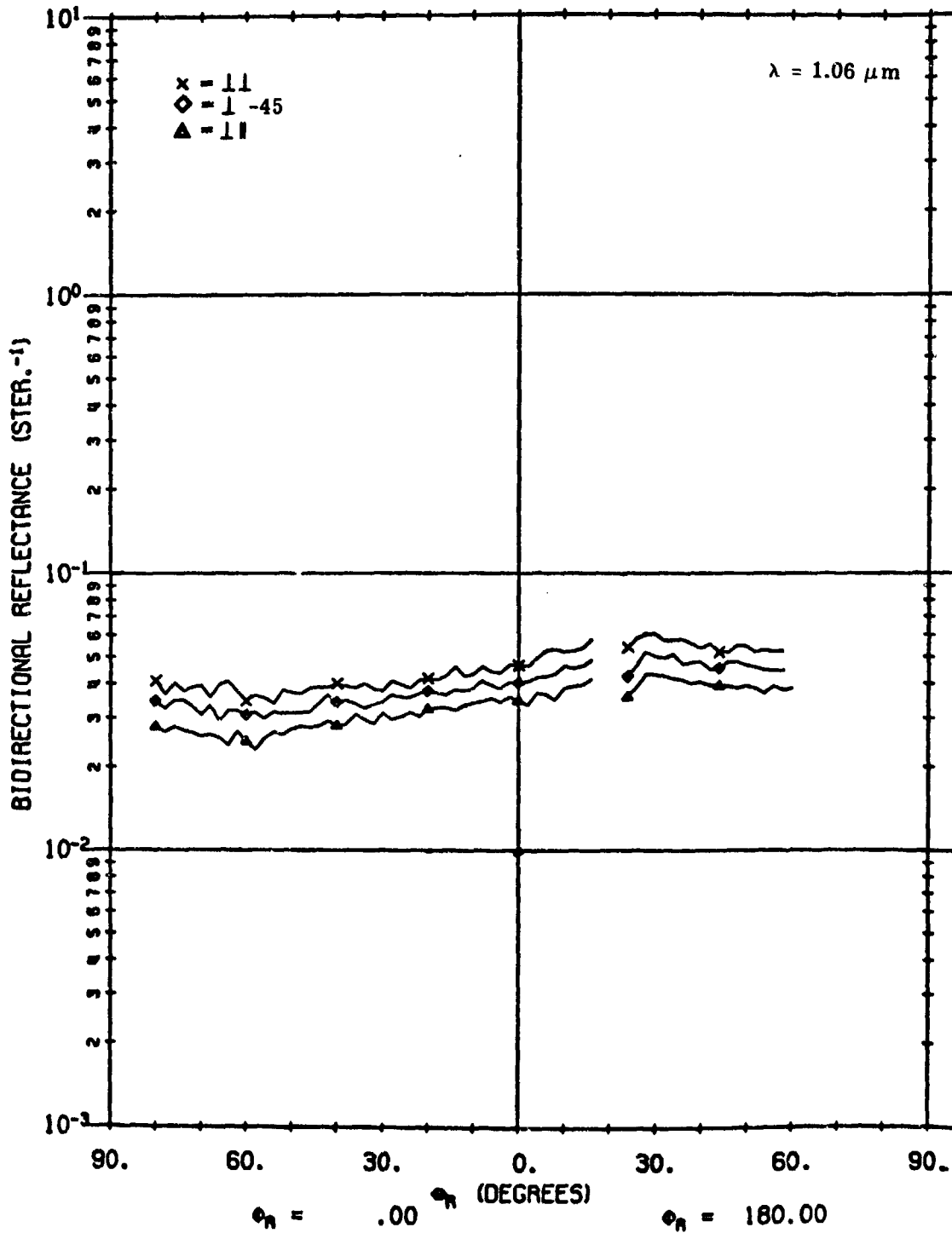


FIGURE 43. MEASURED ρ^* FOR A02100 AT 20° , 180° , 0° , 180° .

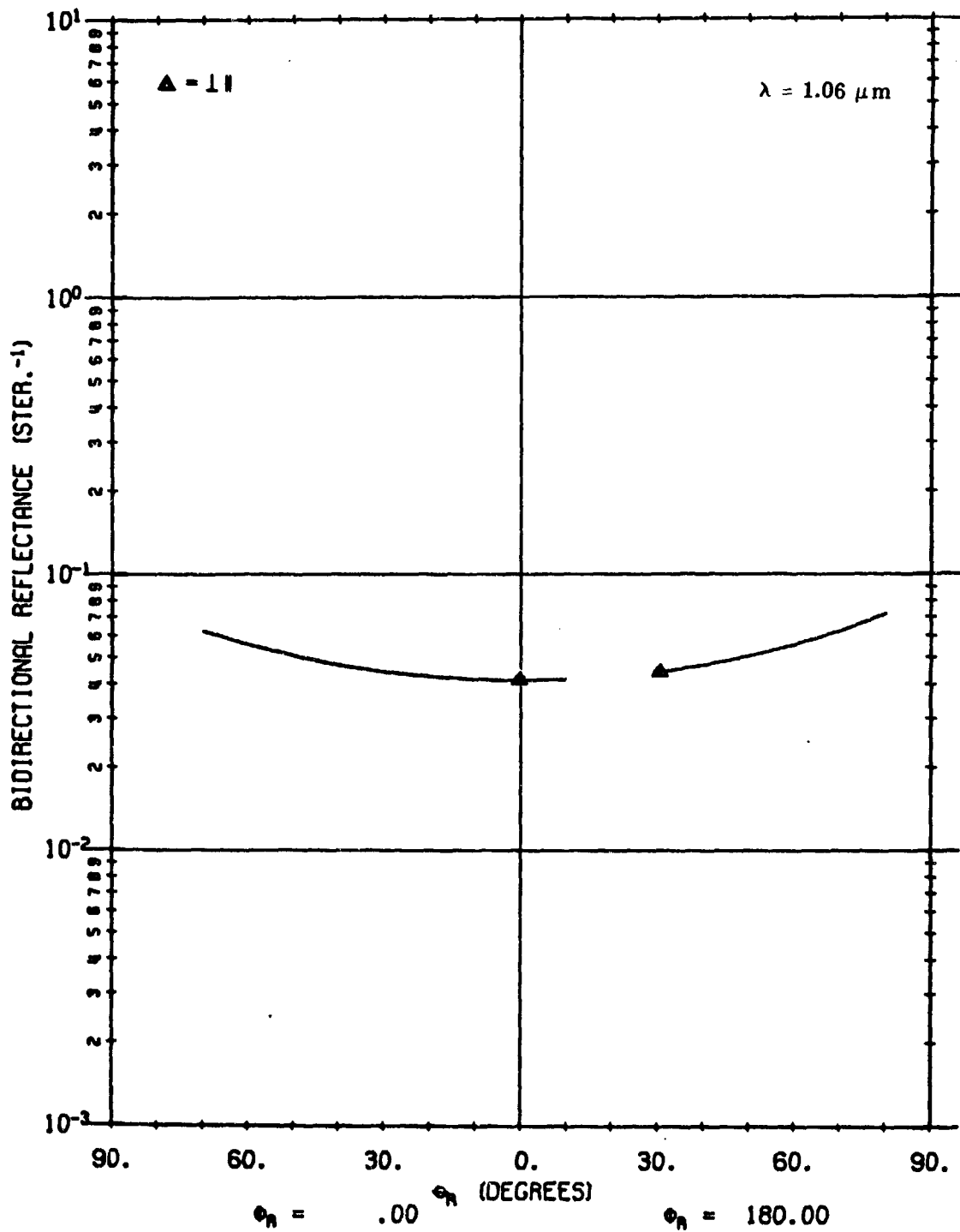


FIGURE 44. CALCULATED ρ' FOR A02100 USING NON-LAMBERTIAN VOLUME MODEL. $\theta_i = 20^\circ$, $\phi_i = 180^\circ$, $\phi_r = 0^\circ, 180^\circ$.

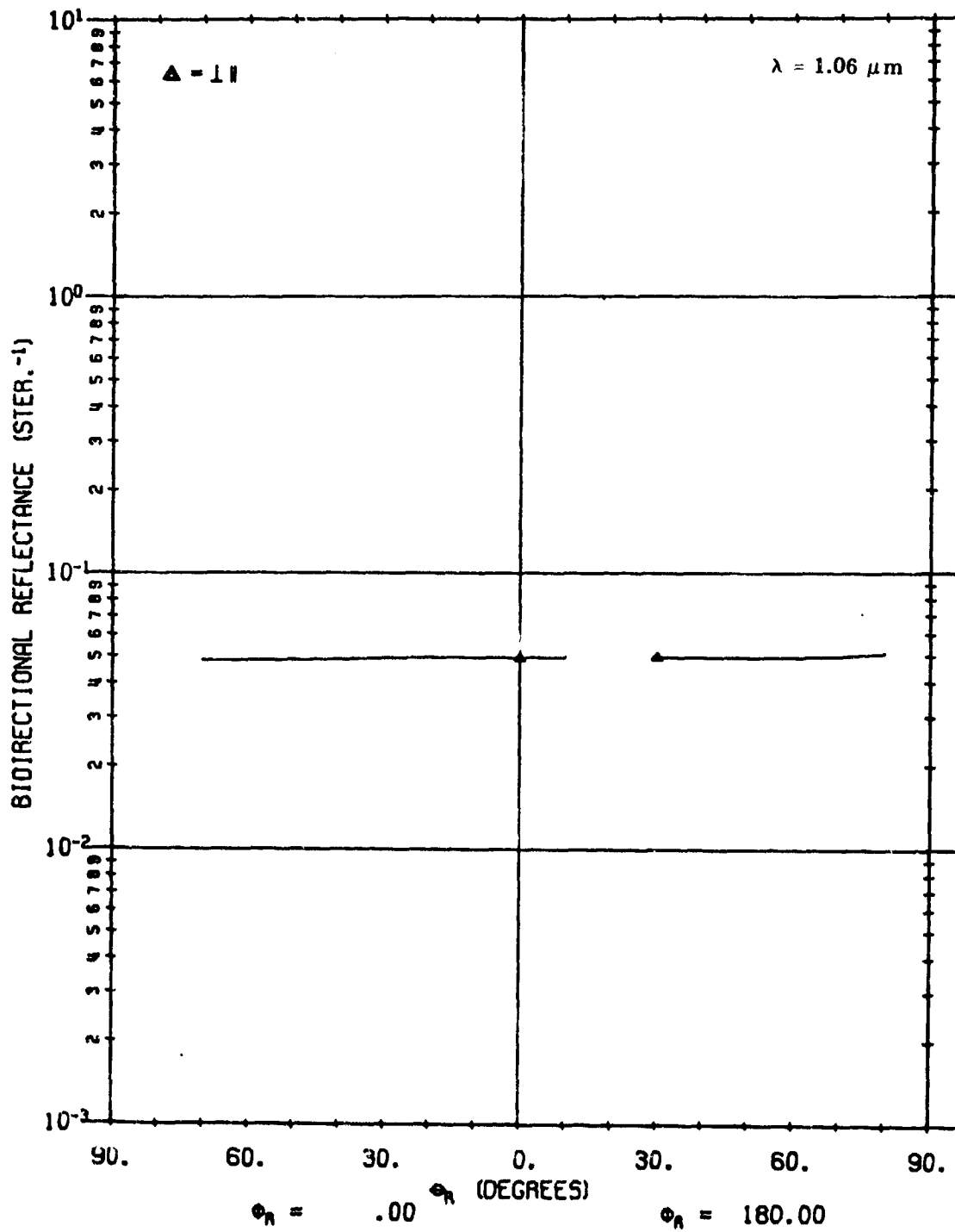


FIGURE 45. CALCULATED ρ' FOR A02100 USING LAMBERTIAN VOLUME MODEL.

$$\theta_i = 20^\circ, \phi_i = 180^\circ, \phi_r = 0^\circ, 180^\circ.$$

A02100 101

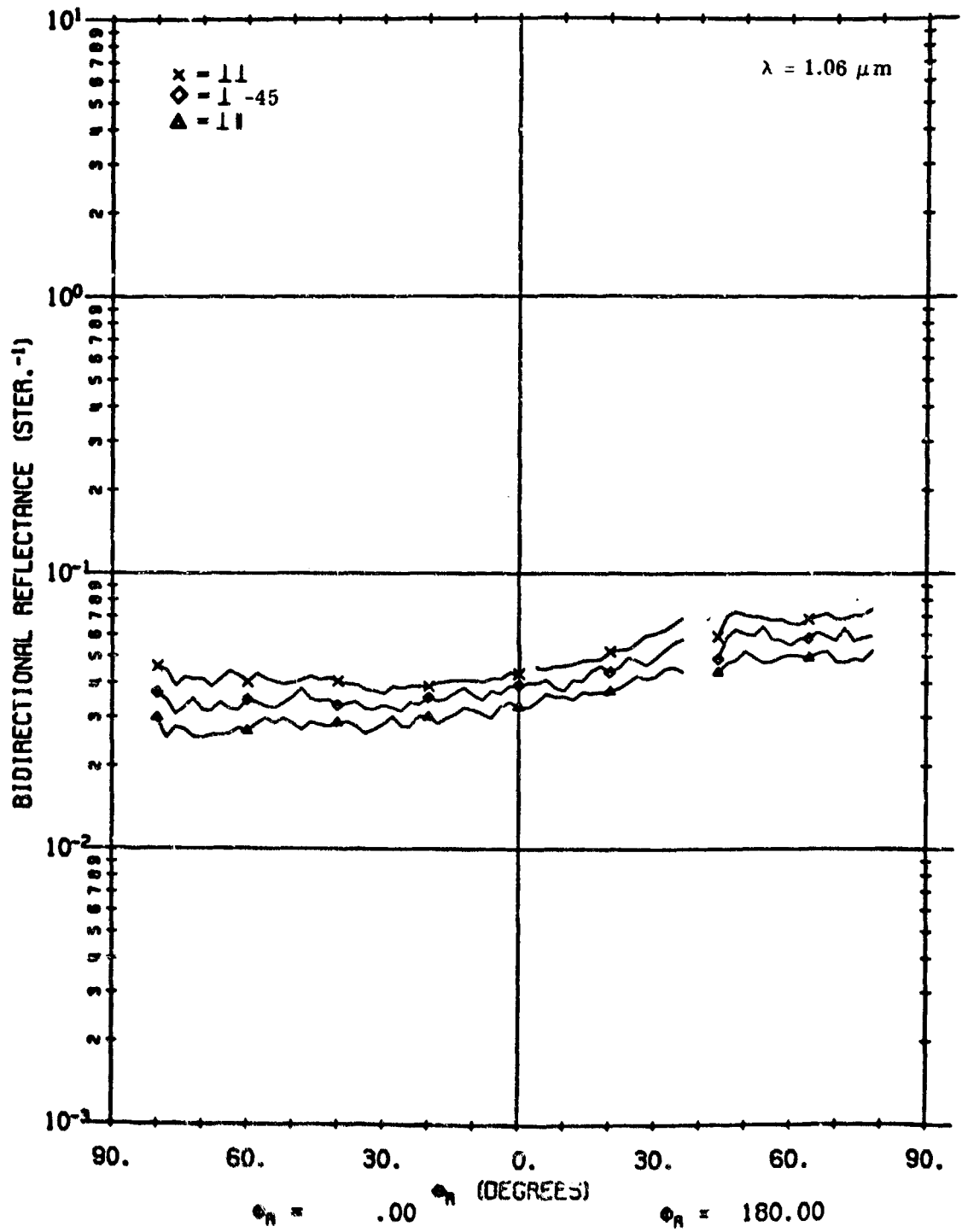


FIGURE 46. MEASURED ρ' FOR A02100. $\theta_i = 40^\circ$, $\phi_i = 180^\circ$, $\phi_r = 0^\circ, 180^\circ$.

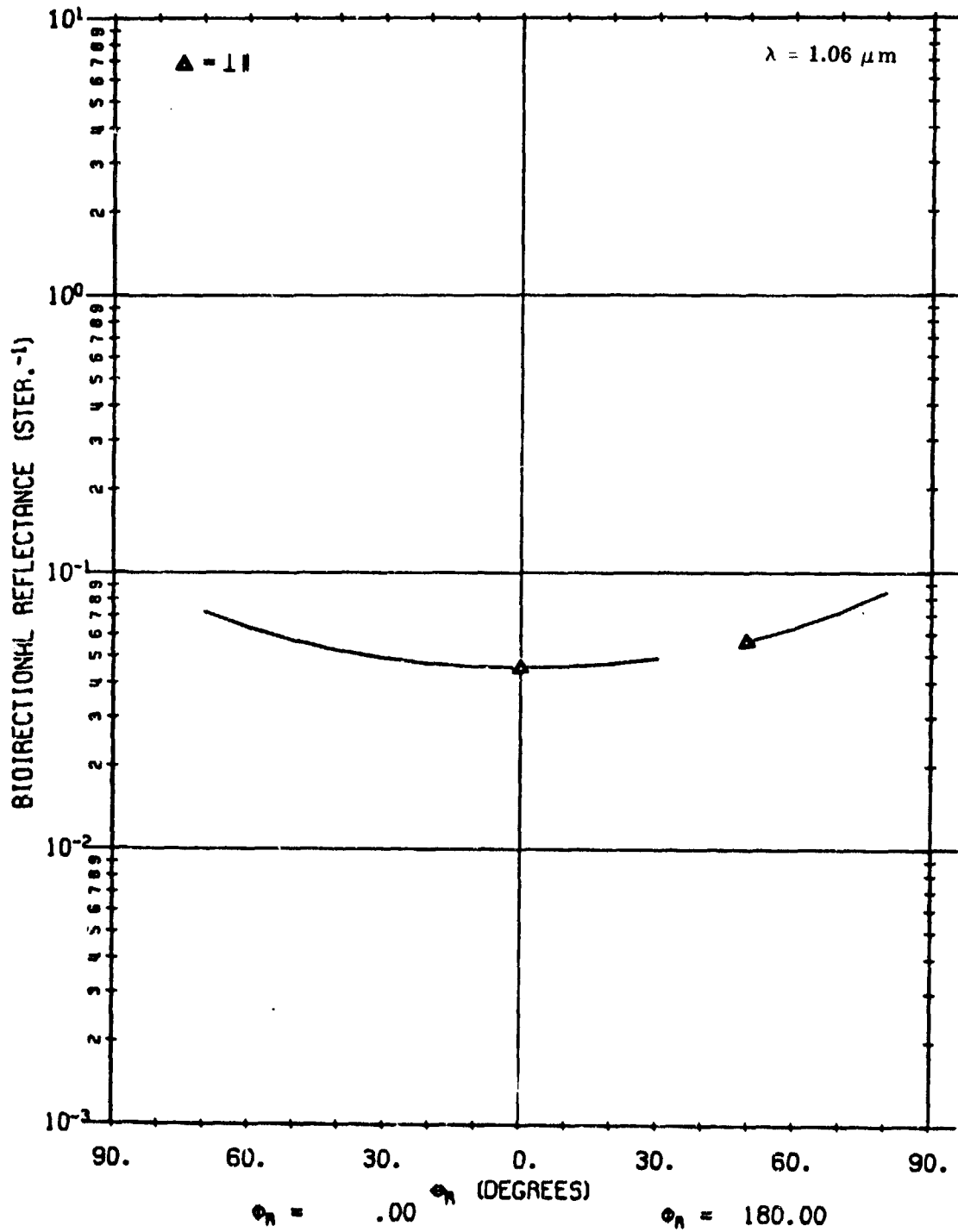


FIGURE 47. CALCULATED ρ' FOR A02100 USING NON-LAMBERTIAN VOLUME MODEL. $\phi_i = 40^\circ$, $\phi_i = 180^\circ$, $\phi_r = 0^\circ$, 180° .

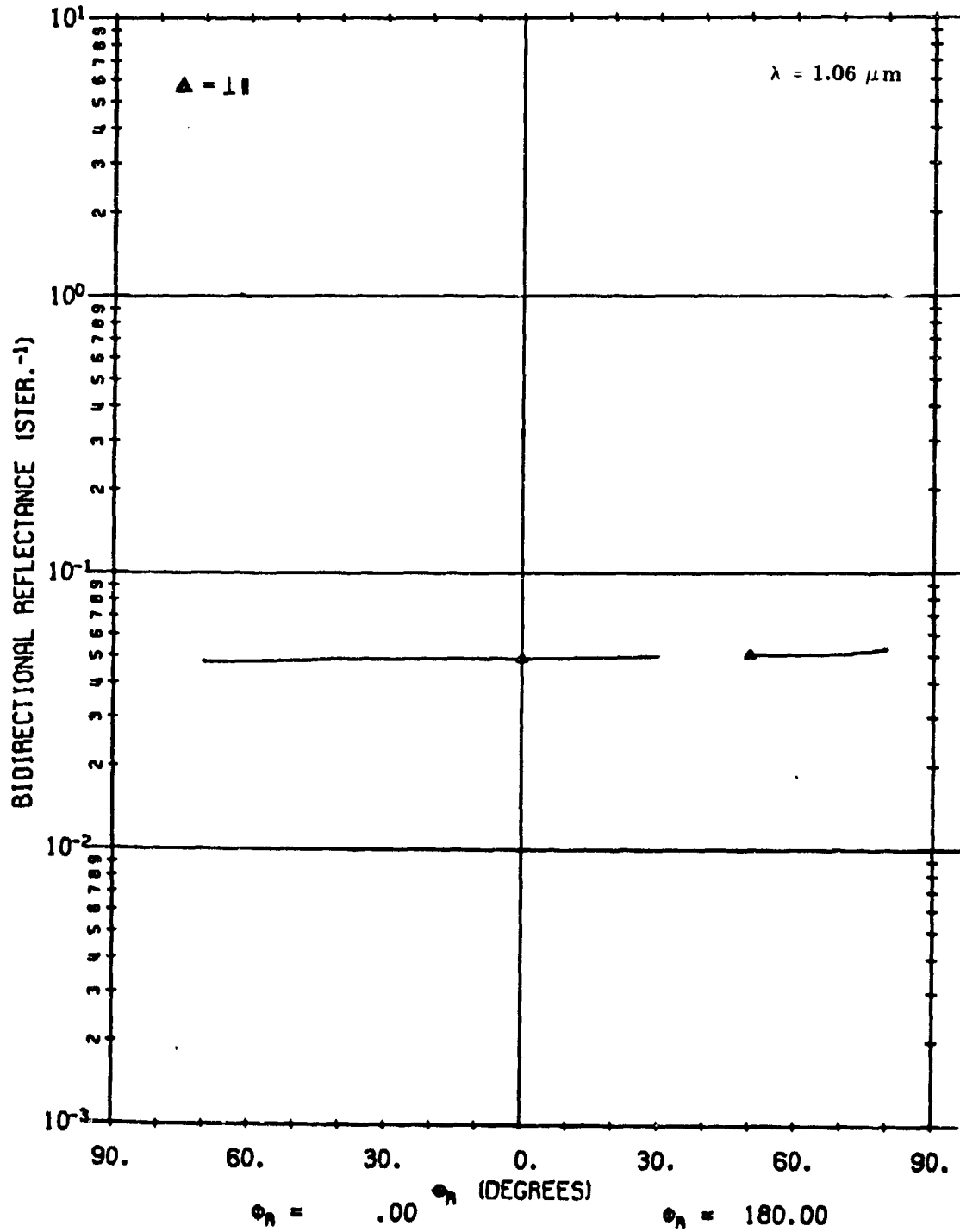


FIGURE 48. CALCULATED ρ' FOR A02100 USING LAMBERTIAN VOLUME MODEL.

$$\theta_i = 40^\circ, \phi_i = 180^\circ, \phi_r = 0^\circ, 180^\circ.$$

MODEL PARAMETERS

This section briefly describes the model parameters that can be used in the bidirectional reflectance program and explains how their values are derived. The choice of parameters for use in the program depends to some extent on the mode of the model being run. Basically, the model is run in three different modes:

- (1) Surface and Lambertian volume components
- (2) Non-Lambertian volume component (no surface contribution included)
- (3) Surface and non-Lambertian volume components

Therefore, we have grouped the model parameters as follows:

- (1) Polarization parameters
- (2) Surface model parameters
- (3) Lambertian volume model parameters
- (4) Non-Lambertian volume model parameters

7.1. SOURCE POLARIZATION PARAMETERS

The present model has been designed to account for polarization dependence in both surface and volume components.

In the surface component, polarization is accounted for automatically in the Fresnel reflectance coefficients. In the most general case, such polarization can be elliptical and can be decomposed into linear and circular components. To date, only a linearly polarized source and receiver have been used in measurements. However, for some applications, circularly polarized sources or receivers may be of interest. Therefore, in the model, we have provided program subroutines which take into consideration the ellipticity and handedness (i.e., direction of rotation in an elliptically polarized source) of both incident and reflected beam.

For volume components in both Lambertian and non-Lambertian cases, it is assumed that reflectance will be depolarized to some extent. In both cases, in fact, we assume total depolarization. Therefore, although a depolarization factor has been included in the non-Lambertian volume model for future flexibility, we assume $DP(j) = 1$.

The source polarization may most generally be defined as partially polarized with the polarized component elliptically polarized. The state of polarization of the source will be defined by its degree of polarization, P , and parameters A , B , ψ , and H to define the elliptical polarization of the polarized component. Here, A and B are the intensities along the semi-major and semi-minor axes, respectively. The angle ψ is the angle between the semi-major axis of the ellipse and the direction normal to the plane of incidence, measured looking into the source beam; ψ is equivalent to α except that $0^\circ < \psi < 180^\circ$ and $-90^\circ < \alpha < 90^\circ$. The handedness $H = \pm 1$.

The Stokes vectors provide a convenient formalism for defining the polarization state of the reflected radiance. (Reference [5] provides a general discussion of Stokes vectors in this context.)

$$S = \begin{bmatrix} I_p + I_u \\ I_p \cos 2\chi \cos 2\psi \\ I_p \cos 2\chi \sin 2\psi \\ I_p \sin 2\chi \end{bmatrix}$$

where I_p and I_u are the polarized and unpolarized components, respectively, in the reflected radiance. The degree of polarization in the reflected radiance is $P = I_p / (I_p + I_u)$. Angles χ and ψ define the polarization state of the reflected radiance: ψ is the angle between the semi-major axis of the ellipse and the direction normal to the plane of reflection; $\tan \chi = \pm \sqrt{B/A}$ where A and B are the intensities along the semi-major and semi-minor axes of the polarization ellipse and $\tan \chi < 0$ for left-handed elliptically polarized radiation.

The RHOPRIME program produces the Stokes vector S for unit irradiance in the input beam; the area may also be defined to be unity and then S represents a reflectance Stokes vector. The program also produces the components of the reflected radiance transmitted with a receiver polarization analyzer oriented parallel or perpendicular to the reflectance plane for computing $\rho'_{\psi, \parallel}$ and $\rho'_{\psi, \perp}$.

7.2. SURFACE MODEL PARAMETERS

n and k. These are the real and imaginary parts of the refractive index. As discussed earlier in this report, they are used for the determination of $R(\beta)$, the Fresnel reflectance. Values for n and k are estimated for the paint surfaces in this study. Moreover, the surface is assumed to be essentially nonconducting so that $k = 0$. Based on experience with similar paint samples, n is taken to be 1.65. For a given sample, n and k can be determined accurately by measuring the Brewster angle and calculating n and k as outlined in Section 4 on the surface model. At the present time the program used, RHOPRIME, does not do this.

τ and Ω . These parameters are used in the function which provides a correction to the program to account for shadowing and obscuration effects resulting from the roughness of the surface. Values for τ and Ω have been selected, based on observed characteristics of reflectance properties. They have been established as $\tau = 15$ and $\Omega = 40$.

ρ' $\rho'(\theta_i, \phi_i; \theta_r, \phi_r) \cos^2 \theta_i$. One of the quantities in Eq. (9) from which $\rho'(\theta_i, \phi_i; \theta_r, \phi_r)$ is determined is $\rho'(\theta_i, \phi_i; \theta_i, \phi_i) \cos^2 \theta_i$. As previously discussed, $\rho'(\theta_i, \phi_i; \theta_i, \phi_i)$ is obtained from zero bistatic data. Values for $\rho'(\theta_i, \phi_i; \theta_i, \phi_i) \cos^2 \theta_i$ must be calculated (preferably for increments of two degrees) and made into a table which is one of the model inputs. Values are provided in Tables III-VI for materials A02017-001, A02018-001, A02018-002, and A02100.

7.3. LAMBERTIAN VOLUME MODEL PARAMETERS

$\rho_{\chi 1}$ and $\rho_{\chi 2}$. These are the cross components of polarized radiation used in the model to account for the diffuse contribution, $\rho_{\chi 1} = 2\rho_{\parallel\perp}$ and $\rho_{\chi 2} = 2\rho_{\perp\parallel}$, where $\rho_{\perp\parallel}$ and/or $\rho_{\parallel\perp}$ is determined by taking the average value of the cross component from the measured data. According to the reciprocity theorem, $\rho_{\chi 1} = \rho_{\chi 2}$ [Ref. 6]. It is important to remember that ρ_{χ} values only used when the volume scatter model is not used. When the volume model is used, $\rho_{\chi 1} = \rho_{\chi 2} = 0$.

7.4. NON-LAMBERTIAN VOLUME MODEL PARAMETERS

ρ_V . This represents the non-Lambertian volume scatter component; it is determined by extracting $\rho'_{\perp\parallel}$ or $\rho'_{\parallel\perp}$ at the point which would lie under the peak of the zero bistatic scan if the measured curve were smooth; $\rho_V = 2\rho'_{\perp\parallel} = 2\rho'_{\parallel\perp}$ at the peak point. (The fact that a hump sometimes occurs on the measured cross component curve is discussed in the section on Model Validations.)

Here again, it is important to remember that when the Lambertian volume model is used, $\rho_V = 0$ and $\rho_{\chi} \neq 0$. When the non-Lambertian volume model is used, $\rho_V \neq 0$ and $\rho_{\chi} = 0$. Also, ρ_V and ρ_{χ} are never simultaneously nonzero in models which have been validated to date.

$DP(i), f(j), g\left(\frac{\theta}{\hat{n}}\right)$. Integral parts of SUBROUTINE FUNC, these parameters currently are all set equal to 1. They have been included to provide flexibility for later model modifications.

TABLE III. $\rho'(\theta_n, \phi_n; \theta_n, \phi_n) \cos^2 \theta_n$ VALUES FOR A02017-001

θ_n	$\rho'(\theta_n, \phi_n; \theta_n, \phi_n) \cos^2 \theta_n$
.9	.14528
2.9	.08415
4.9	.0529
6.9	.03705
8.9	.03077
10.9	.02315
12.9	.01829
14.9	.01786
16.9	.01524
18.9	.01344
20.9	.01169
22.9	.01091
24.9	.01148
26.9	.00984
28.9	.0086
30.9	.00925
32.9	.00908
34.9	.00815
36.9	.00625
38.9	.00649
40.9	.00664
42.9	.00617
44.9	.00531
46.9	.00465
48.9	.00474
50.9	.00406
52.9	.00354
54.9	.00291
56.9	.00323
58.9	.00265
60.9	.00224
62.9	.00217
64.9	.00211
66.9	.00205
68.9	.00196
70.9	.0027

TABLE IV. $\rho'(\theta_n, \phi_n; \theta_n, \phi_n) \cos^2 \theta_n$ VALUES FOR A02018-001

$\hat{\theta}_n$	$\rho'(\hat{\theta}_n, \hat{\phi}_n; \hat{\theta}_n, \hat{\phi}_n) \text{Cos}^2 \hat{\theta}_n$
1.1	.5143
3.1	.27294
5.1	.11897
7.1	.05797
9.1	.03291
11.1	.02348
13.1	.02058
15.1	.01614
17.1	.0143
19.1	.0118
21.1	.01191
23.1	.01056
25.1	.01055
27.1	.00924
29.1	.00918
31.1	.00672
33.1	.00708
35.1	.00612
37.1	.00597
39.1	.00578
41.1	.00549
43.1	.00469
45.1	.00459
47.1	.00433
49.1	.00417
51.1	.0046
53.1	.00376
55.1	.00292
57.1	.0023
59.1	.00179
61.1	.00168
63.1	.00132
65.1	.0013
67.1	.00109

TABLE V. $\rho'(\theta_n, \phi_n; \theta_n, \phi_n) \cos^2 \theta_n$ VALUES FOR A02018-002

θ_n	$\rho'(\theta_n, \phi_n; \theta_n, \phi_n) \cos^2 \theta_n$
1.15	.02497
3.15	.02520
5.15	.02388
7.15	.01975
9.15	.02135
11.15	.02177
13.15	.02335
15.15	.02353
17.15	.02300
19.15	.02243
21.15	.02338
23.15	.02022
25.15	.02056
27.15	.01726
29.15	.01885
31.15	.01966
33.15	.01875
35.15	.02089
37.15	.01882
39.15	.01709
41.15	.01785
43.15	.01604
45.15	.01545
47.15	.01295
49.15	.01319
51.15	.01434
53.15	.01180
55.15	.01385
57.15	.01190
59.15	.00922
61.15	.01149
63.15	.00869
65.15	.00954
67.15	.00808
69.15	.01349

TABLE VI. $\rho'(\theta_n, \phi_n; \theta_n, \phi_n) \cos^2 \theta_n$ VALUES FOR A02100

θ_n	$\rho'(\theta_n, \phi_n; \theta_n, \phi_n) \cos^2 \theta_n$
0.1	.21399
2.1	.16918
4.1	.1096
6.1	.08454
8.1	.05494
10.1	.03917
12.1	.03869
14.1	.02547
16.1	.03465
18.1	.02112
20.1	.02753
22.1	.02155
24.1	.02261
26.1	.01906
28.1	.02055
30.1	.01637
32.1	.01799
34.1	.01778
36.1	.01601
38.1	.01559
40.1	.01337
42.1	.01626
44.1	.01101
46.1	.01054
48.1	.00894
50.1	.01003
52.1	.00898
54.1	.00648
56.1	.00815
58.1	.00701
60.1	.00470
62.1	.00552
64.1	.00497
66.1	.00387
68.1	.00343
70.1	.00292

Appendix I
DOCUMENTATION OF BIDIRECTIONAL REFLECTANCE PROGRAM (RHOPRIME)

Program RHOPRIME is the main calling program for subroutines to read and store materials data, perform geometrical calculations, compute bidirectional reflectances for any source/receiver position and polarization, and prepare the output in a convenient format. The calling sequence, purpose, and calculations performed by each subroutine are given below, followed by details on the input data formats.

III.1. DESCRIPTIONS OF SUBROUTINES

SUBROUTINE INDATA. This is the first subroutine called. Material parameters needed for the calculation of bidirectional reflectance are read and stored. Material parameters are

MAT = material specifier

N = n = real part of refractive index

K = k = imaginary part of refractive index

RX1 = $\rho_{\chi 1}$ = diffuse reflectance for \perp polarized source

RX2 = $\rho_{\chi 2}$ = diffuse reflectance for \parallel polarized source

RHOV = ρ_v = volume reflectance

SIGMA } parameters available to calculate $\rho'(\theta_{\hat{n}}, \phi_{\hat{n}}; \theta_{\hat{n}}, \phi_{\hat{n}})$ in subroutine FUNC
RPO }

TAU = τ (deg)

OMEGA = Ω (deg) } parameters to calculate a shadowing and obscuration factor to be applied to ρ' ($\cos \beta_{NP}$) in subroutine FUNC
Q1 }
Q2 }

RCOSBNP = $\rho'(\theta_{\hat{n}}, \phi_{\hat{n}}; \theta_{\hat{n}}, \phi_{\hat{n}}) \cos^2 \theta_{\hat{n}}$ } table of zero-degree bistatic bidirectional reflectance data
BNP = $\theta_{\hat{n}}$ (deg) }

TITLE. A title card (optional) is read and used to identify on the printed output the calculations to be performed.

FACET. The source and receiver are located in an earth-fixed, right-handed XYZ coordinate system. The XYZ components of the unit normal vector of the reflecting surface are read (optional). If the facet definition card is not supplied, the facet unit normal vector defaults to (0, 0, 1).

COMPUTATION REQUEST. The specification of source and receiver positions and source polarization for computation of the bidirectional reflectance is read.

ISW = model selector
 TS = zenith angle of source (deg)
 PS = azimuth angle of source (deg)
 TD = zenith angle of receiver (deg)
 PD = azimuth angle of receiver (deg)
 A = intensity of major axis of polarization ellipse
 B = intensity of minor axis of polarization ellipse
 PSI = angle of major axis of polarization ellipse from the normal to the plane of incidence
 measured CCW looking into the source, $0 \leq \text{PSI} \leq 180$ (deg)
 P = polarization of source ($0 \leq P \leq 1.0$)
 H = handedness of polarization ellipse (± 1.0 or 0.0)
 MI = material specifier

SUBROUTINE SCAN. This subroutine defines a sequence of detector positions for a specified source position and polarization.

ISW = model selector
 TS = zenith angle of source (deg)
 PS = azimuth angle of source (deg)
 TDS = start zenith angle of receiver (deg)
 TDE = end zenith angle of receiver (deg)
 TSTEP = zenith angle scan increment (deg)
 PDS = start azimuth angle of receiver (deg)
 PDE = end azimuth angle of receiver (deg)
 PSTEP = azimuth angle scan increment (deg)
 A = intensity of major axis of polarization ellipse
 B = intensity of minor axis of polarization ellipse
 PSI = angle of major axis of polarization ellipse from the normal to the plane of incidence
 measured CCW looking into the source, $0 \leq \text{PSI} \leq 180$ (deg)
 P = polarization of source ($0 \leq P \leq 1.0$)
 H = handedness of polarization ellipse (± 1.0 or 0.0)
 MI = material specifier

SUBROUTINE GEOM. This subroutine does the necessary geometrical calculations of angles needed for the bidirectional reflectance calculations (see Fig. 49).

OR = (0, 0, 1) is a unit vector along the earth-fixed Z axis
 PSI = the angle of the major axis of polarization ellipse from the normal vector of the OR,
 E plane measured CCW looking into the source, $0 \leq \text{PSI} \leq 180$ (deg)

X D = E
 D = E
 Y OR = E
 OR = E

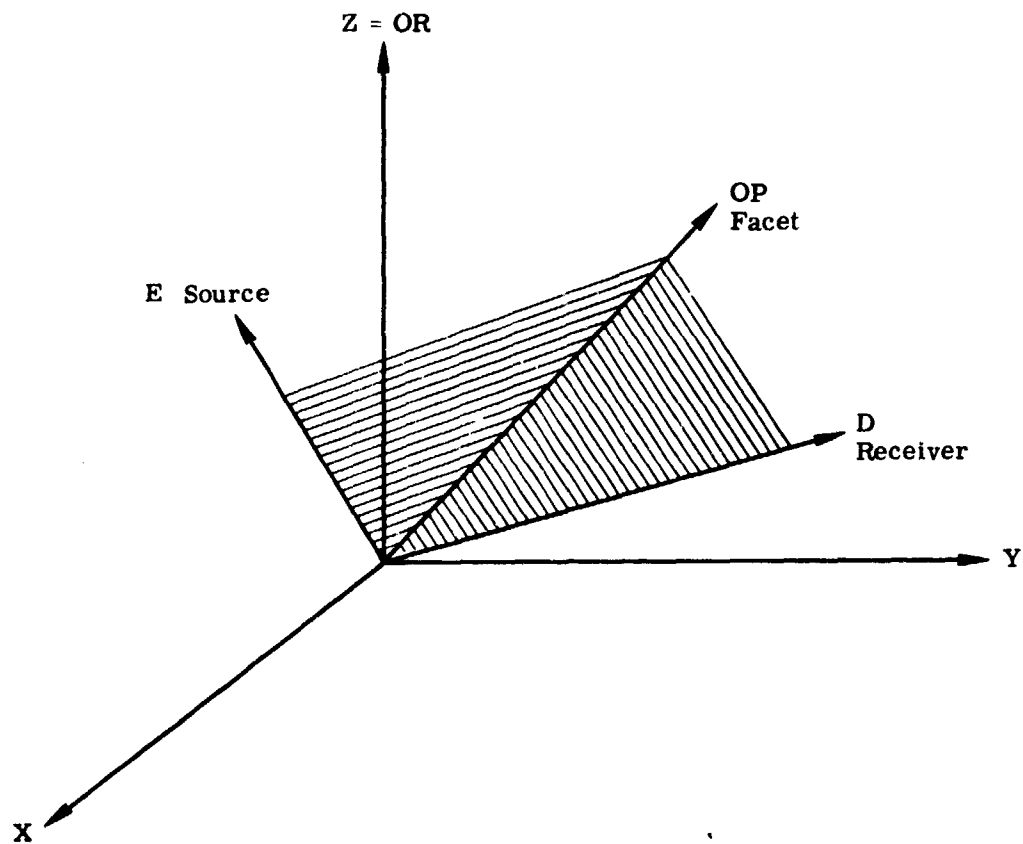


FIGURE 49. BIDIRECTIONAL REFLECTANCE GEOMETRY

$$YA = \frac{OR \times D}{|OR \times D|}$$

$$XA = \frac{E \times D}{|E \times D|}$$

$$U = \frac{D \times E}{|D \times E|}$$

$$XAP = \frac{OP \times E}{|OP \times E|}$$

$$YAP = \frac{OP \times D}{|OP \times D|}$$

$$COSB = X \cdot D$$

$$COSBDP = OP \cdot D$$

$$COSBEP = OP \cdot E$$

$$COSBNP = OP \cdot X$$

$$PSIPE = PSI - SIGN(-XAP \cdot OR)ARCOS(XAP \cdot Y)$$

= angle of major axis of polarization ellipse from the normal vector of the OP, E plane

$$PSIDE = PSI - SIGN(Y \cdot D)ARCOS(U \cdot Y)$$

= angle of major axis of polarization ellipse from the normal vector of the D, E plane

$$WADE = -SIGN(-YA \cdot E)ARCOS(XA \cdot YA)$$

= angle for transforming the output angle of polarization from E, D plane to OR, D plane

EDPHI = ARCOS(XAP \cdot YAP) = the relative azimuth angle between E and D in the facet coordinate system

DC = (-SINBEP, 0, COSBEP) = direction of specular ray in the facet coordinate system

D1 = (SINBDP COS EDPHI, SINBDP SIN EDPHI, COSBDP) = direction of reflected ray in the facet coordinate system

$$NZ1 = DC \cdot OP$$

$$NZ = NZ1 \cdot DC$$

$$DN = D1 \cdot NZ$$

PHIEN = 0 IF DN > 0
 = 2 - ARCOS(-DN) IF DN < 0 } parameter required in FUNCTION FUNC for shadowing and obscuration

SUBROUTINE GFRM. GFRM does all of the bidirectional reflectance calculations. The subroutine requires:

F = series of switches which can be set (optional) to reduce the number of redundant computations when GFRM is used as part of the multifaceted target model

COSB defined in SUBROUTINE GEOM

COSBDP defined in SUBROUTINE GEOM

COSBEP defined in SUBROUTINE GEOM

RCOSBNP = defined in SUBROUTINE GEOM

PSIPE = defined in SUBROUTINE GEOM

PSIDE = defined in SUBROUTINE GEOM

WADE = defined in SUBROUTINE GEOM

AP = area of facet (if AP = zero, GFRM returns a bidirectional reflectance Stokes vector; if AP ≠ 0, GFRM returns a Stokes vector for the reflected radiant intensity for unity irradiance in the incident beam)

MI = material specifier (available in COMMON)

ISW = model selector (available in COMMON)

W = wavelength specifier (available in COMMON), not used

TABLE = array containing all of the materials properties data read in SUBROUTINE IN-DATA

GFRM returns the bidirectional reflectance Stokes vector (AP = 0) or radiant intensity Stokes vector (AP ≠ 0).

I11 = Stokes vector for surface plus Lambertian model with polarized source

I21 = Stokes vector for surface plus Lambertian model with unpolarized source

I13 = Stokes vector for non-Lambertian volume model with polarized source

I23 = Stokes vector for non-Lambertian volume model with unpolarized source

I14 = Stokes vector for combined model with polarized source

I24 = Stokes vector for combined model with unpolarized source

FUNCTION GETDAT returns the appropriate material parameters for bidirectional reflectance calculations, namely N, K, RX1, RX2, RHOV, RCOSBNP, DP0, DP90, F, G.

FUNCTION FUNC provides the optional capability for deriving RCOSBNP analytically (if SIGMA ≠ 0) and for deriving a shadowing and obscuration correction factor (optional) to the RCOSBNP used in the specular model. In addition, the depolarization factors DP0(B) and DP90(B), as well as F(B) and G(BNP) needed in the volume model, are defined analytically. FUNCTION FUNC currently yields

$$DP0(B) = 1.0$$

$$DP90(B) = 1.0$$

$$F(B) = 1.0$$

$$G(BNP) = 1.0$$

$$RCOSBNP = (COSBNP)^2 RPO \left[Q1 e^{-1/2} e^{-\frac{1}{2} \left(\frac{BNP^2}{SIGMA^2} \right)} + Q2 RHOV \right]$$

for BNP < SIGMA

$$= (COSBNP)^2 RPO \left(Q1 e^{-\frac{BNP}{SIGMA}} + Q2 RHOV \right)$$

for BNP > SIGMA

The shadowing and obscuration factor applied to RCOSBNP (measured values read during the input phase of RHOPRIME or defined analytically in FUNC) is

$$\frac{1 + \frac{BNP}{OMEGA} e^{-\frac{2B}{TAU}}}{1 + \frac{BNP}{OMEGA}} \cdot \frac{1}{1 + \frac{PHIEN}{OMEGA} \cdot \frac{BEP}{OMEGA}}$$

(a) SURFACE-PLUS-LAMBERTIAN MODEL CALCULATION

$$R0 = \frac{(N+1)^2 + K^2}{(N-1)^2 + K^2} \cdot \frac{(V2 - COSB)^2 + V3}{(V2 + COSB)^2 + V3}$$

= normalized reflectance for \perp polarized incidence

$$R90 = \frac{(V2COSB + COS^2 B - 1)^2 + V3COS^2 B}{(V2COSB - COS^2 B + 1)^2 + V3COS^2 B} \cdot R0$$

= normalized reflectance for \parallel polarized incidence

where

$$V2 = \sqrt{\frac{4N^2K^2 + (N^2 - K^2 - 1 + COS^2 B)^2 + (N^2 - K^2 - 1 + COS^2 B)}{2}}$$

$$V3 = \frac{\sqrt{4N^2K^2 + (N^2 - K^2 - 1 + COS^2 B)^2 - (N^2 - K^2 - 1 + COS^2 B)}}{2}$$

If $H = 0$ the calculation is made for a plane polarized source (polarization angle PSI). The calculation ignores the induced elliptical polarization for $K \neq 0$.

$$PSIED = ATAN \left[\sqrt{\frac{R90}{0}} \cdot TAN PSIDE \cdot SIGN(COSATAN(N) - COSB) \right]$$

polarization angle with respect to D, E reference plane, after reflection

C = 1 if $AP = 0$, then a bidirectional reflectance Stokes vector is computed

C = $AP \cdot COSBEP \cdot COSBDP$ if $AP \neq 0$, then a reflected radiant intensity Stokes vector is computed

$$I(1) = C \left[\frac{RCOSBNP}{COSBEP \cdot COSBDP} (R0 \cdot COS^2 PSIDE + R90 \cdot SIN^2 PSIDE) \right. \\ \left. + (RX1 \cdot COS^2 PSIDE + RX2 \cdot SIN^2 PSIDE) \right]$$

$$I(2) = C \left[\frac{RCOSBNP}{COSBEP \cdot COSBDP} (R0 \cdot COS^2 PSIDE + R90 \cdot SIN^2 PSIDE) COS2 (PSIED-WADE) \right]$$

$$I(3) = C \left[\frac{RCOSBNP}{COSBEP \cdot COSBDP} (R0 \cdot COS^2 PSIDE + R90 \cdot SIN^2 PSIDE) SIN2 (PSIED-WADE) \right]$$

$$I_{21}(1) = C \left[\frac{R \cos B \sin \phi}{\cos B \sin \phi \cos \delta} \frac{1}{2} (R_0 + R_{90}) + \frac{1}{2} (R_{X1} + R_{X2}) \right]$$

$$I_{21}(2) = C \left[\frac{R \cos B \sin \phi}{\cos B \sin \phi \cos \delta} \frac{1}{2} (R_0 - R_{90}) \cos^2 (-\text{WADE}) \right]$$

$$I_{21}(3) = C \left[\frac{R \cos B \sin \phi}{\cos B \sin \phi \cos \delta} \frac{1}{2} (R_0 - R_{90}) \sin^2 (-\text{WADE}) \right]$$

If $H = \pm 1$ the calculation includes the phase difference and ellipticity induced by reflection for $K \neq 0$ and is an exact treatment of the Fresnel equations.

SUBROUTINE ELIPS1 (AA, AB, PSIDE, H; AA1, AA2, D) defines the following input elliptical polarization parameters: the amplitudes perpendicular (AA1) and parallel (AA2) to the D, E plane and the relative phase $D = \phi_{\parallel} - \phi_{\perp}$ of the amplitudes of the major (AA) and minor (AB) axes of polarization ellipse; the orientation of the ellipse with respect to the D, E plane; PSIDE; and the handedness, H.

$DR = \phi_{\parallel} - \phi_{\perp}$ induced by reflection

FOR $K = 0$, $DR = 0$ if $\cos B < \cos \text{ARTAN}(N)$
 $= -\pi$ if $\cos B > \cos \text{ARTAN}(N)$

FOR $K \neq 0$, $DR = -\pi + \text{ATAN} \left(\frac{2 \sqrt{V3} (1 - \cos^2 B) \cos B}{(1 - \cos^2 B)^2 - \cos^2 B (V2^2 + V3)} \right)$
 if () < 0

$DR = -\text{ATAN} \left(\frac{2 \sqrt{V3} (1 - \cos^2 B) \cos B}{(1 - \cos^2 B)^2 - \cos^2 B (V2^2 + V3)} \right)$
 if () > 0

The intensities A_{1R} and A_{2R} , and the relative phase of the parallel and perpendicular components of the reflected radiance induced by the reflections, are

$A_{1R} = A_1 \cdot R_0$

$A_{2R} = A_2 \cdot R_0$

$DR = DR + D$

SUBROUTINE ELIPS2 (AA1, AA2, DR, AAR, ABR, PSIED, HR) defines the elliptically polarized reflected radiance as amplitudes AAR and ABR of the major and minor axes, the angle of the ellipse relative to the D, E plane, PSIED, and the handedness, HR. PSIDE = PSIED-WADE is the angle that the polarization ellipse of the reflected radiance makes with the normal vector to the OR, D plane.

$\text{CHI} = \text{HR} \cdot \text{ATAN}(ABR / AAR)$ is the parameter used to define the ellipticity of the reflected radiance.

$C = 1$ if $AP = 0$

$$C = AP \cdot \text{COSBEP} \cdot \text{COSBDP} \text{ if } AP \neq 0$$

$$I11(1) = C \left[\frac{AR + BR}{A + B} \frac{R \text{COSBNP}}{\text{COSBEP} \text{COSBDP}} + (RX1 \text{COS}^2(\text{PSIPE}) + RX2 \text{SIN}^2(\text{PSIPE})) \right]$$

$$I11(2) = C \left[\frac{AR + BR}{A + B} \frac{R \text{COSBNP}}{\text{COSBEP} \text{COSBDP}} \text{COS}(2\text{PSIDE})\text{COS}(2\text{CHI}) \right]$$

$$I11(3) = C \left[\frac{AR + BR}{A + B} \frac{R \text{COSBNP}}{\text{COSBEP} \text{COSBDP}} \text{SIN}(2\text{PSIDE})\text{COS}(2\text{CHI}) \right]$$

$$I11(4) = C \left[\frac{AR + BR}{A + B} \frac{R \text{COSBNP}}{\text{COSBEP} \text{COSBDP}} \text{SIN}(2\text{CHI}) \right]$$

$$I21(1) = C \left[\frac{R \text{COSBNP}}{\text{COSBEP} \text{COSBDP}} \frac{1}{2} (R0 + R90) + \frac{1}{2} (RX1 + RX2) \right]$$

$$I21(2) = C \left[\frac{R \text{COSBNP}}{\text{COSBEP} \text{COSBDP}} \frac{1}{2} (R0 - R90) \text{COS}(-2\text{WADE}) \right]$$

$$I21(3) = C \left[\frac{R \text{COSBNP}}{\text{COSBEP} \text{COSBDP}} \frac{1}{2} (R0 - R90) \text{SIN}(-2\text{WADE}) \right]$$

$$I21(4) = 0$$

(b) VOLUME MODEL CALCULATION

The angular-dependent, volume reflectance model, Stokes vector is given by

$$I13(1) = C \frac{1}{\text{DP90}(1+\text{DP0})} \frac{2\text{RH0V} \cdot \text{F} \cdot \text{G}}{\text{COSBEP} + \text{COSBDP}} \left[\text{COS}^2 \text{PSIDE} \cdot \text{DP90}(1+\text{DP0}) + \text{SIN}^2 \text{PSIDE} \cdot \text{DP90}(1-\text{DP90}) \right]$$

$$I13(2) = C \frac{1}{\text{DP90}(1-\text{DP0})} \frac{2\text{RH0V} \cdot \text{F} \cdot \text{G}}{\text{COSBEP} + \text{COSBDP}} \left[\text{COS}^2 \text{PSIDE} \cdot \text{DP90}(1-\text{DP0}) + \text{SIN}^2 \text{PSIDE} \cdot \text{DP0}(1-\text{DP90}) \right] \text{COS}^2 2\text{AD}$$

$$I13(3) = C \frac{1}{\text{DP90}(1-\text{DP0})} \frac{2\text{RH0V} \cdot \text{F} \cdot \text{G}}{\text{COSBEP} + \text{COSBDP}} \left[\text{COS}^2 \text{PSIDE} \cdot \text{DP90}(1-\text{DP90}) + \text{SIN}^2 \text{PSIDE} \cdot \text{DP0}(1-\text{DP90}) \right] \text{SIN}^2 2\text{AD}$$

$$I23(1) = C \frac{1}{\text{DP90}(1-\text{DP0})} \frac{2\text{RH0V} \cdot \text{F} \cdot \text{G}}{\text{COSBEP} + \text{COSBDP}} \frac{1}{2} [\text{DP90}(1-\text{DP0}) + \text{DP0}(1-\text{DP90})]$$

$$I23(2) = C \frac{1}{\text{DP90}(1-\text{DP0})} \frac{2\text{RH0V} \cdot \text{F} \cdot \text{G}}{\text{COSBEP} + \text{COSBDP}} \frac{1}{2} [\text{DP90} - \text{DP0}] \text{COS}(-2\text{WADE})$$

$$I23(3) = C \frac{1}{\text{DP90}(1-\text{DP0})} \frac{2\text{RH0V} \cdot \text{F} \cdot \text{G}}{\text{COSBEP} + \text{COSBDP}} \frac{1}{2} [\text{DP90} - \text{DP0}] \text{SIN}(-2\text{WADE})$$

where

$$C = 1 \text{ for } AP = 0$$

$$C = AP \cdot \text{COSBEP} \cdot \text{COSBDP} \text{ for } AP \neq 0$$

The angle of polarization of the reflected radiance, AED, from the normal vector of the D, E plane is

$$AED = ATAN \left[\sqrt{\frac{DP0(1 - DP90)}{DP90(1 - DP0)}} \cdot TAN(PSIDE) \cdot SIGN(COS ATAN(N) - COSB) \right]$$

and the angle of polarization referred to the OR, D plane is

$$AD = AED - WADE$$

SUBROUTINE OUTPUT. This subroutine prints the Stokes vectors for the bidirectional reflectance ($AP = 0$) or reflected radiant intensity for unit incident irradiance ($AP \neq 0$) for the surface model, the volume models, and for the combined specular and volume model. Stokes vectors are printed for a completely polarized source, for a completely unpolarized beam, and also for a partially polarized beam (polarization defined by the input parameter P).

In addition, several calculations are made with the Stokes vectors. For a bidirectional reflectance (or radiant intensity) Stokes vector, the bidirectional reflectance (or radiant intensity) for a receiver polarized \perp or \parallel to the OR, D plane is

$$\text{receiver } \perp = \frac{A + B}{2}$$

$$\text{receiver } \parallel = \frac{A - B}{2}$$

where the Stokes vector is of the form:

$$\begin{bmatrix} A \\ B \\ C \\ D \end{bmatrix}$$

The angle of the major axis of the reflected radiance and the percent polarization of the reflected radiance are also given; they are

$$AL = \pm \frac{1}{2} ATAN \left| \frac{C}{B} \right| \quad -90 \leq AL \leq 90 \quad \begin{array}{l} \text{(looking into the source, } AL > 0 \text{ is a CCW angle;} \\ AL < 0 \text{ is a CW angle)} \end{array}$$

$$P = \frac{\sqrt{B^2 + C^2 + D^2}}{A} \times 100\%$$

The output includes TS, PS, TD, PD, P, as well as the input and output values of A, B, PSI, H from the surface model calculation (if the input H = 0, the input and output values of A, B, H default to 1, 0, and 0).

SUBROUTINE ELIPSI (A, B, PSI, H; A1, A2, DELTA). The basic equations which relate two specifications of an elliptically polarized beam (A, B, PSI, H) and (A1, B1, DELTA) are

$$\tan \alpha = \frac{A1 - A2}{0} \cdot \alpha \cdot \pi \cdot 2$$

$$\tan \chi = \pm \frac{B}{A} \text{ for } \frac{r_t}{l_t} \quad -\pi \cdot 4 \leq \chi \leq \pi \cdot 4$$

$$\tan 2\psi = \tan 2\alpha \cos \delta$$

$$\sin 2\lambda = \sin 2\alpha \sin \delta$$

from which we obtain

$$\sin^2 2\alpha = \frac{\sin^2 2\lambda + \tan^2 2\psi}{1 + \tan^2 2\psi}$$

or equivalently

$$\cos 2\alpha = \cos 2\lambda \cos 2\psi$$

Subroutine ELIPS1 determines A1, A2, DELTA from A, B, PSI, H

$$\text{LAMBDA} = \sqrt{A^2 + B^2}$$

If B = 0, A1 = LAMBDA COS PSI

A2 = LAMBDA SIN PSI

DELTA = 0 when $0 \leq \text{PSI} < \pi/2$

DELTA = π when $\pi/2 \leq \text{PSI} < \pi$

Otherwise:

CHI = H * ATAN(B, A)

TI = |COS 2CHI COS 2PSI|

ALPHA = 1/2 ARCCOS(-TI) if $\pi/4 \leq \text{PSI} < 3\pi/4$

= 1/2 ARCCOS(TI) if $\text{PSI} < \pi/4$ or $\text{PSI} > 3\pi/4$

If ALPHA = 0, A1 = LAMBDA, A2 = 0, DELTA = 0

If ALPHA = $\pi/4$, A1 = A2 = LAMBDA/√2, DELTA = 2CHI if $\text{PSI} = \pi/4$,

= H * π - 2 CHI if $\text{PSI} = 3\pi/4$,

If ALPHA = $\pi/2$, A1 = 0, A2 = LAMBDA, DELTA = 0

Otherwise

TI = SIN 2CHI SIN 2ALPHA

MU = ARSIN TI

A1 = LAMBDA COS ALPHA

A2 = LAMBDA SIN ALPHA

COSD = TAN 2PSI / TAN 2ALPHA

If COSD > 0 DELTA = H * MU

If COSD < 0 DELTA = H * (π - MU)

SUBROUTINE ELIPS2 (A1, A2, DELTA; A, B, PSI, H). Subroutine ELIPS2 determines A, B, PSI, H from A1, A2, DELTA.

$$\text{LAMBDA} = \sqrt{A_1^2 + A_2^2}$$

If $A_1 = 0$ or $A_2 = 0$, then $A = \text{LAMBDA}$, $B = 0$, $H = 1$, and

$\text{PSI} = 0$ if $A_2 = 0$

$\text{PSI} = \pi/2$ if $A_1 = 0$

If $A_1 = A_2$, then $\text{CHI} = 1/2|\text{DELTA}|$, $A = \text{LAMBDA} \cos \text{CHI}$, $B = \text{LAMBDA} \sin \text{CHI}$, and

$H = 1$ if $\text{DELTA} > 0$

$= -1$ if $\text{DELTA} < 0$

$\text{PSI} = \pi/4$ if $\text{CHI} < \pi/4$

$= 3\pi/4$ if $\text{CHI} > \pi/4$

If $\text{DELTA} = \pm\pi$, $A = \text{LAMBDA}$, $B = 0$, $H = 1$, $\text{PSI} = \pi - \text{ATAN } A_2/A_1$

If $\text{DELTA} = 0$, $A = \text{LAMBDA}$, $B = 0$, $H = 1$, $\text{PSI} = \text{ATAN } A_2/A_1$

If $\text{DELTA} = \pm\pi/2$, $H = +1$ if $\text{DELTA} > 0$

-1 if $\text{DELTA} < 0$

If $A_1 > A_2$, $A = A_1$, $B = A_2$, $\text{PSI} = 0$

If $A_1 < A_2$, $A = A_2$, $B = A_1$, $\text{PSI} = \pi/2$

Otherwise

If $A_1 > A_2$, $\text{ALPHA} = \text{ATAN } A_2/A_1$

$\text{CHI} = 1/2 \text{ ARSIN} |\sin 2\text{ALPHA} \sin \text{DELTA}|$

$\text{LAMBDA} = |\tan 2\text{ALPHA} \cos \text{DELTA}|$

$A = \text{LAMBDA} \cos \text{CHI}$

$B = \text{LAMBDA} \sin \text{CHI}$

$H = \pm$ if $\text{DELTA} \gtrless 0$

Part 1: $0 < |\text{DELTA}| < \pi/2$; $\text{PSI} = 1/2 \text{ ATANLAMDA}$

Part 2: $\pi/2 < |\text{DELTA}| < \pi$; $\text{PSI} = \pi - 1/2 \text{ ATANLAMDA}$

and

If $A_1 < A_2$, $0 < |\text{DELTA}| < \pi/2$ $\text{PSI} = \pi/2 - 1/2 \text{ ATANLAMDA}$

$\pi/2 < |\text{DELTA}| < \pi$ $\text{PSI} = \pi/2 + 1/2 \text{ ATANLAMDA}$

III.2. INPUT DATA FORMATS

The input to the RHOPRIME program is segmented into logical blocks. Each block is initiated by a block header and terminated by an end card. Blocks may be in any order, but a data block is assumed to precede any computation request blocks or scan request blocks. If a block header specifies an invalid block types, all input up to and including the next end card is ignored.

DATA TABLES BLOCK. The data tables block specifies all physical characteristics of the materials to be studied. The block header is one card with the following format:

<u>Columns</u>	<u>Description</u>
1-4	'TABL'
5-19	ignored
20-25	maximum material index to be expected
26-80	ignored

The data tables block is itself segmented into material blocks each characterizing one material to be studied. Each material block is initiated by a material header and terminated by an end card. The material header is two cards with the following format:

Card 1

<u>Columns</u>	<u>Description</u>
1-4	'MATR'
5-8	ignored
9-10	material index
11-20	n
21-30	k
31-40	$\rho_{\setminus 1}$
41-50	$\rho_{\setminus 2}$
51-60	ρ_v
61-70	SIGMA [if SIGMA \neq 0, RCOSBNP is computed]
71-80	RPO

Card 2

<u>Columns</u>	<u>Description</u>
1-10	ignored
11-20	τ
21-30	Ω
31-40	Q1
41-50	Q2
51-80	blank

Following a material header, there may be a set of ρ' data. If present, the ρ' is a function of $\theta_{\hat{n}}$ and the $\theta_{\hat{n}}$'s must be in ascending order. The format is

<u>Columns</u>	<u>Description</u>
1-4	blank or 'ANGL'
5-10	ignored
11-20	$\theta_{\hat{n}}$ (deg)
21-30	$\rho'(\theta_{\hat{n}}, \phi_{\hat{n}}; \theta_{\hat{u}}, \phi_{\hat{n}}) \cos^2 \theta_{\hat{n}}$
31-80	ignored

WARNING: Each material block must be terminated by an end card. The entire data tables block must also be terminated by an end card.

COMPUTATION REQUEST BLOCK. The computation requests block contains all information needed to perform desired computations. The block header is one card with the following format:

<u>Columns</u>	<u>Description</u>
1-4	'COMP'
5-19	ignored
20-25	model selector
26-80	ignored

The model selector, ISW, is:

1—if specular and diffuse models are desired

3—if volume model is desired

7—if combined model is desired

Following the block header, computation requests are processed sequentially until an end card is encountered. The format of a computation request is:

<u>Columns</u>	<u>Description</u>
1-4	blank
5-9	ignored
10-16	source zenith (deg)
17	ignored
18-24	source azimuth (deg)
25	ignored
26-32	detector zenith (deg)
33	ignored
34-40	detector azimuth (deg)
41	ignored
42-48	polarization major axis length
49	ignored
50-56	polarization minor axis length
57	ignored
58-64	angle of source polarization (deg)
65	ignored
66-72	source percent polarization + 100
73	ignored
74-76	handedness of polarization (if $\neq 0$, elliptical polarization is assumed)
77	ignored
78-80	material index

SCAN REQUEST BLOCK. If a scan of the detector zenith and/or azimuth is desired, a scan request block may be used. The block header is one card with the following format:

<u>Columns</u>	<u>Description</u>
1-4	'SCAN'
5-19	ignored
20-25	model selector
26-80	ignored

One card follows the block header giving all required parameters. The format of this card is:

<u>Columns</u>	<u>Description</u>
1-6	source zenith (deg)
7-12	source azimuth (deg)
13-18	initial detector zenith (deg)
19-24	final detector zenith (deg)
25-30	zenith increment (deg)
31-36	initial detector azimuth (deg)
37-42	final detector azimuth (deg)
43-48	azimuth increment (deg)
49-54	polarization major axis length
55-60	polarization minor axis length
61-66	angle of source polarization (deg)
67-72	source percent polarization ÷ 100
73-76	handedness of polarization
77-80	material index

TITLE SPECIFICATION BLOCK. A title may be printed at the top of each page of long form output using the title specification block. The block header is one card in the following format:

<u>Columns</u>	<u>Description</u>
1-4	'TITL'
5-19	ignored
20-25	blank
26-80	ignored

One card following the block header specifies the title. The format of this card is:

<u>Columns</u>	<u>Description</u>
1-60	title
61-80	ignored

FACET DEFINITION BLOCK. If default facet definition is not desired, the facet may be redefined using the facet definition block. The block header is one card in the following format:

<u>Columns</u>	<u>Description</u>
1-4	'FACE'
5-19	ignored
20-25	blank
26-80	ignored

One card following the block header defines the facet. The format of this card is:

<u>Columns</u>	<u>Description</u>
1-4	blank
5-9	ignored
10-16	facet area (default = 0)
17	ignored
18-24	facet normal - x (default = 0)
25	ignored
26-32	facet normal - y (default = 0)
33	ignored
34-40	facet normal - z (default = 1)
41-80	blank

END BLOCK. The end block terminates the program. The format of the block header is the same as that of the end card.

<u>Columns</u>	<u>Description</u>
1-4	'END'
5-80	blank

This block does not need an end card.

Appendix II
INSTRUCTIONS FOR USE OF PROGRAM
WITH SAMPLE COMPUTER OUTPUT

The program documentation in Appendix I, together with the sample computations included in this appendix should enable the user to (1) modify this program to accommodate the requirements of his own computer and (2) verify output from his modified program by comparison with the samples given herein.

Note that the input parameter values shown in Table VII are the ones with which the program has been run.

Sample outputs presented in this appendix include

- (1) a listing of the input information (Table VII)
- (2) the computed output of the program (long form) (Table VIII)
- (3) a short form of the computed output, containing only that information necessary to feed into a computer program for the purpose of obtaining plots of the data (Table IX)

The three tables mentioned above appear at the end of this appendix. All of the sample information is keyed and labelled so that elements may be identified easily. However, the further descriptive detail below may be helpful in studying the samples given.

RHOPRIME Input Listing

The following items appear across the top of Table VII. One line 2:

- n = real part of index of refraction
- k = imaginary part of index of refraction
- $\rho_{\chi 1}$ = cross component ($2\rho_{\perp 1}$)
- $\rho_{\chi 2}$ = cross component ($2\rho_{\perp 1}$)
- ρ_V = volume component used for volume model
- SIGMA = generating function parameter
- RPO = generating function parameter

And on line 3:

- τ = shadowing and obscuration parameter
- Ω = shadowing and obscuration parameter
- Q1 = generating function parameter
- Q2 = generating function parameter

Following these items in Table VII is the $\rho'(\theta_{\hat{n}} \phi_{\hat{n}}; \theta_{\hat{n}} \phi_{\hat{n}}) \cos^2 \theta_{\hat{n}}$ tabulation which, in this case, was extracted from measured data and determined from the zero bistatic scan. Alternatively, such a tabulation can be generated by use of a generating function specified in the SUBROUTINE FUNC.

Note in the sample input information of Table VII that values are provided for $\rho_{\chi 1}$, and $\rho_{\chi 2}$ and also for ρ_V . In practice, $\rho_{\chi 1}$, and $\rho_{\chi 2}$ will be used or ρ_V will be used; all three values will never be nonzero simultaneously.

If the table is supplied as part of the input, the parameters SIGMA and RPO are set to 0 and Q1 = Q2 = 1.

The $\rho' \left(\begin{matrix} \theta_{\hat{n}} \\ \phi_{\hat{n}} \end{matrix}; \begin{matrix} \theta_{\hat{n}} \\ \phi_{\hat{n}} \end{matrix} \right) \cos^2 \theta_{\hat{n}}$ tabulation is followed by scan request information telling the computer what source-receiver combinations are to be computed and what model is to be selected:

- θ_i = θ for source
- ϕ_i = ϕ for source
- θ_{r1} = initial θ for receiver
- θ_{r2} = maximum θ for receiver
- θ_{r3} = size of angular step for θ_r scan
- ϕ_{r1} = ϕ for receiver
- ϕ_{r2} = ϕ for receiver (value for second scan)
- ϕ_{r3} = size of angular step for ϕ_r
- A = semi-major axis of polarization ellipse (normalized to 1.0)
- B = semi-minor axis of polarization ellipse (B = 0 implies linear polarization)
- PSI = angle of source polarization
- P = percent polarization (1.0 = 100%)
- MI = material index
- ISW = 7 for combined model. (When volume model is used, set $\rho_{\chi 1} = \rho_{\chi 2} = 0$.)

Note that in addition to these input parameters, others must be added in the SUBROUTINE FUNC:

- DP0, DP90 = depolarizations for perpendicular and parallel components of incident beam
- f, g = volume model parameters.

For the materials in the sample listing, values for DP0, DP90, f, and g have been set equal to 1.0.

Computer Output (Long Form)

As exemplified by Table VIII, each page of the computed output corresponds to one source-receiver configuration. Items at the upper left are self-explanatory. However it should be borne in mind that MAJOR refers to the semi-major elliptical axis (a), which is taken to be 1.0. Since MINOR, which refers to the semi-minor axis (b), is 0, the MAJOR-MINOR combination implies linear polarization with polarization angle PSI for the incident beam. HANDED = 0 whenever the polarization is linear only.

The entries in the three main columns are reflectances. From the top, the first four entries in each column are the surface model elements of the Stokes vector which describes the polarization state of the beam as it leaves the target:

A = total reflectance

B = reflectance with receiver polarization angle = 0 (perpendicular polarization)

C = reflectance with receiver polarization angle = 45°

D = reflectance with receiver circularly polarized

The second four entries, still in the surface model block, are

$\frac{A+B}{2}$ = reflectance recorded from receiver with analyzer set for perpendicular polarization

$\frac{A-B}{2}$ = reflectance recorded from receiver with analyzer set for parallel polarization

AL = angle of polarization for reflected beam

P = percent polarization of reflected beam

Thus far the first two blocks of four entries have been discussed. The foregoing, as previously stated, apply to the surface plus Lambertian volume model.

The third and fourth blocks apply to the non-Lambertian volume model and are to be interpreted in exactly the same manner as above.

The fifth and sixth blocks consist of the sum of the surface + volume models and are printed out for convenience.

Note that in the volume model output and in the summed output, item D (circularly-polarized component) is not present.

Computer Output (Short Form)

The short form of the computer output consists of the information in the last four entries of the summed output (surface + volume), $\frac{A+B}{2}$, $\frac{A-B}{2}$, AL, P (see Table IX). Moreover, the data are compressed so that, whereas the long form has only one source-receiver configuration per page, the short form contains a complete scan in one block.

One scan consists of four item numbers. Preceding each of the first two item numbers in each scan are

Wavelength (1.06 μ m)

θ_i (0°)

ϕ_i (180°)

ϕ_r (0° or 180°)

The first item number in each scan contains $\frac{A+B}{2}$. Each output entry is preceded by the θ_r scan angle — i.e., 0.0, 0.0268 means that the reflectance at $\theta_r = 0$ is 0.0268. The second item number contains $\frac{A-B}{2}$. The third item number contains the polarization angle, AL, at each receiver angle. The fourth item number contains the percent polarization.

The scans are in the same overall order as those in the long form of the output

TABLE IX. SHORT FORM OUTPUT

SL	Item No.	$\frac{A-B}{2}$	$\frac{A+B}{2}$	λ	θ_i	ϕ_i	ϕ_F
1	4021009015001	0.0	0.0	0.0	0.0	0.0	0.0
2	9001	$\frac{A-B}{2}$	$\frac{A+B}{2}$	1.06	0.0	180.00	0.0
3		0.0	0.0647	20.000.0620	30.000.0601	30.000.0642	40.000.0641
4		50.000.0733	60.000.0837	70.000.1101	80.000.1580	80.000.1580	80.000.1580
5	First Set of 4-Item Numbers	0.0	0.0402	20.000.0405	30.000.0414	30.000.0430	40.000.0454
6		50.000.0448	60.000.0534	70.000.0547	80.000.0683	80.000.0683	80.000.0683
7	3(AL)	0.0	-5.0	20.00	-4.6	30.00	-4.6
8		50.00	-3.9	70.00	-2.9	80.00	-2.4
9	4(P)	0.0	23.76	21.33	20.00	18.72	30.00
10		50.00	20.23	22.22	20.00	29.79	30.00
11		0.0	0.0647	20.000.0620	30.000.0601	30.000.0642	40.000.0641
12		50.000.0733	60.000.0837	70.000.1101	80.000.1580	80.000.1580	80.000.1580
13	Second Set of 4-Item Numbers	0.0	0.0402	20.000.0405	30.000.0414	30.000.0430	40.000.0454
14		50.000.0448	60.000.0534	70.000.0547	80.000.0683	80.000.0683	80.000.0683
15		0.0	-5.0	20.00	-4.6	30.00	-4.6
16		50.00	-3.9	70.00	-2.9	80.00	-2.4
17		0.0	23.76	21.33	20.00	18.72	30.00
18		50.00	20.23	22.22	20.00	29.79	30.00
19		0.0	0.0647	20.000.0620	30.000.0601	30.000.0642	40.000.0641
20		50.000.0733	60.000.0837	70.000.1101	80.000.1580	80.000.1580	80.000.1580
21		0.0	0.0402	20.000.0405	30.000.0414	30.000.0430	40.000.0454
22		50.000.0448	60.000.0534	70.000.0547	80.000.0683	80.000.0683	80.000.0683
23		0.0	-5.0	20.00	-4.6	30.00	-4.6
24		50.00	-3.9	70.00	-2.9	80.00	-2.4
25		0.0	23.76	21.33	20.00	18.72	30.00
26		50.00	20.23	22.22	20.00	29.79	30.00
27		0.0	0.0647	20.000.0620	30.000.0601	30.000.0642	40.000.0641
28		50.000.0733	60.000.0837	70.000.1101	80.000.1580	80.000.1580	80.000.1580
29		0.0	0.0402	20.000.0405	30.000.0414	30.000.0430	40.000.0454
30		50.000.0448	60.000.0534	70.000.0547	80.000.0683	80.000.0683	80.000.0683
31		0.0	-5.0	20.00	-4.6	30.00	-4.6
32		50.00	-3.9	70.00	-2.9	80.00	-2.4
33		0.0	23.76	21.33	20.00	18.72	30.00
34		50.00	20.23	22.22	20.00	29.79	30.00
35		0.0	0.0647	20.000.0620	30.000.0601	30.000.0642	40.000.0641
36		50.000.0733	60.000.0837	70.000.1101	80.000.1580	80.000.1580	80.000.1580
37		0.0	0.0402	20.000.0405	30.000.0414	30.000.0430	40.000.0454
38		50.000.0448	60.000.0534	70.000.0547	80.000.0683	80.000.0683	80.000.0683
39		0.0	-4.8	20.00	-3.9	30.00	-3.5
40		50.00	-2.9	70.00	-1.8	80.00	-1.2
41		0.0	18.72	10.00	23.13	20.00	27.73
42		50.00	24.17	60.00	25.87	70.00	28.92
43		0.0	0.0401	20.000.0401	30.000.0478	30.000.0599	40.000.0626
44		50.000.0703	60.000.0769	70.000.0904	80.000.0904	80.000.0904	80.000.0904

Appendix III
RHOPRIME PROGRAM LISTING

```

PHOPRIME AS OF 02.20.73
1 DIMENSION K(500),MP(3),F(3),D(3),OR(3),LABEL(15),TABLE(500)
2 EQUIVALENCE (TABLE,K)
3 INTERGR CODE,TABLES/'TABLE'/,COMP/'COMP'/,END/'END'/,SCANT/'SCANT'/
4 INTERGR TITLE/'TITL'/,FACE/'FACE'/
5 REAL T21(4),I11(4),T23(3),I13(3),T24(3),I14(3)
6 COMMON MI,ISW,w,TABLE,IP1,I11,IP3,I13,IP4,I14
7 COMMON /CMPT/PS1,PD1,BETA,BFTAB,KPO,COSTNF,SIGMA,PHIEN,REP,TS
8 DATA DP/0.0,0.0,1.0/,AP/0.0/,DK/0.0,0.0,1.0/
9 C*****
10 C
11 C FORMATS
12 C
13 C*****
14 100 FORMAT(A4,15X,I6)
15 110 FORMAT(A4,5X,A(F7.2,1X),F3.0,1X,I3)
16 120 FORMAT('NORMAL TERMINATION')
17 140 FORMAT('1','***** END-OF-FILE ENCOUNTERED')
18 150 FORMAT('1','***** TABLE READ ERROR -- CONDITION CODE =',F3.0)
19 170 FORMAT('1','***** WARNING EOF IN COMPUTATION REQUESTS')
20 180 FORMAT('1','***** INVALID CARD TYPE')
21 190 FORMAT('1','***** EOF IN SCAN DATA.')
22 200 FORMAT(15A4)
23 C*****
24 C
25 C DATA BLOCK READ-IN PHASE
26 C
27 C*****
28 1000 READ(2,100,END=8000)CODE,NMAT
29 C*****
30 C MATERIAL TABLES
31 C*****
32 1010 IF(CODE.NE. TABLES)GO TO 1020
33 CALL TNDATA(NMAT,CC)
34 IF(CC.GT. 0.0)GO TO 8010
35 GO TO 1000
36 C*****
37 C COMPUTATION REQUEST
38 C*****
39 1020 IF(CODE.NE. COMP)GO TO 1040
40 ASSIGN 1030 TO MODE
41 ISW = NMAT
42 1030 READ(2,110,END=8030)CODE,TS,PS,TU,PD,P,A,R,PST,D,H,MI
43 IF(CODE.EQ. END)GO TO 5000
44 IF(M.GT. 0.0)H = 1.0
45 IF(M.LT. 0.0)H = -1.0
46 IF(M.EQ. 0.0)A = 1.0
47 IF(M.EQ. 0.0)B = 0.0
48 GO TO 2000
49 C*****
50 C DEFECTOR SCAN REQUEST
51 C*****
52 1040 IF(CODE.NE. SCANT)GO TO 1060
53 ISW = NMAT
54 ASSIGN 1050 TO MODE
55 1050 CALL SCANC(C,TS,PS,TU,PD,P,A,R,PST,H)
56 IF(CC.GT. 0.0)GO TO 5000
57 GO TO 2000
58 C*****
59 C TITLE SPECIFICATION

```

```

60 C*****
61 1060 IF(CODE .NE. TITLE)GO TO 1070
62 READ(2,200)LABEL
63 CALL AUX17(LABEL,0.0,0.0,0.0,0.0,0.0,0.0,1)
64 IF(OP(3) .EQ. 1.0)GO TO 1090
65 JP(1) = 0.0
66 JP(2) = 0.0
67 JP(3) = 1.0
68 GO TO 1090
69 C*****
70 C FACET DEFINITION
71 C*****
72 1070 IF(CODE .NE. FACET)GO TO 1080
73 READ(2,110)CODE,AP,OP
74 GO TO 1090
75 C*****
76 C PROGRAM TERMINATION
77 C*****
78 1080 IF(CODE .NE. END)GO TO 8040
79 WRITE(3,120)
80 CALL SYSTEM
81 C*****
82 C READ END CARD
83 C*****
84 1090 READ(2,100,END=8000)CODE
85 IF(CODE .NE. END)GO TO 1090
86 GO TO 1000
87 C*****
88 C
89 C COMPUTATION PHASE
90 C
91 C*****
92 2000 PSI1 = PST/57.29577
93 TS1 = TS/57.29577
94 PS1 = PS/57.29577
95 TD1 = TD/57.29577
96 PD1 = PD/57.29577
97 E(1) = SIN(TS1)*COS(PS1)
98 E(2) = SIN(TS1)*SIN(PS1)
99 E(3) = COS(TS1)
100 U(1) = SIN(TD1)*COS(PD1)
101 U(2) = SIN(TD1)*SIN(PD1)
102 U(3) = COS(TD1)
103 CALL GERM(C,E,JP,TP,PSI1,PSTDF,PSTPF,CJSB,COSHP,CJSBF,
104 C CSR2,WAUF)
105 CALL GERM(CSR,CJSBP,CD,HEP,COSHP,COSR2,PSIPE,PSIDE,WAUF,AP,
106 C A,AP,H,RR,H,HR,PSID)
107 PSID = PSTJ*57.29577
108 C*****
109 C
110 C OUTPUT PHASE
111 C
112 C*****
113 C*****
114 C LOG FORM
115 C*****
116 CALL OUTP(ITR,PS,TD,PD,P,A,AP,P,RR,PSI,PSID,H,HR,LABEL,AP)
117 GO TO MDPF,(1030,1050)
118 C*****
119 C SHORT FORM

```

```

120 C*****
121 5000 IF(CC .GT. 2.0)GO TO R050
122 CALL AUX17(LABEL,0,0,0,0,0,0,0,0,0,3)
123 IF(CC .EQ. 1.0)GO TO P000
124 CC = 0.0
125 GO TO 1000
126 C*****
127 C
128 C ERROR HANDLING PHASE
129 C
130 C*****
131 8000 WRITE(0,140)
132 STOP R000
133 8010 WRITE(0,150)CC
134 STOP R010
135 8030 WRITE(0,170)
136 STOP R030
137 8040 WRITE(0,180)
138 GO TO 1090
139 8050 WRITE(0,190)
140 STOP R050
141 END
142 SUBROUTINE INDATA(NMAT,CC)
143 DIMENSION TABLE(500),KTAB(500)
144 EQUIVALENCE (TABLE,KTAB)
145 REAL N,K
146 INTEGER NRS,CODE,FND/'END '/,ANGLE/'ANGL'/,BLANK/' /
147 DATA MATR/'MATR'/
148 COMMON /I,I9,N,KTAB,I21,I11,I23,I13,I24,I14
149 C*****
150 C FORMATS
151 C*****
152 100 FORMAT(A4,4X,T2,7F10.3)
153 110 FORMAT(A4,5X,2E10.3)
154 120 FORMAT('/ ***** WARNING -- ANGLES OUT OF ORDER. '/)
155 130 FORMAT(10X,7E10.3)
156 CC = 0.0
157 NRS = NMAT+2
158 C*****
159 C HEAD MATERIAL HEADER
160 C*****
161 1000 HEAD(2,100,FND=R000)CODE,MAT,N,K,RX1,RX2,RHOV,SIGMA,RPO
162 IF(CODE .EQ. FND)RETURN
163 IF(CODE .NE. MATR)GO TO 8010
164 READ(2,130,FND=R000)TAU,OMEGA,Q1,Q2
165 IF(MAT .GT. NMAT)GO TO R020
166 BETA0 = -5.0
167 C*****
168 C STORE MATERIAL CONSTANTS
169 C*****
170 KTAB(MAT) = NRS
171 TABLE(NRS+1) = N
172 TABLE(NRS+2) = K
173 TABLE(NRS+3) = RX1
174 TABLE(NRS+4) = RX2
175 TABLE(NRS+5) = RHOV
176 TABLE(NRS+6) = SIGMA*0.0174533
177 TABLE(NRS+7) = RPO
178 TABLE(NRS+8) = TAU*0.0174533
179 TABLE(NRS+9) = OMEGA*0.0174533

```

```

180         TABLE(WRS+10) = J1
181         TABLE(WRS+11) = J2
182     C*****
183     C     READ AND STORE SCORING TABLE IF GIVEN
184     C*****
185         K1 = WRS+12
186         NA = 0
187     1010 READ(2,110,FND=8000)CODE,RETA,RCUR
188         IF(CODE .EQ. FND)GO TO 1020
189         IF(CODE .NE. ANGLE .AND. CODE .NE. BLANK)GO TO 8030
190         IF(RETA .LE. RETA7)WRITE(0,120)MAT
191         BETA0 = BETA
192         BETA = RETA+0.01/4533
193         TABLE(K1) = COS(BETA)
194         TABLE(K1+1) = RCUR
195         K1 = K1+2
196         NA = NA+1
197         GO TO 1010
198     C*****
199     C     SET NUMBER OF BETAS
200     C*****
201     1020 KTAB(WRS) = NA
202         WRS = WRS+NA+NA+1
203         GO TO 1000
204     C*****
205     C     ERROR HANDLING
206     C*****
207     8000  CF = 1.0
208         RETURN
209     8010  CF = 2.0
210         RETURN
211     8020  CF = 3.0
212         RETURN
213     8030  CF = 4.0
214         RETURN
215     END
216     SIBERITINE SCAN(CF,TS,PS,TU,PD,P,A,B,PSI,H)
217     COMMON MI,ISW,A,TABLE,IPI,I11,IPS,I13,I14,I14
218     DIMENSION TABLE(500)
219     REAL I21(4),I11(4),I23(3),I13(3),I24(3),I14(3)
220     INTEGER CODE,FND/END //
221     DATA ENTER/0.0/
222     C*****
223     C     FORMATS
224     C*****
225     100  FORMAT(12F5.2,F4.0,T4)
226     110  FORMAT(A4)
227     C*****
228     C     READ SCAN PARAMETERS
229     C*****
230         CF = 0.0
231         IF(ENTER .GT. 0.0)GO TO 2000
232         ENTER = 1.0
233         READ(2,100,FND=9000)TS,PS,IPS,IDE,ISTEP,POS,PDE,PSIFP,A,B,PSI,P,H,
234         1
235         IF(TDE = TDR)1000,1000,1010
236     1000  IPS = 0.0
237         IDE = 83.0
238     1010  ID = TDR-TSTEP
239         IF(PDE=PD9)1020,1020,1030

```

```

240      1020 PDS = 0.0
241          PDE = 180.0
242          PSTFP = 180.0
243      1030 IF(PSTEP .LT. 5.0)PSTEP = 5.0
244          IF(TSTEP .LT. 2.0)TSTEP = 2.0
245          IF(H .GT. 0.0)H = 1.0
246          IF(H .LT. 0.0)H = -1.0
247          IF(H .EQ. 0.0)A = 1.0
248          IF(H .EQ. 0.0)B = 0.0
249          PD = PD9
250      1040 READ(2,110,END=9000)CODE
251          IF(CODE .NE. END)GO TO 1040
252      C*****
253      C      INCREMENT THETA
254      C*****
255      2000 TD = TD+TSTEP
256          IF(TD .LE. TDF)RETURN
257      C*****
258      C      INCREMENT PHI
259      C*****
260          PD = PD+PSTEP
261          IF(PD .GE. PDF)GO TO 3000
262          TD = TD9
263          CF = 1.0
264          RETURN
265      C*****
266      C      SCAN COMPLETE
267      C*****
268      3000 CC = 2.0
269          ENTER = 0.0
270          RETURN
271      C*****
272      C      ERROR HANDLING
273      C*****
274      9000 CC = 3.0
275          ENTER = 0.0
276          RETURN
277      END
278      SUBROUTINE GETDATA(R,COS9)
279          DIMENSION TABLE(500),KTAB(500),P(TO)
280          EQUIVALENCE (TABLE,KTAB)
281          INTEGER NRS
282          COMMON MI,ISW,W,TABLE,IP1,I11,IP3,I13,IP4,I14
283          COMMON /CMPT/PS,PD,RETA,BETA,B,RP0,COSINF,SIGMA,PHIEN,REP,TS
284      C*****
285      C
286      C      THIS SUBROUTINE RETRIEVES DATA FROM TABLE
287      C      INPUT:
288      C          COS9 = COS(BETA)
289      C          COSINE = COS(BETA-N,P)
290      C
291      C      OUTPUT:
292      C          R(1) = N
293      C          R(2) = K
294      C          R(3) = RHO-CHI,1
295      C          R(4) = RHO-CHI,2
296      C          R(5) = RHO-V
297      C          R(6) = RHO(ETA=N,P)
298      C          R(7) = DP-PFRP
299      C          R(8) = DP-PAR

```

```

300 C R(0) = F
301 C R(10) = G
302 C
303 C*****
304 C*****
305 C RETRIEVE MATERIAL CONSTANTS
306 C*****
307 1000 IF(MI .LT. 1 .OR. MT .GT. 500)STOP 4000
308 WRS = KTAR(MI)
309 NA = KTAR(WRS)
310 K(1) = TABLE(WRS+1)
311 R(2) = TABLE(WRS+2)
312 K(3) = TABLE(WRS+3)
313 R(4) = TABLE(WRS+4)
314 R(5) = TABLE(WRS+5)
315 SIGMA = TABLE(WRS+6)
316 KPO = TABLE(WRS+7)
317 R(10) = TABLE(WRS+8)
318 K(7) = TABLE(WRS+9)
319 R(8) = TABLE(WRS+10)
320 R(9) = TABLE(WRS+11)
321 C*****
321.25 R(6) = 0.0
322 C TABLE LOOK-UP FOR KPOBMP
323 C*****
324 IF(NA .LE. 0)GO TO 3000
325 K1 = WRS+12
326 IF(NA .EQ. 1)GO TO 2020
327 K2 = K1+NA+NA
328 2010 IF(ABS(COSINE-TABLE(K1)) .LE. 0.0001)GO TO 2020
329 K3 = K1+2
330 IF(K3 .GE. 42)GO TO 2030
331 IF(TABLE(K3) .LT. COSINE)GO TO 2030
332 K1 = K3
333 GO TO 2010
334 C*****
335 C COSINE FUNCTION, RETRIEVE POLISH UP
336 C*****
337 2020 R(6) = TABLE(K1+1)
338 GO TO 3000
339 C*****
340 C INTERPOLATE KPOBMP
341 C*****
342 2030 FACT = (COSINE-TABLE(K1))/(TABLE(K3)-TABLE(K1))
343 R(6) = FACT*(TABLE(K3+1)-TABLE(K1+1))+TABLE(K1+1)
344 GO TO 3000
345 C*****
346 C COMPUTE JPO, DPO, F, G (KPOBMP = 1 IF SIGMA = 0)
347 C*****
348 3000 BETA = ARCTAN(COS4)
349 RFIAB = ATAN(R(1))
350 CALL FU(4)
351 RETURN
352 END
353 DIMENSION R(0),E,UP,OP,PSI,PSIDE,PSIDE,COSR,COSRDP,COSREP,
354 C COSR2,WALF,
355 DIMENSION J(3),F(3),UP(3),OP(3),X(3),Y(3),XA(3),YA(3),UF(3),
356 XAF(3),YAF(3),J1(3),JF(1),J7(3),N71(3),YAM(3)
357 REAL N2,N71
358 EXTERNAL SIG4
359 COMMON /CHPT/PS,PD,BETA,RFIAB,KPO,COSRDP,SIGMA,PHIEN,REP,TS

```

```

360 C*****
361 C FORMATS
362 C*****
363 100 FORMAT(' ***** FACET NOT VISIBLF. ')
364 C
365 IF(PSI .GT. 1.5707963)PSI = PSI-3.1415927
366 IT = 0
367 C*****
368 C
369 C*****
370 X(1) = D(1)+E(1)
371 X(2) = D(2)+E(2)
372 X(3) = D(3)+E(3)
373 T1 = VNORM(X,Y)
374 C*****
375 C
376 C*****
377 IF(ABS(F(3)-1.0) .GT. 0.0001)GO TO 1000
378 Y(1) = COS(PS+1.57079)
379 Y(2) = SIN(PS+1.57079)
380 Y(3) = 0.0
381 GO TO 1010
382 1000 CALL CROSSR(TH,E,Y)
383 T1 = VNORM(Y,Y)
384 C*****
385 C
386 C*****
387 1010 IF(ABS(D(3)-1.0) .GT. 0.0001)GO TO 1020
388 YA(1) = COS(PD+1.57079)
389 YA(2) = SIN(PD+1.57079)
390 YA(3) = 0.0
391 GO TO 1030
392 1020 CALL CROSSR(TH,D,YA)
393 T1 = VNORM(YA,YA)
394 C*****
395 C
396 C*****
397 1030 IF(ABS(F(1)-D(1)) .GT. 0.0001 .OR. ABS(F(2)-D(2)) .GT. 0.0001)
398 1 GO TO 1040
399 U(1) = Y(1)
400 U(2) = Y(2)
401 U(3) = Y(3)
402 XA(1) = YA(1)
403 XA(2) = YA(2)
404 XA(3) = YA(3)
405 IT = 1
406 GO TO 1050
407 1040 CALL CROSSR(F,D,YA)
408 T1 = VNORM(YA,XA)
409 U(1) = -XA(1)
410 U(2) = -XA(2)
411 U(3) = -XA(3)
412 C*****
413 C
414 C*****
415 1050 IF(ABS(TH(1)-F(1)) .GT. 0.0001 .OR. ABS(TH(2)-E(2)) .GT. 0.0001)
416 1 GO TO 1060
417 XAP(1) = Y(1)
418 XAP(2) = Y(2)
419 XAP(3) = Y(3)

```

```

420          GO TO 1070
421      1060  CALL CROSS(7P,L,XAP)
422          T1 = VNORM(XAP,YAP)
423      C*****
424      C
425      C*****
426      1070  IF (ABS(7P(1)-0(1)) .GT. 0.0001 .OR. ABS(0P(2)-0(2)) .GT. 0.0001)
427          )   GO TO 1080
428          YAP(1) = YA(1)
429          YAP(2) = YA(2)
430          YAP(3) = YA(3)
431          GO TO 1090
432      1080  CALL CROSS(7P,D,YAP)
433          T1 = VNORM(YAP,YAP)
434      C*****
435      C
436      C*****
437      1090  CCSR = DDT(X,D)
438          CCSRDP = DDT(7P,D)
439          CCSRSP = DDT(7P,E)
440          CCSRNP = DDT(7P,X)
441          CCSR2 = CCSR+CCSR
442          PSIPR = PSI-ARCS(DDT(XAP,Y)) + STGN(-DDT(XAP,0P))
443          PSIDR = PSI-ARCS(DDT(0,Y)) * STGN(DDT(Y,D))
444          IF (T1 .LT. 1) GO TO 1100
445          IF (ABS(F(1)-0P(1)) .GT. 0.0001 .OR. ABS(E(2)-0R(2))
446          )   .GT. 0.0001) GO TO 1100
447          WADF = 0.0
448          IF (WADF .GE. 3.14159) WADF = WADF-3.14159
449          IF (WADF .LT. 0.0) WADF = WADF+3.14159
450          GO TO 1110
451      1100  YAM(1) = -YA(1)
452          YAM(2) = -YA(2)
453          YAM(3) = -YA(3)
454          WADF = -ARCS(DDT(XA,YA)) + STGN(DDT(YAM,F))
455      C*****
456      C
457      C*****
458      1110  BRP = ARCS(CCSRDP)
459          BRP = ARCS(CCSRSP)
460          IF (BRP .GT. 1.57079 .OR. RUP .GT. 1.57079) WRITE(0,100)
461          ERPR1 = ARCS(DDT(XAP,YAP))
462          PHIFN = 0.0
463          IF (ABS(Y(1)-0P(1)) .LT. 0.0001 .AND. ABS(Y(2)-0P(2)) .LT. 0.0001)
464          )   RETURN
465          IF (ABS(0(1)-0P(1)) .LT. 0.0001 .AND. ABS(0(2)-0P(2)) .LT. 0.0001)
466          )   RETURN
467          IF (ABS(F(1)-0P(1)) .LT. 0.0001 .AND. ABS(F(2)-0P(2)) .LT. 0.0001)
468          )   RETURN
469      C
470          UP(1) = -SIN(BRP)
471          UP(2) = 0.0
472          UP(3) = CCSRSP
473      C
474          U1(1) = STN(BRP)*COS(FUPR1)
475          U1(2) = STN(BRP)*SIN(FUPR1)
476          U1(3) = CCSRDP
477      C
478          CALL CROSS(0C,UP,NZ1)
479          T1 = VNORM(NZ1,NZ1)

```

```

4A0      CALL CROSS(NZ1,DC,N7)
4A1      T1 = VNORM(NZ,N7)
4A2      DN = DUT(N1,N7)
4A3      IF(DN .LT. 0.0)PHTEN = 1.57079-ARCOS(-DN)
4A4      RETURN
4A5      END
4A6      SUBROUTINE GFRM(COSR,COSBP,COSRP,COSBNP,COSR2,PSIPE,PSIDE,
4A7      1      WADE,AP,A,AR,R,RR,H,HR,PSID)
4A8      DIMENSION TABLE(500),KTAB(500),P(10),ST(5)
4A9      LOGICAL MOD1,MOD2,MOD3,MOD4
490      EQUIVALENCE (MOD1,MOD2,I1),(MOD3,T3),(MOD4,I4),(R(1),N),(R(2),K),
491      1      (R(3),RY1),(R(4),RX2),(R(5),RHUV),(R(6),RMD),
492      2      (R(7),DPO),(R(8),DP90),(R(9),FF),(R(10),G)
493      INTFGR SHFTR
494      HFAL I21(4),I11(4),I23(3),I13(3),I24(3),I14(3),T12,T22,N,K
495      COMMON MI,ISW,W,TABLE,I21,I11,I23,I13,I24,I14
496      DATA MASK/200000001/
497      EXTERNAL SIGN
498      C*****
499      C
500      C      CHOOSE MODEL AND RETRIEVE DATA
501      C
502      C*****
503      I1 = LAND(MASK,ISW)
504      I3 = LAND(MASK,SHFTR(ISW,1))
505      I4 = LAND(MASK,SHFTR(ISW,2))
506      CALL GETDAT(R,COSR)
507      DO 1000 I = 1,5
508      I21(I) = 0.0
509      I11(I) = 0.0
510      I23(I) = 0.0
511      I13(I) = 0.0
512      I24(I) = 0.0
513      1000 I14(I) = 0.0
514      C*****
515      C
516      C      SPECULAR AND DIFFUSE MODEL (MOD1 & MOD2)
517      C
518      C*****
519      IF(.NOT. MOD1 .AND. .NOT. MOD2)GO TO 3000
520      C*****
521      C      COMPUTE FRESNEL COEFFICIENTS
522      C*****
523      V1 = DIVIDE((N+1.0)*(N+1.0)+K*K),(N-1.0)*(N-1.0)+K*K)
524      U = N*N*K*K-1.0+COSR2
525      P = SQRT(4.0*N*N*K*K+U*U)
526      V2 = SQRT(ABS(P+U)+0.5)
527      V3 = ABS(P-U)*0.5
528      C
529      H0 = V1*(1+(V2-COSR)*(V2-COSR)+V3)/(1+V2+CU98)*(V2+CU98)+V3)
530      C
531      V4 = V2+COSR
532      H90 = H0*((V4+CU98-1.0)**2+V3+COSR2)/(V4-COSR2+1.0)**2+
533      1      V3+CU98)
534      I21(4) = 0.0
535      I11(4) = 0.0
536      IF(M .NE. 0)GO TO 2000
537      AR = 0.0
538      BR = 0.0
539      PRI0 = 0.0

```

```

540      HP = 0.0
541      C*****
542      C      PLANE POLARIZED MODEL
543      C*****
544      T1 = ABS(ABS(PSTDF)-1.570796)
545      T2 = ABS(ABS(PSTDF)-4.712389)
546      IF(T1 .GT. 0.001 .AND. T2 .GT. 0.001) PSTED = ATAN(SQRT(DIVIDE
547      1 (R90,P0))*TAN(PSIDE)*SIGN(COS(ATAN(N))-COSB))
548      IF(T1 .LE. 0.001 .OR. T2 .LE. 0.001) PSTED = PSTDF*SIGN(COS(ATAN
549      1 (N))-COSB)
550      AR11 = PSTED-WADE
551      T1 = AR11+AP11
552      ST(1) = COS(T1)
553      ST(2) = SIN(T1)
554      T1 = -WADE-WAUF
555      V1 = (R0-R90)*0.5
556      ST(3) = (R0+R90)*0.5
557      ST(4) = V1*COS(T1)
558      ST(5) = V1*SIN(T1)
559      C
560      IF(AP .GT. 0.0) GO TO 1010
561      V1 = RMD/(COSREP*COSBDDP)
562      V4 = 1.0
563      GO TO 1020
564      C
565      1010 V1 = RMD*AP
566      V4 = COSBFP+COSRJP*AP
567      C*****
568      C      COMPUTE STOKES VECTOR
569      C*****
570      C
571      C      UNPOLARIZED SOURCE
572      C
573      1020 I22 = (RX1+RX2)*V4*0.5
574      I21(1) = V1+ST(3)+I22
575      I21(2) = V1+ST(4)
576      I21(3) = V1+ST(5)
577      C
578      C      POLARIZED SOURCE
579      C
580      I12 = (RX1+CJS(PSTDF)**2+RX2*91*(PSTDF)**2)*V4
581      C
582      V1 = (COS(PSIDE)**2*W0+SIN(PSTDF)**2*RY0)*V1
583      I11(1) = V1+I12
584      I11(2) = V1+ST(1)
585      I11(3) = V1+ST(2)
586      GO TO 3000
587      C*****
588      C      ELLIPTICAL MODEL
589      C*****
590      2000 IF(PSTDF .GT. 3.141593) PSTDF = PSTDF-3.141593
591      IF(PSTDF .LT. 0.0) PSIDE = PSIDE+3.141593
592      IF(PSTDF .LT. 0.0) PSIDE = PSIDE+3.141593
593      AA = SQRT(A)
594      AB = SQRT(B)
595      CALL FLTP91(AA,AB,PSIDE,M,AA1,AA2,0)
596      A1 = AA1*AA1
597      A2 = AA2*AA2
598      C
599      IF(ABS(CJ93-1.0) .LT. 0.001) C0 = -3.141593

```

```

600      IF(ABS(C09B) .LT. 0.001)DR = 0.0
601      C
602      IF(K .NE. 0.0160 TO 2040
603      BFTAB = C7S(ATAN(N))
604      IF(C09B=BFTAB)2010,2020,2030
605      2010 DR = 0.0
606      GN TU 2060
607      2020 DR = -1.570796
608      GN TU 2060
609      2030 DR = -3.141593
610      GN TU 2060
611      C
612      2040 T3 = 2.0*SQRT(V3)*(1.0-C09B2)+C09B
613      T4 = (1.0-C09B2)**2-C09B2*(V2*V2+V3)
614      IF(ABS(T4) .GT. 0.00001)GN TU 2050
615      DR = -1.570796
616      GN TU 2060
617      C
618      2050 T1 = T3/T4
619      IF(T1 .LT. 0.0)DR = -3.141593+ATAN(-T1)
620      IF(T1 .GE. 0.0)DR = -ATAN(T1)
621      C
622      2060 DR = DR+D
623      A1R = A1*90
624      A2R = A2*90
625      A41R = 90RT(A1R)
626      A42R = 90RT(A2R)
627      CALL FLTP92(A41R, A42R, DR, A4R, ABR, PSTED, HR)
628      C
629      AP = A4R*A4R/(A+B)
630      BP = ABR*ABR/(A+B)
631      IF(PSTED .GE. 3.141593)PSTED = PSTED-3.141593
632      PRIN = PSTED-WAVE
633      IF(PSTU .GE. 3.141593)PRIN = PSTU-3.141593
634      IF(PSTU .LE. 0.0)PSTU = PRIN+3.141593
635      T1 = PSTU+PRIN
636      T2 = 1.570796
637      IF(ABS(AAP) .GT. 0.0001)T2 = HR*ATAN(ABR/AAP)
638      T2 = T2+T2
639      C
640      IF(AP .GT. 0.0)GN TU 2070
641      V1 = RM7/(C09BEP+C09BNP)
642      V2 = 1.0
643      GN TU 2080
644      C
645      2070 V1 = R07*AP
646      V2 = C09BEP+C09BNP*AP
647      C
648      C*****
649      C      COMPLETE STOKES VECTOR
650      C*****
651      C
652      C      UNPOLARIZED SOURCE
653      C
654      2080 IP2      = (RV1+RV2)*V2*0.5
655      IP1(1) = V1*(R0+R90)*0.5+T22
656      IP1(2) = V1*(R0-W90)*0.5+C09(-WADF-WANB)
657      IP1(3) = V1*(R0-R90)*0.5+91N(-WADF-WANB)
658      C
659      C      POLARIZED SOURCE

```

```

660 C
661 I12 = (RY1*CNS(PRIPE)**2+RY2*STN(PRIPE)**2)*V2
662 C
663 V3 = V1*(AP+RR)
664 I11(1) = V3+I12
665 I11(2) = V3*CNS(T1)+CNS(T2)
666 I11(3) = V3*STN(T1)+CNS(T2)
667 I11(4) = V3*STN(T2)
668 C*****
669 C
670 C POLYMER MODEL (M003)
671 C
672 C*****
673 3000 IF(.NOT. MJD3160 TU 4000
674 V1 = 1.0
675 IF(AP .GT. 0.0)V1 = CNSREP*FOSBOP*AP
676 V1 = 2.0*V1*RHOU*FF*G/(COSBEP+COSPOP)
677 AFD = 0.0
678 T1 = ABS(ABS(PSTDF)-1.570796)
679 T2 = ABS(ABS(PSTDE)-4.712389)
680 IF(T1 .GE. 0.001 .AND. T2 .GE. 0.001)GO TO 3010
681 AFD = PSIDE
682 GO TO 3030
683 C
684 3010 IF(DH90 .GT. 0.001 .AND. DPO .LT. 0.999)GO TO 3020
685 AFD = 1.57079
686 GO TO 3030
687 3020 VP = SQRT(DPO*(1.0-DPO)/(DH90*(1.0-DPO)))*TAN(PSIDE)*SIGN
688 1 (COS(ATAN(N))-FOSB)
689 AFD = ATAN(V2)
690 C
691 3030 AN = AFD-WADE
692 C1 = COS(PSTDF)
693 C1 = C1*C1*DH90
694 S1 = SIN(PSTDF)
695 S1 = S1*S1*DH90
696 V1 = V1/(C1.0+DPO)*DH90)
697 C*****
698 C COMPUTE STOKES VECTOR
699 C*****
700 C
701 C POLARIZED SOURCE
702 C
703 I13(1) = V1*(C1*(1.0+DH90)+S1*(1.0-DH90))
704 I13(2) = V1*(C1*(1.0-DH90)+S1*(1.0+DH90))*COS(AU+AN)
705 I13(3) = V1*(C1*(1.0-DH90)+S1*(1.0+DH90))*SIN(AU+AN)
706 C
707 C UNPOLARIZED SOURCE
708 C
709 V1 = V1*0.5
710 I23(1) = V1*(DH90*(1.0+DH90)+DPO*(1.0+DH90))
711 I23(2) = V1*(DH90-DPO)*COS(-WADE-WADE)
712 I23(3) = V1*(DH90-DPO)*SIN(-WADE-WADE)
713 C*****
714 C
715 C INTERFACE MODEL (M004)
716 C
717 C*****
718 4000 IF(.NOT. MJD4)RETURN
719

```

```

720      END
721      SUBROUTINE OUTPUT(TS,PS,TD,PD,P,AA,AR,BR,RR,PSI,PSID,M,MR,LABEL,
722      1      AP)
723      DIMENSION A(3),R(3),C(3),AES(3,3),AFP(3,3),AL(3,3),PP(3,3)
724      DIMENSION LABEL(15),D(1),TABLE(500)
725      LOGICAL MOD1,MOD2,MOD3,MOD4
726      REAL T21(4),I11(4),T23(3),I13(3),T24(3),I14(3)
727      INTEGER SHFTB
728      COMMON MI,I9M,M,TABLE,I21,I11,I23,I13,I24,I14
729      EQUIVALENCE (MOD1,MOD2,T1),(MOD2,T3),(MOD4,T4)
730      DATA MASK/Z00000001/,ZERO/0.0/,ONE/1.0/
731      C*****
732      C      FORMATS
733      C*****
734      100  FORMAT(T1,10X,'REFLECTANCE',2X,4L1,2X,15A4//21X,'THETA',6X,'PHI',
735      1      13X,'POLARIZED',13X,'UNPOLARIZED',12X,'PARTIAL POL. ')
736      110  FORMAT(T1,10X,'INTENSITY',2X,4L1,2X,15A4//21X,'THETA',6X,'PHI',
737      1      13X,'POLARIZED',13X,'UNPOLARIZED',12X,'PARTIAL POL. ')
738      120  FORMAT(11Y,'SOURCE',2(4X,F6.2),3(10X,F13.5)/11X,'DETECTION',2X,
739      1      F6.2,4X,F6.2,3(10X,F13.5)/11X,'PERCENT POLAR.',4X,F6.2,3(10X,
740      2      E13.5)/37X,3(10X,F13.5))
741      130  FORMAT(23Y,'IN',8X,'OUT'/11X,'MAJOR',1X,2(4X,F6.2),3(10X,F13.5)/
742      1      11X,'MINOR',1X,2(4X,F6.2),3(10X,E13.5)/11X,'PSI',3X,2(4X,F6.2)
743      2      3(10X,F13.5)/11X,'HANDLED',2(4X,F5.0),2Y,3(10X,E13.5)//)
744      140  FORMAT(3(37Y,3(10X,F13.5))/4(37X,3(10X,E13.5))//)
745      PA = ABS(P)
746      IT = 1
747      I1 = IAND(MASK,TSW)
748      I3 = IAND(MASK,SHFTB(TSW,1))
749      I4 = IAND(MASK,SHFTB(TSW,2))
750      IF(.NOT. MOD1 .AND. .NOT. MOD2)GO TO 2000
751      A(1) = PA*I11(1)+(1.0-PA)*I21(1)
752      A(2) = PA*I11(2)+(1.0-PA)*I21(2)
753      C(1) = PA*I11(3)+(1.0-PA)*I21(3)
754      D(1) = PA*I11(4)+(1.0-PA)*I21(4)
755      AFS(1,1) = (I11(1)+T11(2))/2.0
756      AFS(2,1) = (I21(1)+T21(2))/2.0
757      AFS(3,1) = (A(1)+D(1))/2.0
758      AFP(1,1) = (I11(1)-T11(2))/2.0
759      AFP(2,1) = (I21(1)-T21(2))/2.0
760      AFP(3,1) = (A(1)-D(1))/2.0
761      AI(1,1) = 0.9999999
762      IF(T11(2) .NE. 0.0 .OR. I11(3) .NE. 0.0)
763      1  AL(1,1) = ATAN2(T11(3),I11(2))+28.6498
764      AI(2,1) = 0.9999999
765      IF(T21(2) .NE. 0.0 .OR. I21(3) .NE. 0.0)
766      1  AL(2,1) = ATAN2(T21(3),I21(2))+28.6498
767      AI(3,1) = 0.9999999
768      IF(R(1) .NE. 0.0 .OR. C(1) .NE. 0.0)
769      1  AL(3,1) = ATAN2(C(1),R(1))+28.6498
770      PP(1,1) = SQRT((I11(2)+T11(2)+I11(3)+T11(3)+I11(4)+T11(4))/
771      1      T11(1)+100.0)
772      PP(2,1) = SQRT((I21(2)+T21(2)+I21(3)+T21(3)+I21(4)+T21(4))/
773      1      T21(1)+100.0)
774      PP(3,1) = SQRT(D(1)*R(1)+L(1)*C(1)+U(1)+O(1))/A(1)+100.0
775      2000 IF(.NOT. MOD3)GO TO 3000
776      A(2) = PA*I13(1)+(1.0-PA)*I23(1)
777      A(2) = PA*I13(2)+(1.0-PA)*I23(2)
778      C(2) = PA*I13(3)+(1.0-PA)*I23(3)
779      AFS(1,2) = (I13(1)+T13(2))/2.0

```



```

840      2      (PP(T,3),I=1,3)
841      RETURN
842 4020  IF(.NOT. MJD3)GO TO 4030
843      WRITE(3,120)TS,PS,I13(1),T23(1),A(2),TD,PD,T13(2),I23(2),R(2),PA,
844      1      T13(3),I23(3),C(2)
845      WRITE(3,130)ONE,ZFRQ,(AFS(I,2),T=1,3),ZFRQ,ZERU,(AEP(T,2),I=1,3),
846      1      PSI,ZERU,(AL(I,2),T=1,3),ZFRQ,ZERU,(PP(I,2),T=1,3)
847      IF(.NOT. MJD4)RETURN
848      WRITE(3,140)I14(1),T24(1),A(3),T14(2),I24(2),R(3),I14(3),T24(3),
849      1      C(3),(AEP(T,3),I=1,3),(AFP(I,3),T=1,3),(AL(I,3),T=1,3),
850      2      (PP(T,3),I=1,3)
851      RETURN
852 4030  IF(.NOT. MJD4)RETURN
853      WRITE(3,120)TS,PS,I14(1),T24(1),A(3),TD,PD,T14(2),I24(2),R(3),PA,
854      1      T14(3),I24(3),C(3)
855      WRITE(3,130)ONE,ZFRQ,(AFS(I,3),T=1,3),ZFRQ,ZERU,(AEP(T,3),I=1,3),
856      1      PSI,ZFRQ,(AL(T,3),I=1,3),ZERU,ZFRQ,(PP(T,3),I=1,3)
857      RETURN
858      END
859      SUBROUTINE AUXIN(TITLE,Y1,Y1,Y2,Y3,Y4,ICODE)
860      COMMON /CMPT/PS1,PD1,RETA,BETA,BF1AB,KPU,COSINF,SIGMA,PHTEN,REP,TS
861      DIMENSION TITLE(3),Y(5,46)
862      DATA WL/1.04/
863      C*****
864      C
865      C      FORMATS
866      C
867      C*****
868      100  FORMAT(A4,A4,A1,'5001',1/Y,'0101')
869      110  FORMAT(9X,'9001',T5,27X,I3,2X,3F6.2,6X,F6.1)
870      120  FORMAT(20X,5(F6.2,F6.4)/(20X,5(F6.2,F6.4)))
871      130  FORMAT(20X,5(F6.2,F6.1)/(20X,5(F6.2,F6.1)))
872      140  FORMAT(20X,5(F6.2,F6.2)/(20X,5(F6.2,F6.2)))
873      C*****
874      C
875      C      SUBROUTINE CONTROL
876      C
877      C*****
878      GO TO(100,2000,3000),ICODE
879      STOP 1111
880      C*****
881      C
882      C      HEADER
883      C
884      C*****
885      1000  IS = 0
886      10  IP = 0
887      WRITE(4,100)TITLE
888      RETURN
889      C*****
890      C
891      C      STIPE
892      C
893      C*****
894      2000  IP = IP+1
895      X(1,IP) = X1
896      X(2,IP) = Y1
897      X(3,IP) = Y2
898      X(4,IP) = Y3
899      X(5,IP) = Y4

```

```

900         IF (TP .GE. 45) GO TO 3000
901         RETURN
902 C*****
903 C
904 C     WRITE UNIT
905 C
906 C*****
907 3000 CONTINUE
908 C*****
909 C     REFLECTANCES
910 C*****
911         PD = PD1*57.29577
912         PS = PS1*57.29577
913         DO 3010 I=2,3
914             IS = IS+1
915             WRITE(4,110) IS, TP, MI, TS, PS, PD
916             WRITE(4,120)(Y(1,J), X(1,J), J=1, TP)
917 3010 CONTINUE
918 C*****
919 C     ANGLE OF POLARIZATION
920 C*****
921         IS = IS+1
922         WRITE(4,110) IS, TP
923         WRITE(4,130)(X(1,I), X(4,J), I=1, TP)
924 C*****
925 C     PERCENT POLARIZATION
926 C*****
927         IS = IS+1
928         WRITE(4,110) IS, TP
929         WRITE(4,140)(Y(1,I), X(5,J), I=1, TP)
930         IP = 0
931         RETURN
932     END
933     SUBROUTINE FLTPS1(A,B,PS1,M,A1,A2,UFLTA)
934     REAL LAMBDA,MH
935     IF (PST .LT. 0.0 .OR. PST .GT. 3.141593) GO TO 4000
936     LAMBDA = SQRT(A*A+B*B)
937 C*****
938 C     OBLIQUE CASE
939 C*****
940         IF (M .GT. 0.0) GO TO 1000
941         A1 = ABS(COS(PST))*LAMBDA
942         A2 = ABS(SIN(PST))*LAMBDA
943         UFLTA = 0.0
944         IF (PST .GT. 1.570796) DELTA = 3.141593
945         RETURN
946 C*****
947 C     ELLIPTICAL CASE
948 C*****
949 1000 CHI = M*ATAN(M/A)
950         TI = ABS(COS(2.0*CHI))+COS(2.0*PS1)
951         IF (PST .GT. 0.785398 .AND. PST .LT. 2.356195) ALPHA = .5*ARCOS(-TI)
952         IF (PST .LT. 0.785398 .OR. PST .GT. 2.356195) ALPHA = .5*ARCOS(TI)
953         IF (ALPHA .NE. 0.0) GO TO 1100
954         A1 = LAMBDA
955         A2 = 0.0
956         UFLTA = 0.0
957         RETURN
958 1100 IF (ABS(A1/A2-0.785398) .GT. 0.0001) GO TO 1020
959         A1 = LAMBDA/1.414214

```

```

960      A2 = A1
961      DFLTA = 2.0*CHI
962      IF(ABS(PST-2.356195).LT.0.0001) DFLTA = H*3.141593 - 2.0*CHI
963      RETURN
964      C
965      1020 IF(ABS(ALPHA-1.570796) .GT. 0.0001)GO TO 1030
966      A1 = 0.0
967      A2 = LAMBDA
968      DFLTA = 0.0
969      RETURN
970      C
971      1030 T1 = ABS(SIN(2.0*CHI)/SIN(2.0*ALPHA))
972      IF(T1 .GT. 1.0)T1 = 1.0
973      MU = ARSIN(T1)
974      A1 = LAMBDA*COS(ALPHA)
975      A2 = LAMBDA*STN(ALPHA)
976      COSD = TAN(2.0*PST)/TAN(2.0*ALPHA)
977      IF(COSD .GT. 0.0)DELTA = H*MU
978      IF(COSD .LE. 0.0)DELTA = H*(3.141593-MU)
979      RETURN
980      C*****
981      C      ERROR HANDLING
982      C*****
983      8000 WRITE(3,100)PSI
984      100  FORMAT(///' *****PST ANGLE OUT OF RANGE --',F10.5)
985      STOP
986      END
987      SUBROUTINE FLTPS2(A1,A2,DFLTA,A,B,PSI,H)
988      REAL LAMBDA,LAMDA
989      IF(DELTA .LT. -3.141593)DFLTA = DFLTA+6.283185
990      IF(DELTA .GT. 3.141593)DFLTA = DFLTA-6.283185
991      LAMBDA = SQRT(A1*A1+A2*A2)
992      C*****
993      C      CASE 1 (A1 = 0 OR A2 = 0)
994      C*****
995      IF(A1 .NE. 0.0 .AND. A2 .NE. 0.0)GO TO 1010
996      A = LAMBDA
997      B = 0.0
998      H = 1.0
999      IF(A1 .EQ. 0.0)PST = 1.570796
1000     IF(A2 .EQ. 0.0)PST = 0.0
1001     RETURN
1002     C*****
1003     C      CASE 2 (A1 = A2)
1004     C*****
1005     1010 IF(A1 .NE. A2)GO TO 1020
1006     CHI = 0.5*ARS(DFLTA)
1007     A = LAMBDA*COS(CHI)
1008     B = LAMBDA*STN(CHI)
1009     H = 1.0
1010     IF(DELTA .LT. 0.0)H = -1.0
1011     PSI = 0.785398
1012     IF(CHI .GT. 0.785398)PST = 2.356195
1013     RETURN
1014     C*****
1015     C      CASE 3 (DELTA = PI OR -PI)
1016     C*****
1017     1020 IF(ABS(ABS(DELTA)-3.141593) .GT. 0.0001)GO TO 1030
1018     A = LAMBDA
1019     B = 0.0

```

```

1020           H = 1.0
1021           PSI = 3.141593-ATAN(A2/A1)
1022           RETURN
1023         C*****
1024         C      CASE 4 (DELTA = 0)
1025         C*****
1026         1030 IF (ABS(DELTA) .GT. 0.0001) GO TO 1040
1027           A = LAMDA
1028           B = 0.0
1029           H = 1.0
1030           PSI = ATAN(A2/A1)
1031           RETURN
1032         C*****
1033         C      CASE 5 (DELTA = PT HALVES OR -PT HALVES)
1034         C*****
1035         1040 IF (ABS(ABS(DELTA)-1.570796) .GT. 0.0001) GO TO 1060
1036           H = 1.0
1037           IF (DELTA .LT. 0.0) H = -1.0
1038         C
1039         C      PART 1 (A1 > A2)
1040         C
1041           IF (A1 .LT. A2) GO TO 1050
1042           A = A1
1043           B = A2
1044           PSI = 0.0
1045           RETURN
1046         C
1047         C      PART 2 (A1 < A2)
1048         C
1049         1050 A = A2
1050           B = A1
1051           PSI = 1.570796
1052           RETURN
1053         C*****
1054         C      CASE 6 (A1 > A2)
1055         C*****
1056         1060 ALPHA = ATAN(A2/A1)
1057           CHI = 0.5*ARSTN(ARS(STN(2.0*ALPHA)*SIN(DELTA)))
1058           LAMDA = ARS(TAN(2.0*ALPHA)*COS(DELTA))
1059           A = LAMDA*COS(CHI)
1060           B = LAMDA*SIN(CHI)
1061           H = 1.0
1062           IF (DELTA .LT. 0.0) H = -1.0
1063           IF (A1 .LT. A2) GO TO 1060
1064         C
1065         C      PART 1 (0 < DELTA < PT HALVES)
1066         C
1067           IF (ABS(DELTA) .GT. 1.570796) GO TO 1070
1068           PSI = 0.5*ATAN(LAMDA)
1069           RETURN
1070         C
1071         C      PART 2 (DELTA > PT HALVES)
1072         C
1073         1070 PSI = 3.141593-0.5*ATAN(LAMDA)
1074           RETURN
1075         C*****
1076         C      CASE 7 (A1 < A2)
1077         C*****
1078         C
1079         C      PART 1 (0 < DELTA < PT HALVES)

```

```

1080 C
1081 C 1080 IF(ABS(DELTA) .GT. 1.570796)GO TO 1090
1082 PSI = 1.570796-0.5*ATAN(LAMDA)
1083 RETURN
1084 C
1085 C PART 2(DELTA > PI HALVES)
1086 C
1087 C 1090 PSI = 1.570796+0.5*ATAN(LAMDA)
1088 RETURN
1089 END
1090 FUNCTION DOT(A,R)
1091 DIMENSION A(3), B(3)
1092 C*****
1093 C THIS FUNCTION RETURNS THE DOT PRODUCT OF A AND R
1094 C*****
1095 DOT = A(1)*R(1) + A(2)*R(2) + A(3)*R(3)
1096 RETURN
1097 END
1098 SUBROUTINE CROSS(A,R,X)
1099 DIMENSION A(3), B(3), X(3)
1100 C*****
1101 C THIS FUNCTION RETURNS THE CROSS PRODUCT OF A AND B IN X
1102 C*****
1103 X(1) = A(2)*B(3) - A(3)*B(2)
1104 X(2) = A(3)*B(1) - A(1)*B(3)
1105 X(3) = A(1)*B(2) - A(2)*B(1)
1106 RETURN
1107 END
1108 FUNCTION VNORM(A,X)
1109 DIMENSION A(3),X(3)
1110 C*****
1111 C THIS FUNCTION RETURNS THE NORM OF A AND THE NORMALIZED VECTOR IN X
1112 C*****
1113 VNORM = SQRT ( A(1)*A(1) + A(2)*A(2) + A(3)*A(3) )
1114 X(1) = A(1) / VNORM
1115 X(2) = A(2) / VNORM
1116 X(3) = A(3) / VNORM
1117 RETURN
1118 END
1119 FUNCTION SIGN(A)
1120 C*****
1121 C THIS FUNCTION RETURNS THE ALGEBRAIC SIGN OF THE ARGUMENT
1122 C*****
1123 SIGN = 1.0
1124 IF(A .LT. 0.0)SIGN = -1.0
1125 RETURN
1126 END
1127 FUNCTION DIVIDE(A,B)
1128 DIVIDE = 0.0
1129 IF(ABS(B) .GE. 1.0E-20)DIVIDE=A/B
1130 RETURN
1131 END
END OF FILE

```

```

FUNCTION AS OF 02.20.73
1   SUBROUTINE FUNC(R)
2   COMMON /CMPT/PS,PD,BETA,BETAB,RPO,COSINE,SIGMA,PHIEN,REP,TS
3   DIMENSION R(10)
4   TAU = R(10)
5   OMEGA = R(7)
6   Q1 = R(8)
7   Q2 = R(9)
8   BNP = ARCOS(COSINE)
9   IF(ABS(SIGMA) .LE. 0.001)GO TO 1000
10  IF(BNP .GE. SIGMA)
11  1   R(6) = RPO*COSINE*COSINE*(Q1*EXP(-BNP/SIGMA)+Q2*R(5))
12  IF(BNP .LT. SIGMA)
13  1   R(6) = RPO*COSINE*COSINE*(Q1*EXP(-0.5-0.5*BNP*BNP/(SIGMA*
14  2   SIGMA))+Q2*R(5))
15  1000 R(6) = R(4)
16  R(7) = 1.0
17  R(8) = R(7)
18  R(9) = 1.0
19  R(10) = 1.0
20  RETURN
21  END
51  SUBROUTINE FUNC(R)
52  COMMON /CMPT/PS,PD,BETA,BETAB,RPO,COSINE,SIGMA,PHIEN,REP,TS
53  DIMENSION R(10)
54  TAU = R(10)
55  OMEGA = R(7)
56  Q1 = R(8)
57  Q2 = R(9)
58  BNP = ARCOS(COSINE)
59  IF(ABS(SIGMA) .LE. 0.001)GO TO 1000
60  IF(BNP .GE. SIGMA)
61  1   R(6) = RPO*COSINE*COSINE*(Q1*EXP(-BNP/SIGMA)+Q2*R(5))
62  IF(BNP .LT. SIGMA)
63  1   R(6) = RPO*COSINE*COSINE*(Q1*EXP(-0.5-0.5*BNP*BNP/(SIGMA*
64  2   SIGMA))+Q2*R(5))
65  1000 R(6) = R(4)
66  R(7) = 1.0
67  R(8) = R(7)
68  R(9) = 1.0
69  R(10) = 1.0+EXP(-151.31221*RNP*RNP)
70  RETURN
71  END
101  SUBROUTINE FUNC(R)
102  COMMON /CMPT/PS,PD,BETA,BETAB,RPO,COSINE,SIGMA,PHIEN,REP,TS
103  DIMENSION R(10)
104  C*****
105  C
106  C   THIS IS A REPLACEABLE SUBROUTINE USED TO COMPUTE DPO,DPOU,F,AND G.
107  C   OUTPUT:
108  C   R(6) = RCJRBNP
109  C   R(7) = JPO
110  C   R(8) = JPQA
111  C   R(9) = F
112  C   R(10) = G
113  C
114  C*****
115  TAU = R(10)
116  OMEGA = R(7)
117  Q1 = R(8)

```

```

118      QP = R(9)
119      BNP = ARCS(COSINE)
120      C
121      C      RCO9BNP
122      C
123      IF(ABS(SIGMA) .LE. 0.001)GO TO 1000
124      IF(RNP .GE. SIGMA)
125      1      R(6) = RPO*COSINE*COSINE*(Q1*EXP(-BNP/SIGMA)+Q2*R(5))
126      IF(RNP .LT. SIGMA)
127      1      R(6) = RPO*COSINE*COSINE*(Q1*EXP(-0.5-0.5*BNP*BNP/(SIGMA*
128      2      SIGMA))+Q2*R(5))
129      1000  R(6) = R(A)*((1.0+BNP/UMEGA*EXP(-2.0*BETA/TAU))/(1.0+RNP/OMEGA))
130      1      /((1.0+PHTEN*REP)/(UMEGA+UMEGA))
131      C
132      C      DPO
133      C
134      R(7) = 1.0
135      C
136      C      DP90
137      C
138      R(8) = R(7)
139      C
140      C      F
141      C
142      R(9) = 1.0
143      C
144      C      G
145      C
146      R(10) = 1.0
147      RETURN
148      END
149      SUBROUTINE FUNC(R)
150      COMMON /CMPT/PS,PH,BETA,BETAB,RPO,COSINE,SIGMA,PHTEN,REP,TS
151      DIMENSION R(10)
152      TAU = R(10)
153      UMEGA = R(7)
154      U1 = R(8)
155      U2 = R(9)
156      BNP = ARCS(COSINE)
157      IF(ABS(SIGMA) .LE. 0.001)GO TO 1000
158      IF(RNP .GE. SIGMA)
159      1      R(6) = RPO*COSINE*COSINE*(U1*EXP(-BNP/SIGMA)+U2*R(5))
160      IF(RNP .LT. SIGMA)
161      1      R(6) = RPO*COSINE*COSINE*(U1*EXP(-0.5-0.5*BNP*BNP/(SIGMA*
162      2      SIGMA))+U2*R(5))
163      1000  R(6) = R(A)*((1.0+BNP/UMEGA*EXP(-2.0*BETA/TAU))/(1.0+RNP/OMEGA))
164      1      /((1.0+PHTEN*REP)/(UMEGA+UMEGA))
165      R(7) = 1.0
166      R(8) = R(7)
167      R(9) = 1.0
168      R(10) = 1.0+EXP(-151.31221*RNP*RNP)
169      RETURN
170      END
171      END OF FILE

```

REFERENCES

1. Target Signature Analysis Center: Data Compilation, Eleventh Supplement, Vol. I, Report No. 32210-41-B, Willow Run Laboratories of the Institute of Science and Technology, The University of Michigan, Ann Arbor, AFAL-TR-72-226, October 1972.
2. Target Signature Analysis Center: Data Compilation, Eleventh Supplement, Vol. II, Report No. 32210-41-B, Willow Run Laboratories of the Institute of Science and Technology, The University of Michigan, Ann Arbor, AFAL-TR-72-226, October 1972.
3. M. Born and E. Wolf, Principles of Optics, Pergamon Press, London, 1964.
4. K. E. Torrance and E. M. Sparrow, "Theory for Off-Specular Reflection from Roughened Surfaces," J. Opt. Soc. Amer., Vol. 57, No. 9, September 1967, pp. 1105-1114.
5. W. A. Shurcliff, Polarized Light, Harvard University Press, Cambridge, 1962.
6. H. B. Holl, Reflection of Electromagnetic Radiation, Vol. I, Report RF-TR-63-4, U.S. Army Missile Command, Redstone Arsenal, Huntsville, Alabama, 15 March 1963.